

https://dspace.org/

Applications of high resolution airborne magnetic and radiometric data in the Barberton greenstone belt of South Africa.

Moore, Chris

1994
https://hdl.handle.net/10539/24353

Downloaded from a DSpace repository. https://dspace.org/

APPLICATIONS OF HIGH RESOLUTION AIRBORNE MAGNETIC AND RADIOMETRIC DATA IN THE BARBERTON GREENSTONE BELT OF SOUTH AFRICA

Chris Moore

A Dissertation Submitted to the Faculty of Science
University of the Witwatersrand, Johannesburg
for the degree of Master of Science

Johannesburg 1994

I declare that this dissertation is my own, unaided work. It is being submitted for the degree of Master of Science in the University of the Witwatersrand, Johannesburg. It has not been submitted before for any degree or examination in any other University, nor has it been under the aegis or with the assistance of any other body or organisation or person outside the University of the Witwatersrand, Johannesburg.

Christopher Bruce Moore

21st day of January 1994

CONTENTS

FIGURES v

ATTACHED vii

CHAPTER 1

1 INTRODUCTION 1

1.1 DATA COLLECTION 2

1.2 OBJECTIVES 2

2 GEOLOGY 3

2.1 OVERVIEW 3

2.2 STRATIGRAPHY 4

2.2.1 ONVERWACHT GROUP 4

2.2.2 FIG TREE GROUP 5

2.2.3 MOODIES GROUP 6

2.2.4 INTRUSIVES 6

2.2.5 PHYSICAL PROPERTIES 7

2.3 STRUCTURE 7

2.4 MINING HISTORY 9

2.5 MINERALISATION IN THE BARBERTON GREENSTONE BELT 10

3 DATA ACQUISITION AND PROJECT MANAGEMENT 12

3.1 SUMMARY 12

3.2 PROJECT MANAGEMENT 12

3.2.1 BUDGET CONSIDERATIONS 12

3.2.2 SURVEY DESIGN 14

3.2.2.1 FLIGHT LINES 14

3.2.2.2 AIRCRAFT 16

3.2.3 CONTRACT NEGOTIATION 16

3.2.4 FIELD SUPERVISION 16

3.3 DATA ACQUISITION 17

3.3.1 FLYING HEIGHT 17
3.3.2 NAVIGATION 19
3.3.3 FLIGHT PATH RECOVERY 19
3.3.4 LOCATIONAL ERRORS 20
3.3.5 INSTRUMENTATION 20
3.3.5.1 MAGNETOMETER 21
3.3.5.2 SPECTROMETER 22
3.4 DATA COMPILATION 23
3.4.1 MAGNETICS 23
3.4.2 RADIOMETRICS 24
4 DATA PROCESSING 27
4.1 MAGNETIC DATA 27
4.1.1 DATA VERIFICATION 28
4.1.2 NON-LINEAR FILTER 28
4.1.3 GRIDDING 29
4.1.3.1 MINIMUM CURVATURE GRIDDING 29
4.1.4 SPECTRAL ANALYSIS 30
4.1.5 LOW PASS FILTER 32
4.1.6 DECORRUGATION 32
4.1.7 MERGING 33
4.1.8 IGRF REMOVAL 33
4.1.9 CONTOURING 33
4.1.10 REDUCTION-TO-POLE 34
4.1.11 FIRST VERTICAL DERIVATIVE 36
4.1.12 UPWARD CONTINUATION 37
4.1.13 HANNING FILTER 37
4.1.14 SHADED RELIEF 38
4.1.15 EULER DECONVOLUTION 38
4.2 RADIOMETRIC DATA 40
5 INTERPRETATION 41
5.1 MAGNETICS 41
5.1.1 SUSCEPTIBILITY MEASUREMENTS 43
5.1.2 MODELLING OF MAGNETIC RESPONSES 44
5.1.3 MAGNETIC DOMAINS 44
5.1.4 MAGNETIC DISCONTINUITIES 45

5.1.5 ISOLATED INTRUSIVES 48
5.1.6 ELONGATE MAGNETIC UNITS 50
5.2 RADIOMETRICS 51
5.3 DISCUSSION 53
5.3.1 BARBROOK FAULT 54
5.3.2 SHEBA FAULT 55
5.3.3 EUREKA SYNCLINE 56
5.3.4 JAMESTOWN IGNEOUS COMPLEX 57
5.3.5 DYKES 57
5.4 MINERALISATION 58
6 CONCLUSIONS 59
6.1 SUMMARY OF CONCLUSIONS 59
6.2 SCOPE FOR FURTHER RESEARCH 62
7 BIBLIOGRAPHY 63

APPENDIX 1 70

ATTACHMENTS 71

FIGURES

1 Eastern Transvaal Location Map

2 Barberton Greenstone Belt Stratigraphic Column

3 Northern Barberton Mountain Land Simplified Structure

4 Northern Barberton Mountain Land Gold Distribution Map

5 Geophysical Survey Boundaries with Simplified Geology

6 Radially Averaged Power Spectrum for the East Block

7 IGRF Field over the Barberton Mountain Land

8 Relationship of Susceptibility to Magnetite Content Diagram

9 Barbrook Thrust Development Sequence Diagram

A1 Magnetic Model, A-A' profile

A2 Magnetic Model, B-B' profile

A3 Magnetic Model, C-C' profile

A4 Magnetic Model, D-D' profile

A5 Magnetic Model, E-E' profile

A6 Magnetic Model, F-F' profile

A7 Magnetic Model 1, G-G' profile

A8 Magnetic Model 2, G-G' profile

A9 Magnetic Model, H-H' profile

A10 Magnetic Model, I-I' profile

ATTACHED

Plan No. 1 : Regional Geology	Scale 1 : 100 000
Plan No. 2 : Magnetic Residual field, colour contours	Scale 1 : 100 000
Plan No. 3 : Magnetic Residual Field, shaded relief	Scale 1 : 100 000
Plan No. 4 : Magnetic 1st Vertical Derivative, shaded relief	Scale 1 : 100 000
Plan No. 5 : Euler Deconvolution map	Scale 1 : 100 000
Plan No. 6 : Magnetic Interpretation Map	Scale 1 : 100 000
Plan No. 7 : Radiometric Total-Count, colour contours	Scale 1 : 100 000
Plan No. 8 : Radiometric Interpretation map	Scale 1 : 100 000
Plan No. 9 : Composite Interpretation map	Scale 1 : 100 000

CHAPTER 1

INTRODUCTION

The Barberton mountain land displays an unrivalled succession of some of the oldest rocks on the planet. It is situated in the Eastern Transvaal lowveld region of South Africa and extends into Swaziland (see figure 1). It is an extremely rugged tract of country which remained virtually unexplored until the 1880's, the main deterrent being the mosquito and tsetse fly which infested the low lying land surrounding the mountains. Gold prospectors were the first to brave the malaria and open up the country. In 1881 they were rewarded with a gold strike in northwestern Swaziland - the rush was on! The town of Barberton has always been intimately associated with mining and indeed derives its name from three early prospectors, Graham Barber and his two cousins who exposed Barber's reef behind the present location of the town. Historical gold ore production from the region has exceeded 250 tonnes from over 350 occurrences. Today there are a number of operational mines in the mountain land returning healthy profits to their shareholders. The majority of the gold has been derived from gold quartz lode deposits many of which are located adjacent to major regional faults.

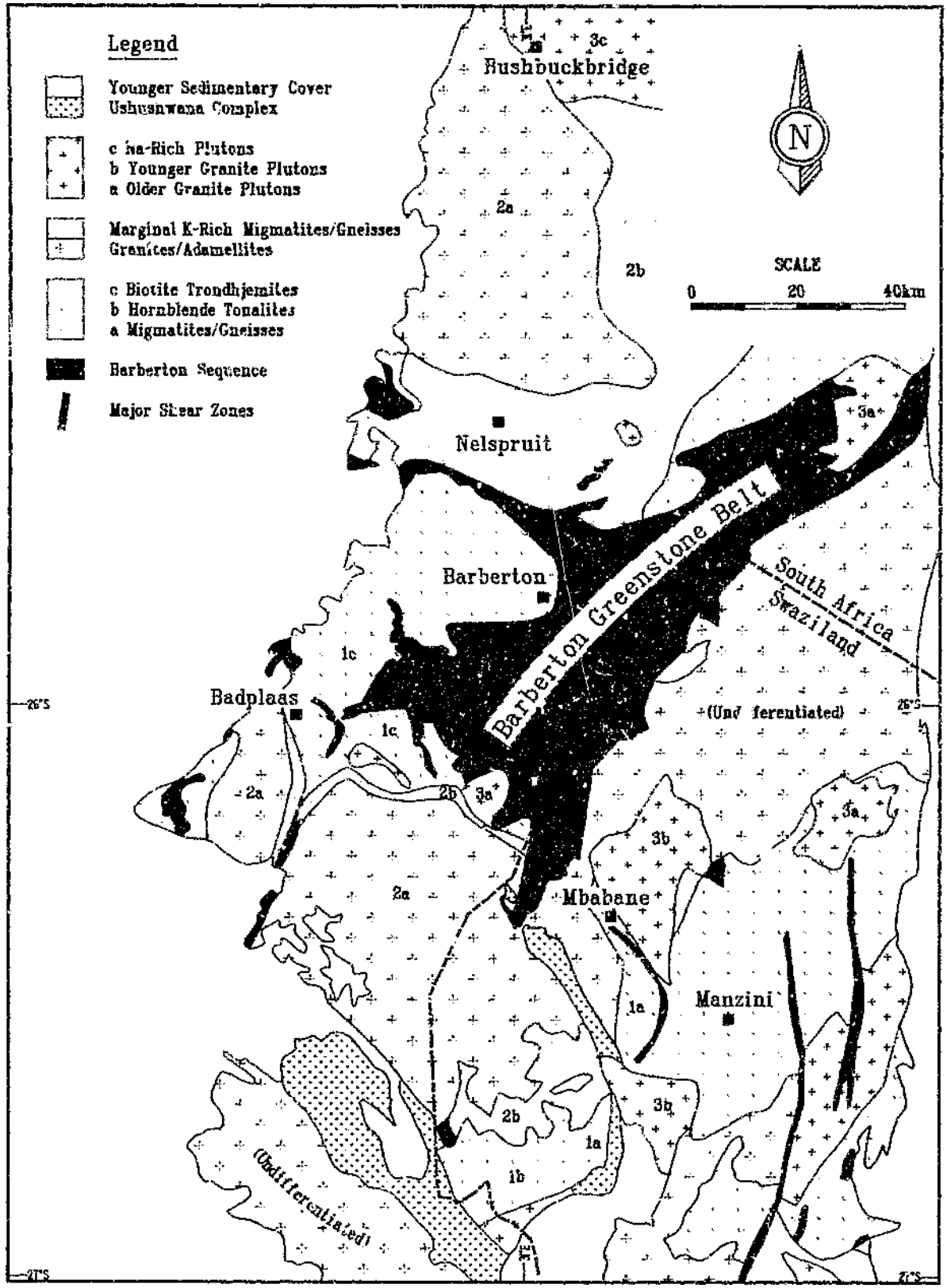
The Barberton mountain land is an elongate, linear Archaean granite-greenstone terrane comprising supracrustal volcanic and sedimentary rocks, termed the Barberton Sequence (SACS 1980). It forms one of the oldest, best developed and best preserved examples of Archaean Strata in southern Africa if not in the world, approximately 3.43 - 3.56Ga (Barton, 1982).

CHAPTER 1

INTRODUCTION

The Barberton mountain land displays an unrivalled succession of some of the oldest rocks on the planet. It is situated in the Eastern Transvaal lowveld region of South Africa and extends into Swaziland (see figure 1). It is an extremely rugged tract of country which remained virtually unexplored until the 1880's, the main deterrent being the mosquito and tsetse fly which infested the low lying land surrounding the mountains. Gold prospectors were the first to brave the malaria and open up the country. In 1881 they were rewarded with a gold strike in northwestern Swaziland - the rush was on! The town of Barberton has always been intimately associated with mining and indeed derives its name from three early prospectors, Graham Barber and his two cousins who exposed Barber's reef behind the present location of the town. Historical gold ore production from the region has exceeded 250 tonnes from over 350 occurrences. Today there are a number of operational mines in the mountain land returning healthy profits to their shareholders. The majority of the gold has been derived from gold quartz lode deposits many of which are located adjacent to major regional faults.

The Barberton mountain land is an elongate, linear Archaean granite-greenstone terrane comprising supracrustal volcanic and sedimentary rocks, termed the Barberton Sequence (SACS 1980). It forms one of the oldest, best developed and best preserved examples of Archaean Strata in southern Africa if not in the world, approximately 3.43 - 3.56Ga (Barton, 1982).



EASTERN TRANSVAAL
GRANITE - GREENSTONE DISTRIBUTION

(after Anhaeusser & Robb 1981)

FIGURE 1

It has become one of the best studied greenstone terranes in the world, yet despite this, the deep structure of the belt and the original stratigraphy of the Barberton Sequence and its surrounding granitoid terrane, remains incomplete and controversial.

1.1 DATA COLLECTION

This project was sponsored by Gencor Ltd who own a number of mineral claims and operating gold mines in the northern Barberton mountain land. During September 1990, Gencor Ltd, acquired extensive high resolution airborne magnetic and radiometric data over the Barberton greenstone belt, under the authors direction. These data provide the basis for this dissertation.

1.2 OBJECTIVES

The objectives of this dissertation are to: design suitable survey parameters for the magnetic/radiometric survey; supervise and ensure adequate quality control of the data acquisition; compile and process the data; evaluate the data and compile an improved regional geological map for the Barberton mountain land and hence derive an improved structural model for the region.

CHAPTER 2

GEOLOGY

This is a geophysical dissertation and as such an in-depth discussion of the geology is beyond the scope of this text. The following is a broad overview.

2.1 OVERVIEW

It was Viljoen and Viljoen (1969a) and Anhaeusser, *et al.*, (1969), who first proposed that the Barberton mountain land represented an undisturbed Archaean greenstone succession. Located in the Eastern Transvaal Lowveld, immediately east of the Drakensburg escarpment, the mountain land is a wedge shaped triangular tract of rugged country, surrounded by a variety of intrusive tonalitic diapirs. These have disrupted the lithologies producing profound metamorphic and structural alterations (Anhaeusser 1966, Hunter 1974, Roering 1965, Urie and Jones 1965).

The granite-greenstone distribution is shown in figure 1, apparent in this are arcuate, narrow, tapering protuberances of stratiform rocks which trend in all directions away from the main east-northeast trending grain of the greenstone belt. These protuberances or schist belts, attain their best development on the northwest, west and southwest sides of the belt. The most spectacular is the Jamestown schist belt, which trends to the northwest of Barberton (figure 1), where it disappears under the younger, flat lying quartzites of the Black Reef Formation and the lavas of the Godwan Formation.

The Jamestown belt is slightly arcuate being concave towards the south and has a strike length of 35 km, (Anhaeusser, 1968). Plan no. 1 presents a detailed geological map of the northern mountain land (derived from the government 1:50 000 sheets), a summarised version can be found in figure 5.

2.2 STRATIGRAPHY

Geologically the area is underlain by a variety of rock types, collectively grouped as belonging to the Barberton Sequence (SACS 1980). This sequence is divided into three major stratigraphic units, based on the work of Viljoen and Viljoen (1969b), and Anhaeusser (1975), (see Figure 2):-

2.2.1 ONVERWACHT GROUP

The Onverwacht Group forms the oldest phase and consists mainly of metamorphosed basaltic and ultramafic rocks, together with siliceous sediments. The assemblage is essentially volcanic in origin and has undergone considerable alteration in places, producing a variety of basic and siliceous schists. The rocks in the sequence constitute the initial magmatic, or ophiolitic, assemblage of the Swaziland geosyncline.

Viljoen and Viljoen (1970) divided the Onverwacht Group into a lower ultramafic-mafic volcanic unit, the Tjakastad Sub-group and an upper mafic-felsic volcanic unit, the Geluk Sub-group, separated by a thick band of cherty limestone and shale, known as the Middle Marker. They recognised three formations in each subgroup with a combined apparent stratigraphic thickness in excess of 15 km, these being: the Sandspruit, Theespruit and Komati Formations of the Tjakastad Sub-group;

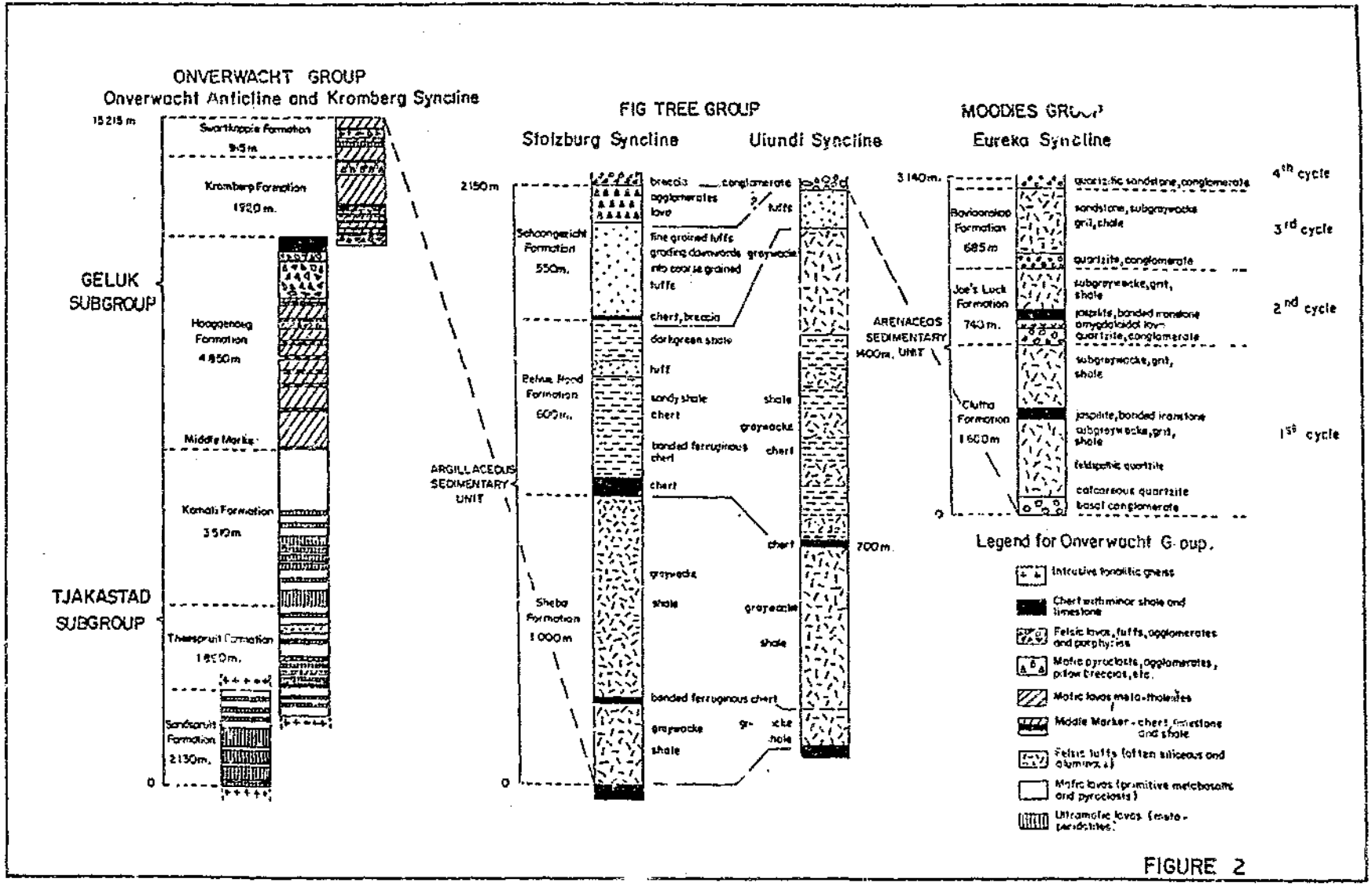


FIGURE 2

STRATIGRAPHY OF THE BARBERTON GREENSTONE BELT (AFTER ANHAEUSSER 1975)

and the Hooggenoeg, Kromberg and Swartkoppie Formations of the Geluk Sub-group. The Swartkoppie Formation is a contentious unit as it contains green and grey schists derived from acid and intermediate volcanics, basic schists derived from basaltic volcanics, cherts, pyroclastics, banded ferruginous cherts and greywackes; (Viljoen and Viljoen 1969c). Steyn (1976) termed this mixture the 'Zwartkoppie Bar'.

Authors have been unsure whether to place it at the top of the Onverwacht or base of the Fig Tree succession. Leinster (1992) surmised that the Swartkoppie Formation has acted as a decollement zone during deformation and may be a tectonic unit that does not, strictly, form part of the stratigraphy.

2.2.2 FIG TREE GROUP

The Fig Tree Group is essentially a sedimentary sequence overlying the Onverwacht rocks, consisting of terrigenous clastics with intercalated volcaniclastic tuffs and felsic lavas. The sediments display deep water turbidity current depositional characteristics. Three Formations have been recognised:-

The Sheba Formation consists of greywackes and shales with minor banded ferruginous cherts. This is overlain by the Belvue Road Formation consisting of sandy shales, tuffs and banded ferruginous cherts. At the top of the succession are course grained tuffs grading upwards through fine grained tuffs to the overlying agglomerates and felsic lavas of the Schoongezicht Formation. A combined stratigraphic thickness of 2000m, has been recognised within the Fig Tree Group, (Anhaeusser 1975).

2.2.3 MOODIES GROUP

The Moodies Group overlies the Fig Tree strata, unconformably in places, and is made up of conglomerates, quartzites, shales, and a few bands of magnetic jaspilite and lava. The Moodies sediments provide evidence of shallow-water deposition, thus contrasting sharply with the essentially deep water environment of the Fig Tree succession and are likened to molasse sediments of geosynclines.

Anhauesser (1975) divided the Group into three sedimentary cycles which he termed the Clutha, Joe's Luck and Baviaanskop Formations. The Clutha Formation consists of a basal conglomerate, considered by Ramsay (1963) to be a disconformity, overlain by felspathic quartzites, magnetite shales and greywacke/shales. The Joes Luck and Baviaanskop Formations essentially repeat the Clutha Formation, with an increasing sandstone content towards the top of the succession. The Moodies facies thicken towards the northern half of the mountain land where they reach a combined stratigraphic thickness of around 3 000 m (Anhaeusser, *et al.*, 1968).

2.2.4 INTRUSIVES

The Barberton greenstone belt is surrounded by intrusive plutonic rocks that are integrally involved with its history. There are two suites, termed the Northern and Southern, which were emplaced 3.2Ga and 3.4Ga respectively, (Kroner, *et al.*, 1991). Both suits display evidence of structural emplacement, with only minor aureoles of amphibolite grade metamorphism developed along the contacts.

It was suggested by Lowe (1991) that the Southern suite of intrusives is co-magmatic with the development of felsic volcanics in the Onverwacht Hooggenoeg Formation.

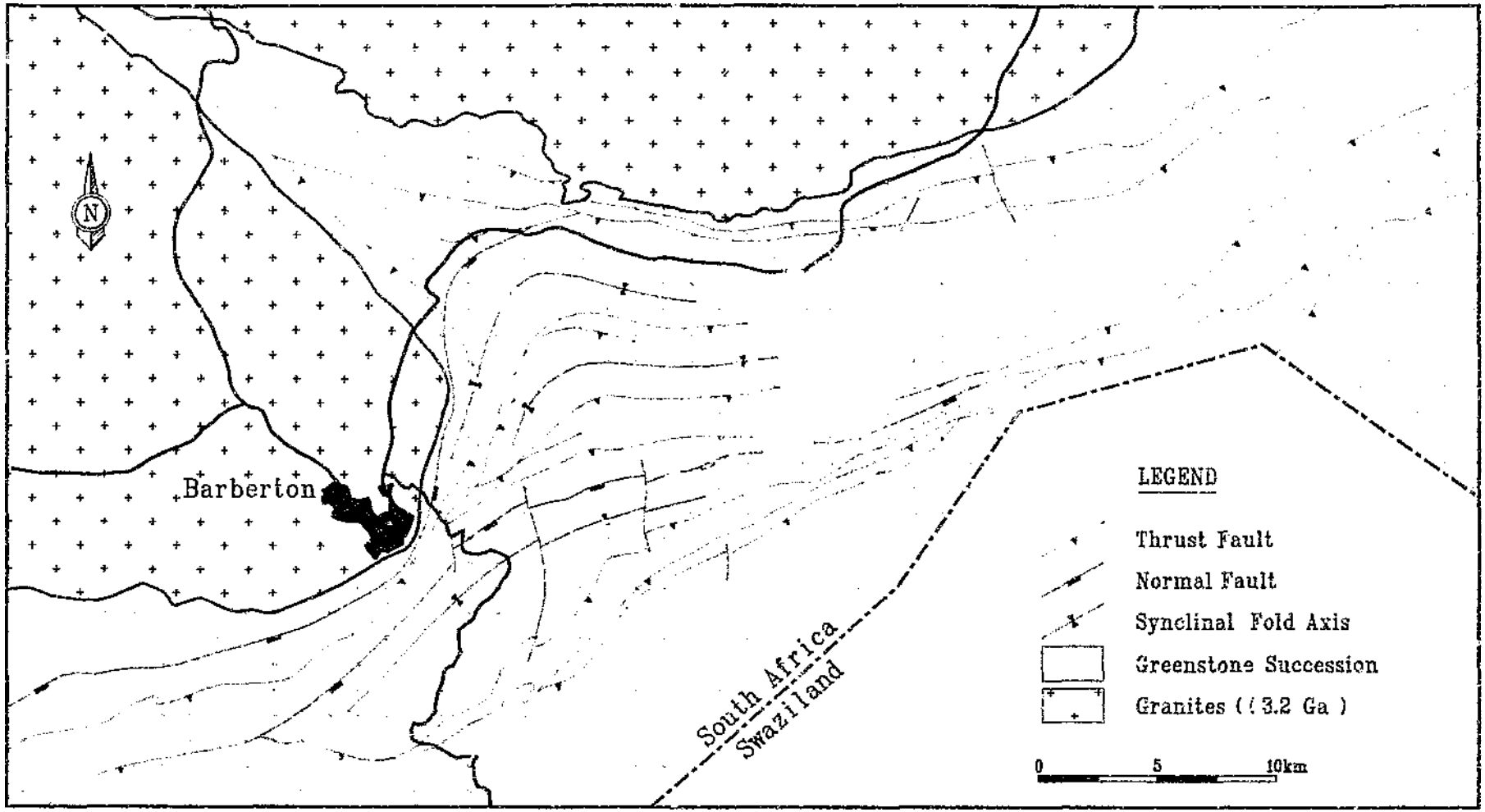
Greenstone fragments have been identified in the Stentor pluton, along the mountain land's northern margin. This would indicate that the pluton is a sheet or sill-like body, implying that the original granite-greenstone margin lies north of the Stentor pluton (Thomkinson and King 1991).

2.2.5 PHYSICAL PROPERTIES

Currently there exists no physical data base for the Barberton lithologies. In particular no measurements of magnetic remanence have been published. A number of susceptibility measurements were taken by the author with a Scintrex hand held susceptibility meter (see table 5.1). These were used to aid the modelling of magnetic anomalies.

2.3 STRUCTURE

The regional structure of the Barberton greenstone belt is that of a broad regional synclinorium with a pronounced east-northeast, west-southwest trend, similar to that of a number of other Archaean greenstone belts within the north-east sector of the Kaapvaal Province. Within this synform, numerous tight synclinal folds occur that plunge south to south-east, with steeply dipping to overturned limbs. These are separated by major normal wrench faults that follow the grain of the belt (Figure 3). These regional faults divide the Barberton greenstone belt into a number of distinct narrow structural zones.



NORTHERN BARBERTON MOUNTAIN LAND
MAJOR FAULT LINEAMENTS MAP

(Source : Geological Survey Of South Africa, Sheet 2530 Barberton)

FIGURE 3

Many faults show evidence of having been reactivated as transcurrent faults and numerous examples of detachments have been identified; (Anhaeusser, *et al.*, 1968, Anhaeusser, 1975).

At surface the limbs of the major folds dip moderately to steeply. This led initial investigators to extrapolate the limbs of the synclines down to extreme depths, resulting in an entrenched view of the belt having a keel at a depth of 20 to 40 km (Anhaeusser, *et al.*, 1969, Viljoen and Viljoen 1969c). The depth was later updated to between 10 and 20 km (Anhaeusser 1973, Hunter 1974). Deformation was modelled as being due to vertical tectonic forces caused by density inversion and diapirism of a down-sagging dense greenstone terrane into an upwelling less dense granitoid terrane.

More recently the traditional model has been scrutinised in the light of modern geophysical and structural investigations. This has led to its rejection and the development of a new scenario for the tectonic evolution of the greenstone belt.

A positive residual gravity anomaly was found to be centred over the belt. Geophysical modelling of this anomaly has yielded a depth for the belt in the order of 3km (Burley, *et al.*, 1970). Darracott, (1975), inferred a maximum depth to the base of the Onverwacht of 6km, but considered a depth of 3km to be the most probable. Geoelectrical soundings were carried out in the belt by de Beer, *et al.*, (1988). These again indicated a depth for the belt in the order of 3km. A shallow broadly tubular structure is therefore more compatible with the geophysical data.

The geophysical evidence is supported by the field work of Fripp, *et al.*, (1980), who mapped large, southward dipping, late stage imbricate thrusts. They interpreted these as shear and mylonite zones that detached into a south dipping sole thrust at the base of the greenstone succession, at a depth of approximately 5-8km. Truncation of the synclines by such a thrust convincingly explains the observed gravity and electrical measurements.

Thrust faulting has been demonstrated at a number of locations in the Barberton greenstone belt (Anhaeusser, *et al.*, 1968; de Wit, 1982; de Wit, *et al.*, 1983). Paris (1987) and de Wit, *et al.*, (1983) have hypothesised that the Onverwacht succession represents an Archaean ophiolite complex that was obducted onto a sialic granitoid margin. de Wit and Armstrong (1987), suggested that felsic volcanics were tectonically emplaced along thrust zones into the mafic/ultramafic ophiolite succession. Lamb and Paris (1988) suggested that the overlying Fig Tree and Moodies sediments represent submarine to alluvial fan deposits derived from the erosion of an advancing thrust wedge, in a foreland basin setting, from south-east to north-west.

2.4 MINING HISTORY

Gold has been mined in the Barberton mountain land for over a century. The earliest recorded discovery was by Tom McLachlan who, in 1881, discovered alluvial gold between Poponyana Creek and Pigs Peak in north-west Swaziland. In June 1882 Jim Murry discovered alluvial gold in the Jamestown area of the De Kaap Valley followed in 1883 by Auguste Robert (French Bob) who located the Pioneer reef, the first payable lode gold to be discovered in the De Kaap goldfields.

It was two years later that Edwin Bray struck gold in the Sheba reef at the Golden Quarry and triggered the famous gold rush that led to the development of the Barberton gold producing district. Production from the 274 recorded gold workings in the Archaean volcano-sedimentary successions of the greenstone belt, during the period 1884 to 1983, was 252 000 kg of Au and 8 900 kg of Ag, at an average grade in the order of 10.7 g/t Au (Anhaeusser, 1986). More than 95% of the gold has been recovered from the northwest flank of the belt. The majority of this mineralisation has come from the Ulundi syncline. In particular two mines, Sheba and Fairview, account for over one third of all gold production.

Several important base metal deposits are located in the greenstone belt. The most notable occurrences are of chrysotile asbestos and iron ore. Lesser occurrences of magnetite, talc, barite and tin also exist.

2.5 MINERALISATION IN THE BARBERTON GREENSTONE BELT

The Archaean gold deposits in the Barberton mountain land occur in a wide variety of host rocks including the principal metavolcanic and metasedimentary units comprising the Onverwacht, Fig Tree and Moodies Groups.

Minor uneconomic occurrences are also found in some of the granites proximal to the belt.

The majority of the gold production in the Barberton greenstone belt stems from quartz lode deposits. It has been demonstrated that structural influences caused by regional and local deformation played a dominant role in the distribution and localisation of epigenetic gold occurrences in the mountain land, (Anhaeusser, *et al.*, 1969; Barton, 1982; Jones, 1969; Poole, 1964; Viljoen and Viljeon, 1969c).

Faulting in particular, played a dominant role in determining the location of ore bodies. Many of the more significant gold deposits are located adjacent to major regional faults, typified by the Sheba, Barbrook, Albion, Lily and Scotsman faults, (see Figure 4).

In most cases, the fault planes have undergone several stages of re-activation by wrench faulting accompanied by second order phenomena associated with horizontal or sub-horizontal strike slip movements and transcurrent dislocation. This has produced loci for the development of mineral ore shoots (Anhaeusser, 1986). The majority of ore bodies are thus located in an environment dictated by the varying influences and effects of fault deformation. Away from the sphere of influence of the major planes of weakness, the incidence of gold mineralisation clearly declines, and is either poorly developed or totally absent. Coupled with the fault control is the effect on a regional scale of intrusive granites and their associated contact metamorphic effects. Again, it has been demonstrated that the more significant gold mineralisation lies in a broad zone adjacent to the periphery of the mountain land, mineralisation decreases progressively away from the influence of the granite contacts (Anhaeusser,*et al.*, 1968; Anhaeusser, *et al.*, 1969; Groeneveld, 1973; Hall 1918).

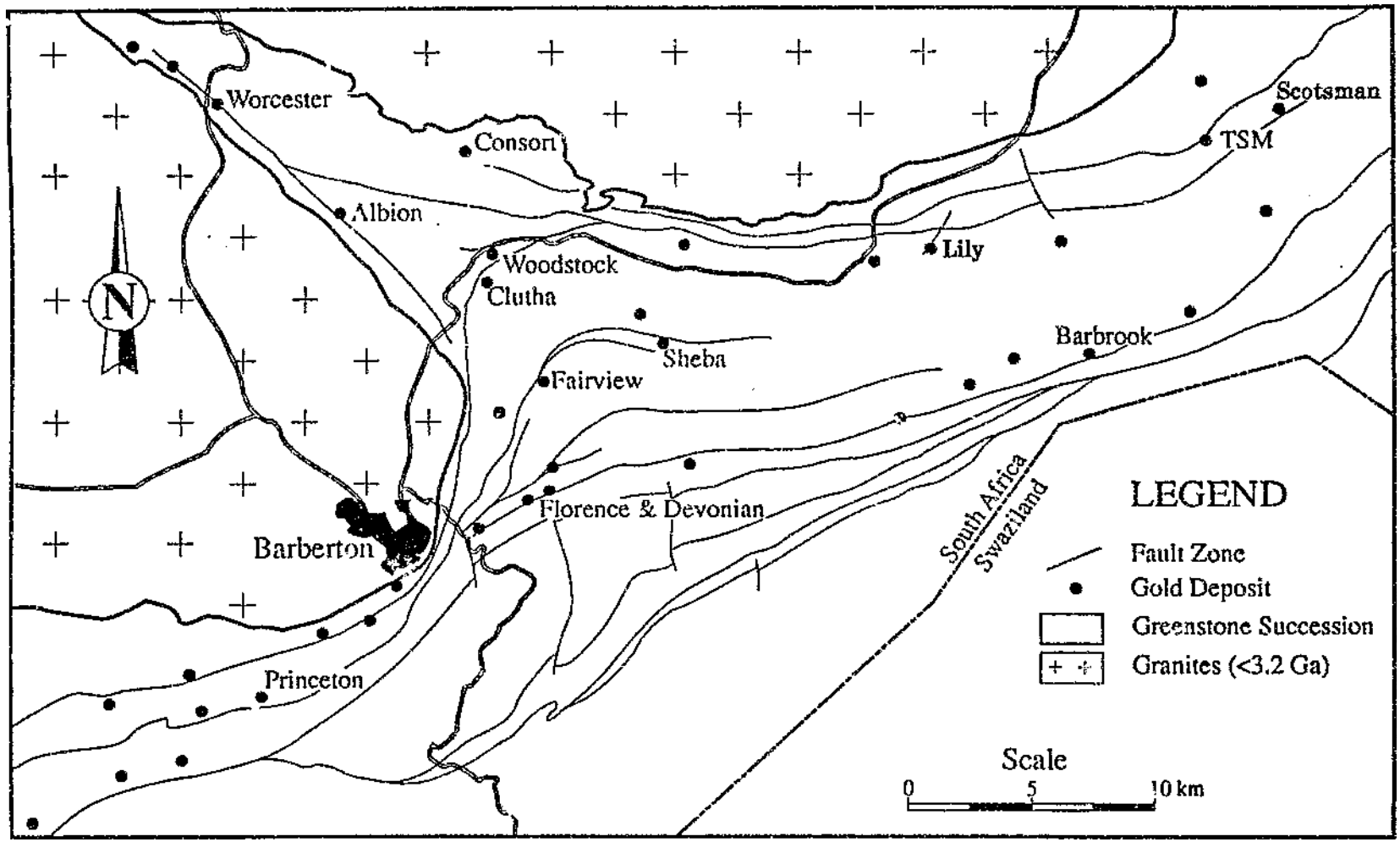


Fig 4 Northern Barberton Mountain Land Gold Deposits Distribution Map

(Source : Geological Survey Of South Africa, Sheet 2530 Barberton)

CHAPTER 3

DATA ACQUISITION AND PROJECT MANAGEMENT

3.1 SUMMARY

The airborne survey provided magnetic and radiometric coverage over a considerable portion of the Barberton greenstone belt.

A total of 10 300 line kilometres of total-field magnetic intensity and spectrometer count rate data was acquired over an 860km² asymmetrical shaped elongate block of roughly 55km x 20km dimensions (see figure 5).

Data acquisition was performed by Geodass (Pty) Ltd, under contract to Gencor Ltd, during the months of November and December 1990. The author was assigned by Gencor to control the project.

3.2 PROJECT MANAGEMENT

3.2.1 BUDGET CONSIDERATIONS

When budgeting for an airborne geophysical survey, a number of factors must be considered. The following is a breakdown of the major cost items that are encountered for a survey of this type.

* Aerial photography: Aerial photography acquisition and ortho-photo production costs.

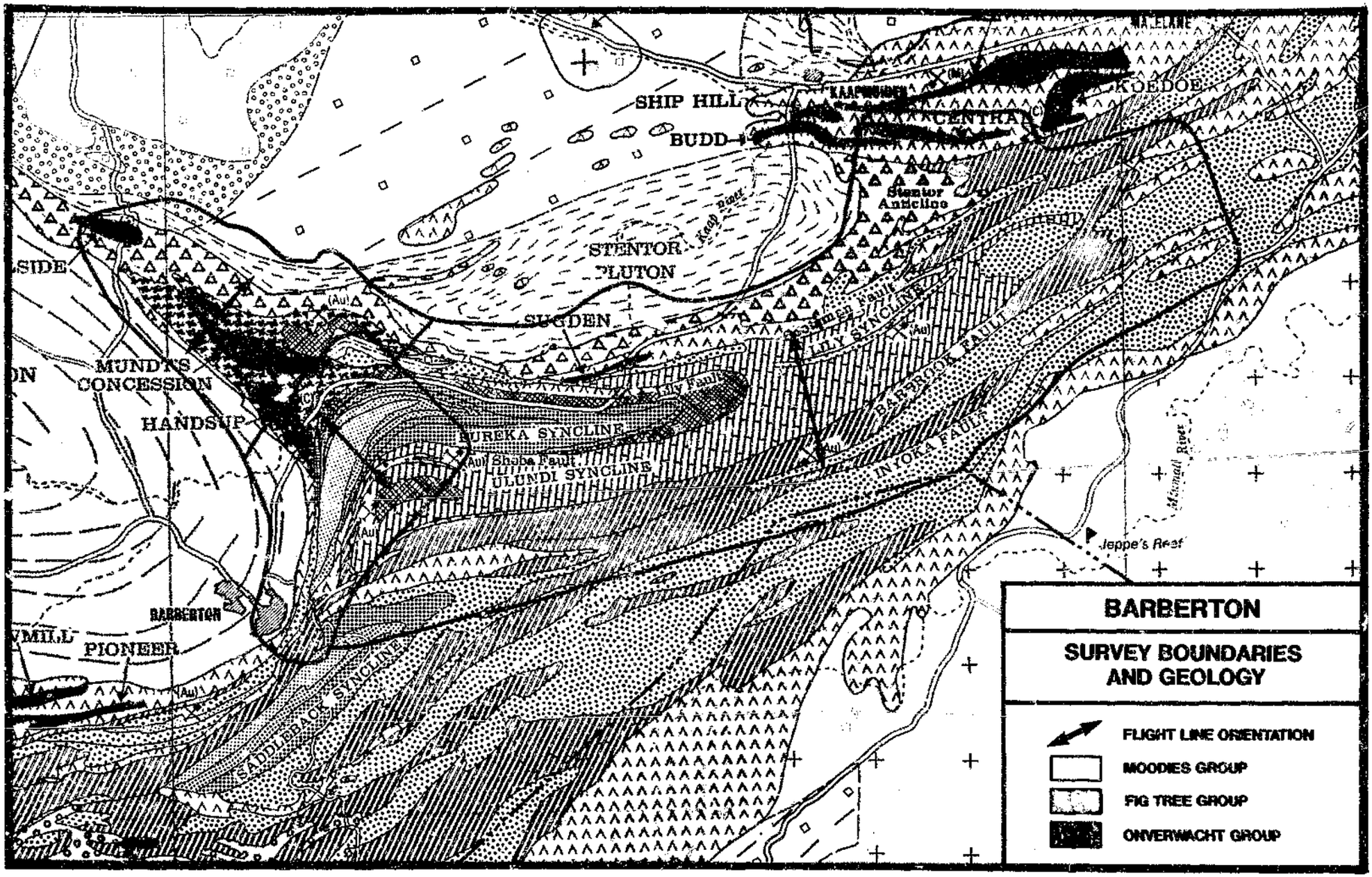

SHIP HILL
BUDD
KOEDOE
CENTRAL
Stentor Anticline
STENTOR
PLUTON
SUGDEN
MUNDTS CONCESSION
HANDSUP
EUREKA SYNCLINE
Shoba Fault
ULUNDI SYNCLINE
BARBERTON
PIONEER
SADDLEBACK SYNCLINE
BARBERTON
SURVEY BOUNDARIES AND GEOLOGY
FLIGHT LINE ORIENTATION
MOODIES GROUP
FIG TREE GROUP
ONVERWACHT GROUP

FIGURE 5

* Mobilisation and demobilisation charges: These cover the transportation of crew, aircraft and equipment to and from the survey area.

* Data acquisition: For this survey the acquisition cost encompassed aircraft hire, fuel charges and the acquisition and compilation of the geophysical data, as a single production based charge. Often clients will chose to negotiate a separate contract for the aircraft hire.

* Accommodation costs for the survey crew: Additional rooms were required for photographic processing and equipment storage.

* Standby charges: A fixed daily rate was applied when poor weather conditions prohibited flying time from exceeding a predefined minimum. This figure is a variable and was budgeted for on a contingency basis.

* Re-flight charges: When the magnetic diurnal exceeds a predefined limit, it becomes necessary to refly the affected lines. The cost of this additional flying was borne by the client.

* Processing charges: The client may require colour maps or filtered products to be produced by the contractor.

* The final major expense is for interpretation of the survey. This item is not paid for upfront with the rest of the survey and hence it often receives scant attention and may be left out of the budget. For this survey interpretation was not a cost item, since the author was already salaried by Gencor.

3.2.2 SURVEY DESIGN

The specifications used for flying and data acquisition during this survey were designed by the author. The cost effectiveness of a survey is dependant on careful planning and design, numerous factors have an effect on the quality of the final product. Discussions were held with geologists working in the area before survey parameters were set. The local geology, expected size and depth of geologic features of interest, depth of weathering and the aerial extent of significant interest were all considered. Parameters were chosen in order to optimally balance the requirement for maximum data resolution against the practical constraints dictated by instrumentation and aircraft dynamics. Budgetary constraints played an important role in parameter selection, however the emphasis was firmly on data quality. The 'garbage in - garbage out' principle is particularly applicable to a survey of this nature. No matter how comprehensive the approach to processing and modelling, results will always be constrained by the quality of the data.

3.2.2.1 FLIGHT LINES

Major variations in lithologic strike occur within the northern mountain land. Irrespective of flight line orientation, a significant proportion of any survey will be orientated at an oblique angle to strike. The effect of which, is a loss in the maximum resolving capacity of the survey, irrespective of line separation. To alleviate this difficulty as far as possible, it was decided to acquire the data in three separate surveys, with each survey having its flight lines orientated to optimise lithologic coupling. The spatial relationship of these surveys is shown in figure 5.

A slight overlap was included between adjoining surveys to enable the data to be merged into a single contiguous block during processing. This procedure increased the complexity of the survey, increasing acquisition costs by 0.5%. It was decided, however, that the benefits gained in data quality warranted the additional expenditure.

The first survey area termed the west block, covers the Jamestown schist belt at the extreme western end of the greenstone remnant. Flight line orientation was 037°, north-northeast.

The second, (central block) covers the Sheba Hills area and includes the Fairview and Sheba mines. Flight line orientation was 135°, southeast.

The third, (east block) lies over the eastern greenstone belt, including the Barbrook Line and Three Sisters Mine. Flight line orientation was 165°, south-southeast.

The Barberton mountain land is covered by regional government magnetics and is well mapped geologically. Hence additional magnetic coverage needed to be detailed if it was to significantly increase the knowledge base. This reasoning led to an extremely narrow flight line spacing of 100m being adopted, in order to provide data of a particularly high resolution.

Tie lines are flown principally to assist the contractor level the data. They were flown perpendicular to the survey lines at a spacing of 500m.

3.2.2.2 AIRCRAFT

The extremely rugged nature of the terrain encountered within the Barberton mountain land precluded the use of a fixed wing survey aircraft. In order to maintain within achievable limits, a constant terrain-sensor clearance, it was necessary to employ a helicopter as the survey platform. The aircraft used for the survey was a Bell 206B Jet Ranger III Helicopter, supplied by Helicopters S.A. C.C.

The mean helicopter velocity for the survey was 27.8m/s. This equates to a magnetic reading every 5m on the ground and a spectrometer reading every 28m. The maximum velocity that was recorded was 44m/s.

3.2.3 CONTRACT NEGOTIATION

Geophysical contractors were invited to tender for the airborne contract in June 1990. Contractual negotiations conducted by the author included: re-flight specifications, penalty clauses for deliverable delays and budgetary matters.

3.2.4 FIELD SUPERVISION

The author spent six weeks in the field with the contractor personnel in order to quality control the operation and provide logistical support. Daily procedures included: a review of the recovered flight path. Where the contract specifications for flight-path deviations were exceeded, the affected lines were assigned to be re-flown. The analogue flight records were checked for noise levels, data dropouts etc., again re-flights were assigned where necessary.

The magnitude of the diurnal variations was checked on the base-station magnetometer readout.

3.3 DATA ACQUISITION

The following sections review the data acquisition procedure in the field and the instrumentation that was employed.

3.3.1 FLYING HEIGHT

Aeromagnetic surveys are generally flown with a wide variety of terrain clearance, line spacing and sampling density. Reid (1980) showed that for a total field survey over three dimensional targets, the fraction of power aliased F_T is given by the equation:

$$F_T = \exp(-2\pi \frac{h}{\Delta x})$$

Where: h is the distance between sensor and magnetic source

Δx is the line spacing

The tolerable aliased power depends on the purpose of the survey. Where signal processing and interpolation such as gridding and contouring is required, as is the case for this survey, Reid believes the aliased power should not exceed 5%, giving a minimum value for $h/\Delta x$ of 0.5. Thus for a 100m line spaced survey, the sensor terrain clearance should be at least 50m. The presence of non-magnetic overburden will decrease this limit as will two dimensionality of the target lithologies.

Taking cognisance of Reid's guideline it was decided to fly the survey using a terrain clearance between the magnetic sensor and the ground of ±45m, which translates to the pilot attempting to maintain a flying height of ±75m. This figure is however not an absolute one as, in rugged topography the limitations of aircraft dynamics must be taken into account. As a helicopter climbs a hill, it's forward velocity decreases rapidly. For this survey it was found that below 40km/hr, the bird became unstable and began to drift around, resulting in positional inaccuracy and increased noise levels. At very low speeds, the bird would rotate about its central axis, causing it to decouple totally with the earth's magnetic field resulting in a subsequent loss of signal. Problems of this nature can be alleviated with the use of a more powerful helicopter, however this option is expensive and not usually viable. A more realistic solution used for this survey, was to adopt a less rigorous approach to the flying and to an extent drape it across the topography. This effectively speeds up survey progress and is thus an area that an unscrupulous contractor could take advantage of. An acceptable trade off must be negotiated between the client and contractor for flying at a realistic terrain clearance, while at the same time maintaining an acceptable quality of data. In Barberton, terrain clearances of up to 150m were recorded over short distances, this is not ideal but clearly preferable to losing data completely as the helicopter struggles up a steep hill.

Data quality is also very dependant on the ability of the pilot. A good pilot experienced in maintaining a long-line can make a huge difference to the final product.

A Sperry AA-200 radar altimeter was mounted in the cabin of the helicopter to provide the pilot with a continuous and accurate measure of the terrain clearance. The altimeter output was recorded digitally for data processing and as an analogue readout for in-field monitoring purposes. Recording resolution was 0.05m.

3.3.2 NAVIGATION

The extreme nature of the terrain encountered in the Barberton mountain land precluded the use of the now commonly used radio-transponder type navigation system. The communication frequencies used for radio navigation require a line of sight to be maintained continuously between helicopter and radio beacons for the system to operate. When beacons are hidden by topographic features, positional information is lost.

Navigation for this survey used the traditional visual method. In July 1990, AOC Ltd was contracted to acquire low level aerial photography over the proposed survey area. This photography was then used to construct a 1:10 000 scale ortho-photograph. A copy of the ortho-photo was used in the helicopter for navigation during the survey. Whilst the aircraft was in flight, a downward looking Geocam 35mm tracking camera, monitored the flight path in continuous frame mode at 1 second intervals. A backup video camera was also used to record the flight-path.

3.3.3 FLIGHT PATH RECOVERY

At the end of each day's flying, the 35mm strip photography was developed.

The data recovery technician spent every night determining accurate positional fixes for the aircraft at regular intervals along each of the flight traverses. From this information, an interpolated flight path was constructed and transferred to the original 1:10000 scale ortho-photograph. Reference markers termed 'fiducials' are recorded on the magnetometer, spectrometer, altimeter and film records.

The points from the flight path that are picked and accurately located on the ortho-photos are termed 'located fiducials'. The maximum distance between located fiducials for this survey was 300m.

3.3.4 LOCATIONAL ERRORS

The human component of this process makes it difficult to estimate locational errors. To establish error limits, the author selected 7 high frequency anomalies from the processed magnetic profiles. Magnetic traverses using a Geometrics 856 proton procession magnetometer were then conducted on the ground beneath the airborne anomalies. Comparison of anomaly peaks gave a mean location error of 65m with a standard deviation of 22m. The overall error limits may be slightly larger because topographic effects can cause peak positions to shift as a function of height.

3.3.5 INSTRUMENTATION

During each survey flight, all digital outputs from the geophysical instrumentation were converted to analogue traces and output to a GR-33 X-Y plotter in real-time. This allowed verification of the system's operation.

3.3.5.1 MAGNETOMETER

The magnetic sensor was mounted in a towed 'bird', which is cylindrical in shape and aerodynamically designed to provide a stable platform over a wide range of aircraft velocity. The bird is suspended 30m beneath the helicopter in order to isolate the sensor from the magnetic field generated by the aircraft and its turbine. This arrangement provides for an additional benefit which is gained through sampling the magnetic field closer to the Earth's surface.

The magnetometer used for the survey was an hand aligned Scintrex VIW 2327 H-8, strapdown, split- beam caesium vapour unit. The Lamour Frequency was counted directly into the acquisition unit. This is the frequency at which the caesium atom electrons precess about the axis of the applied magnetic field. It is proportional to the strength of the Earth's magnetic field and is measured optically with a photo-diode (Telford, *et al.*, 1976). The magnetic field is sampled at 0.17s intervals at a resolution of 0.01nT. This accuracy however, cannot be expected during a field survey. The main culprit is the survey platform; noise levels are increased significantly by the instability inherent in a 'bird' installation. The fourth difference operator of the magnetic field was output to the X-Y plotter, thus allowing noise level estimates to be made (Hood, *et al.*, 1979). The total measurable noise envelope for the survey was found to be in the order of 1nT.

During each survey flight the earth's external diurnal magnetic field was constantly monitored for fluctuations. For this purpose a Geometrics G856 proton precession magnetometer was located at the Barberton airstrip for the duration of the survey.

The magnetic field was sampled at 30 second intervals to an accuracy of 0.1nT. The survey contract specified a maximum diurnal drift of 20nT in any given 20 minute interval. If this limit was exceeded affected lines would require re-flying. No diurnal variation falling outside the specification limit was observed, for the entire duration of the survey.

3.3.5.2 SPECTROMETER

A Geometrics GR800B, multi-channel gamma-ray spectrometer was installed in the helicopter for the duration of the airborne survey. This spectrometer digitally recorded 256 channels of radiometric data, containing information on the near surface concentrations of Potassium, Thorium and Uranium in the survey area. The 256 channels were grouped into 4 windows arranged as follows:

Potassium, ^{40}K	-	1.37 to 1.57 MeV, (1.46MeV peak)
Uranium, ^{214}Bi	-	1.66 to 1.86 MeV, (1.76MeV peak)
Thorium, ^{208}Tl	-	2.41 to 2.81 MeV, (2.62MeV peak)
Total Count	-	0.41 to 2.81 MeV

A reading integration time of one second was used, giving an average of one reading every 28m. Recording resolution was 1cps. Spectrum stabilisation was based on the 662 KeV peak from Caesium sources planted on the crystals.

The crystal pack was a DET-1024, containing 1024in^3 of Thallium activated Sodium Iodide (NaI) crystals, located horizontally in the belly of the helicopter. The crystals were maintained at a constant operating temperature for the duration of the survey. The thermal shock generated by sudden cooling can easily crack the NaI detector crystals, in addition temperature variations can produce calibration changes.

3.4 DATA COMPILATION

Upon completion of the field work the geophysical data were transported to the Johannesburg office of the contractor for compilation. This begins with the located fiducials from the flight path being digitised, plotted and a velocity report check generated. Errors detected at this stage are manually corrected by referring to the ortho-photography and video tape and locating additional fiducials in the problematic area. When the contractor considers the flight path is satisfactory it is loaded into a data base.

The geophysical data are referenced spatially to the flight path by using the located fiducials and added to the data base.

3.4.1 MAGNETICS

The following operational sequence was undertaken on the magnetic data.

* Diurnal correction: The magnetic diurnal was removed by subtracting the digitally recorded base station monitor readings from the field data. An automated lag correction factor was then applied to the data.

* Levelling: The magnetic data were levelled by using the tie-line data to minimise magnetic field differences where flight lines were intersected. Poor levelling results in linear steps along single lines and herringboning, an effect resulting from data on alternating lines being assigned a too high or too low a datum and giving the appearance of a herringbone on contour maps.

* The data were then gridded for verification purposes using an akima spline technique.

3.4.2 RADIOMETRICS

The following operational sequence was undertaken on the spectrometer data.

* Compton Stripping: In order to achieve a quantitative result, spectrometer data must be corrected for Compton scattering of gamma rays. Compton scattering is the process whereby high energy gamma rays interact with the earth, air, aircraft and detector. In so doing they loose energy and appear in the lower regions of the energy spectrum giving rise to the Compton continuum. The correction factors applied are termed Compton correction coefficients or stripping ratios. Their value is defined by the size, geometry and window width of the detector and the geometrical relationship between the detector and the radiation source. The Compton stripping factors used were:

α	-	0.271 (Th into U)
β	-	0.405 (Th into K)
γ	-	0.676 (U into K)
a	-	0.050 (U into Th)
b	-	0.010 (K into U)
g	-	0.001 (K into U)

Where alpha α, β and γ are the forward stripping coefficients and a, b and g are the backward stripping coefficients. These coefficients were determined in part from measurements on pure samples of K, U and Th, recorded at the beginning of each flight.

* Background Radiation: Not all gamma radiations detected in an aircraft are emmited from the ground. Background radiations must be subtracted, these originate from three sources, these are:

  - Aircraft corrections: The background effects due to structural components of the aircraft and the instrumentation package were measured, before, during and after the survey. A correction factor was determined and applied to the data.

  - Radon corrections: Correction for atmospheric radon was necessary. The uranium daughter ^{226}Ra in the near surface soils constantly emits a flux of radon to the atmosphere. The radon content of the air is a source of background gamma radiation noise which must be removed from the data.

  - Cosmic ray corrections: An additional source of background noise is cosmic rays interactions with components of the earth's atmosphere, these produce gamma rays that stimulate the detector.

To estimate background radiation a shielded crystal (termed a 2pi crystal) is directed upward to receive counts from the atmosphere. The ^{214}Bi count from the 2pi is subtracted from the unshielded crystals to give a true reflection of the ^{214}Bi emissions from the ground.

Budgetary constraints necessitated the suspension of work on the spectrometry data at this stage of the processing sequence. For this study, only a qualitative interpretation of the total count data has been attempted.

Two major correction factors are still required before the data can be used to obtain isotopic abundances:

1. Altitude correction: The amount of absorbtion suffered by gamma rays in the air depends on the distance travelled, the density of the air and the energy of the gamma ray, i.e. ^{40}K 1.46MeV rays are attenuated more rapidly than ^{208}Tl 2.615MeV rays.

   Where extreme topographic variations are seen Compton scattering interactions in the atmosphere result in a buildup of photons in the lower energy channels, which are not removed by the normal Compton corrections. To account for these effects an altitude absorptional coefficient should be applied to the data.

   This coefficient is separately determined for each energy channel and is established by flying a test profile at a series of altitudes that cover the observed range of the survey.

2. Calibration: The stripped, background corrected and altitude corrected counts then need to be converted to isotopic abundances by calibration of the system over sources of known radioelement concentrations. This is usually achieved by flying over a calibration test strip (roughly 500m x 2000m), where the radioelement concentrations are uniform and have been measured on the ground. No such facility exists, however, in Southern Africa and all surveys are limited to the production of stripped counts only.

CHAPTER 4

DATA PROCESSING

The author proc ssed the geophysical survey using a 50MHz 486DX Personal Computer. A Canadian computer package 'Geosoft' was the principle software used to signal- and 'nage-process the data. Final plots were generated on an Hewlett Packard Design Jet 650c printer.

4.1 MAGNETIC DATA

Magnetic data by their nature are very 'broad band' in terms of wavelength. A single measurement includes the effect due to all physical sources. The resolution of different sources is dependant on the noise levels of the measuring system and the ability to resolve overlapping signals.

All anomalies including those from single isolated sources consist of a spectrum of frequencies. Small, shallow, short wavelength anomalies comprise a higher band of frequencies than broad deep-sourced anomalies which are dominated by longer wavelengths. Each has a characteristic spectrum which can often overlap. Filtering is a process of removing a specified range of frequencies from a data set, for example, high frequency noise, or low frequency regional components. Usually applied to airborne data sets, digital filters enhance individual or multiple anomalies of similar frequency characteristics.

The following sections describe the processing sequence for the magnetic data:

4.1.1 DATA VERIFICATION

The first step entailed preliminary processing of the data to verify the contractor's compilation and levelling work.

Stacked profiles were constructed for each of the survey blocks and a bi-directional gridding algorithm using an akima spline was used to rapidly interpolate both the levelled and un-levelled data into a gridded format. The resultant plots were used to verify:-

Herringbone effects: The alternate cyclical pattern of contour lines produced by inadequate flight line location, poor aircraft or heading compensation, or improper levelling.

Missing lines: Lines that appear in the un-levelled data but are removed during the levelling process for a variety of reasons.

Noise spikes and areas of poor data along lines.

4.1.2 NON-LINEAR FILTER

A type of non-linear filter is a low-pass filter that operates in the space domain on line based data. A width (wavelength) is specified. If an anomaly in the data has a half wavelength shorter than the specified width, the feature is removed. All of the Barberton data were passed through this filter to remove noise spikes. The advantage of a non-linear filter is that rather than simply leaving a 'hole' where the noise spike is removed the hole is 'filled in' or approximated by interpolated values based on the surrounding valid data.

4.1.3 GRIDDING

When analysing two dimensional data, it is useful to represent the data discretely at points located equally far apart at the nodes of a grid. Data in this format are suitable for a number of two dimensional processes such as computer contouring, filtering and image processing.

The values at the nodes of the grid could be determined by taking readings at the node locations, however in practice this is seldom convenient. For an airborne survey of this nature, the data are collected at a relatively high sample density along more widely separated parallel lines. A minimum curvature technique was applied to create a gridded dataset from the edited flight line data.

4.1.3.1 MINIMUM CURVATURE GRIDDING

A random gridding algorithm 'RANGRID' was used to fit a two-dimensional minimum curvature surface to the data points contained in the XYZ file. The program uses the method described by Briggs (1974). Values are first estimated at the nodes of a course grid whose cells are usually eight times the size of the final grid. The node values are based on the inverse-distance average of the actual data within a specified search radius. An iterative method is then employed to adjust the grid to fit the actual data points nearest the course grid nodes. Once an acceptable fit is achieved, the coarse cell size is halved and the same process repeated, using the coarse grid as the starting surface. This process is repeated until the final grid cell size is generated.

During the gridding process, a de-sampling factor is applied to the data. This factor effectively acts as a 'box car' low-pass filter by means of averaging all X, Y points into the nearest cell defined by this factor. In this case a value of one grid cell was used, this required no prefiltering other than de-aliasing at the size of the grid cell.

Each of the three survey blocks was gridded using the following parameters:

Grid Cell Size	:	50m x 50m
Projection	:	Gaussian Conformable
Spheroid	:	Clark 1880
Reference Longitude	:	31° East
Reference Latitude	:	0° South

4.1.4 SPECTRAL ANALYSIS

Spectral analysis is usually the initial step in analysing magnetic data. It's main purpose is to isolate the dominant periodic components, which are then correlated with the major geologic units. These significant frequencies can similarly be separated from the high frequency noise component of the data; (Gunn, 1975).

Spectral analysis is conducted in the frequency domain and may be defined as the decomposition of a continuous signal into its harmonic constituents. The data are first passed through a Fast Fourier Transform (FFT) to calculate the complex spectrum coefficients of the data. A two dimensional (2D) power spectrum is calculated by taking the square of the modulus ie.

$$power = (real\ co\text{-}efficient)^2 + (imaginary\ co\text{-}efficient)^2$$

This is then normalised, converted to natural logarithms and radially averaged to produce a one-dimensional spectrum termed a '1D Radially Averaged Power Spectrum'. Due to its logarithmic nature, the spectrum displays linear components (Spector, 1968). These represent both magnetic signal contributions of individual assemblages of source bodies, plus noise from the combination of acquisition and processing steps. The individual components of the power spectrum can be separated out for interpretation.

The shortest spatial wavelength λ_N which may be correctly identified by a regular line of samples Δx is termed the Nyquist wavelength given by the equation:

$$\lambda_N = 2\,\Delta x$$

Any wavelength shorter than λ_N is aliased into a wavelength longer than λ_N, (Blackman and Tukey, 1959). Thus for a grid with a 50m cell size the Nyquist frequency is 100m.

Figure 6 is the power spectrum corresponding to the east block. Three linear components have been resolved representing source 'ensembles'. The spectrum can be used to determine the statistical depth to the top of the sources using the relationship:

$$\log E(r) = 4\pi h r$$

Depth is determined by measuring the slope of the power spectrum and dividing by 4π. The east block sources cluster at: 100m, 150m and 350m, the central block at: 100m, 180m and 350m, the west block at: 100m and 250m.

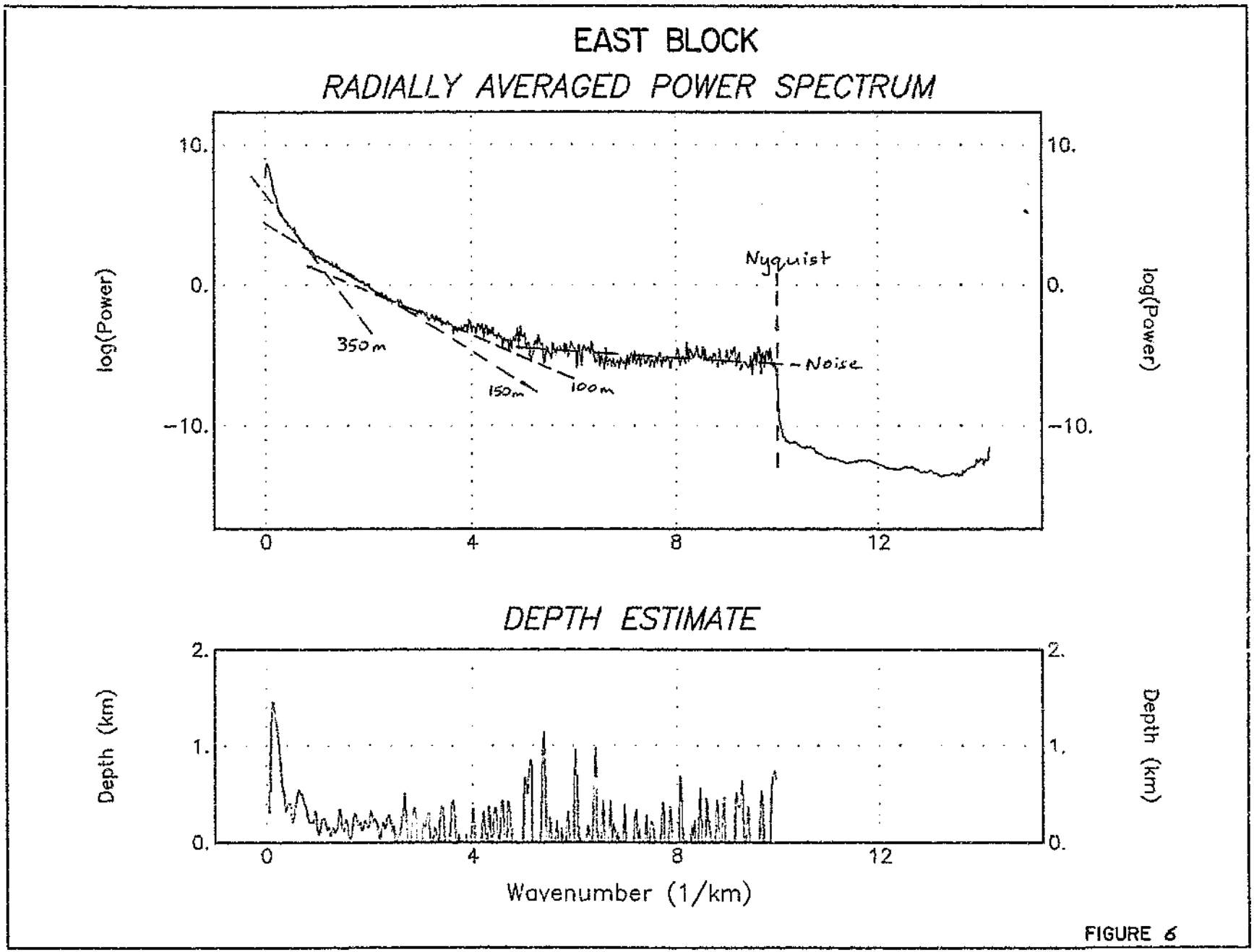

EAST BLOCK
RADIALLY AVERAGED POWER SPECTRUM
log(Power)
10.
0.
-10.
350m
150m
100m
Nyquist
Noise
0
4
8
12
DEPTH ESTIMATE
Depth (km)
2.
1.
0.
Wavenumber (1/km)

FIGURE 6

A power spectrum is useful to determine appropriate filter coefficients. A filter operator should be designed carefully to match the character of the anomalous data. Too much arbitrary smoothing of the data can remove anomalies, too little can leave unwanted noise.

4.1.5 LOW PASS FILTER

The noise identified in the spectral analysis was removed from the gridded data by the use of a low pass filter. A filter employing a cosine roll-off of degree two was selected. This filter has a smooth shape which prevents it from altering the energy spectrum below the beginning of the roll off. Through this approach, ringing (otherwise known as Gibb's phenomena) in the resultant filtered grid is greatly reduced. The east and west blocks had start and end points of the filter set to 0.00282 and 0.006 cycles/metre respectively, while those for the central block was set to 0.0029 and 0.009 cycles/metre.

4.1.6 DECORRUGATION

Flight line noise can be removed from a magnetic grid by applying the following decorrugation operator in the frequency domain, (Spector and Grant, 1970).

$$F(u,v) = [\cos^n(a-\pi+\tfrac{1}{2})]$$

where: u and v are wave numbers.
a is the direction of the filter.
n is the degree of the cosine function.

This is known as a directional cosine filter and is designed to remove sub-parallel directional features from a grid. The rejection notch can be narrowed or widened by setting the degree of the cosine function, thus enabling highly directional features such as line noise to be isolated. The resultant grid is then subtracted from the original to produce a decorrugated grid which is the original data minus line noise.

It should be noted that any geological signal parallel to the filter direction will also be removed. The effect of this was minimised, however, due to the choice of flight-line direction with respect to geological strike.

4.1.7 MERGING

After low pass filtering and decorrugation, the three survey blocks were merged together to form a single large contiguous grid. Areas of overlap between adjoining grids were averaged. All of the following additional processing steps were performed on the merged grid.

4.1.8 IGRF REMOVAL

Total field magnetic data contains long wavelength components derived from the earths main field and deep crustal sources. For a high resolution survey of small aerial extent, this regional magnetic information is superfluous and is normally removed after the data are gridded. A PC based program sourced from the United States Geological Survey (Cordell, *et al.*, 1992) was used to calculate the International Geomagnetic Reference Field (IGRF) over the Barberton mountain land. The results were output in gridded format, (see figure 7). The IGRF grid was subtracted from the merged total field magnetic grid to produce the residual magnetic field. This residual field is often termed an anomaly map.

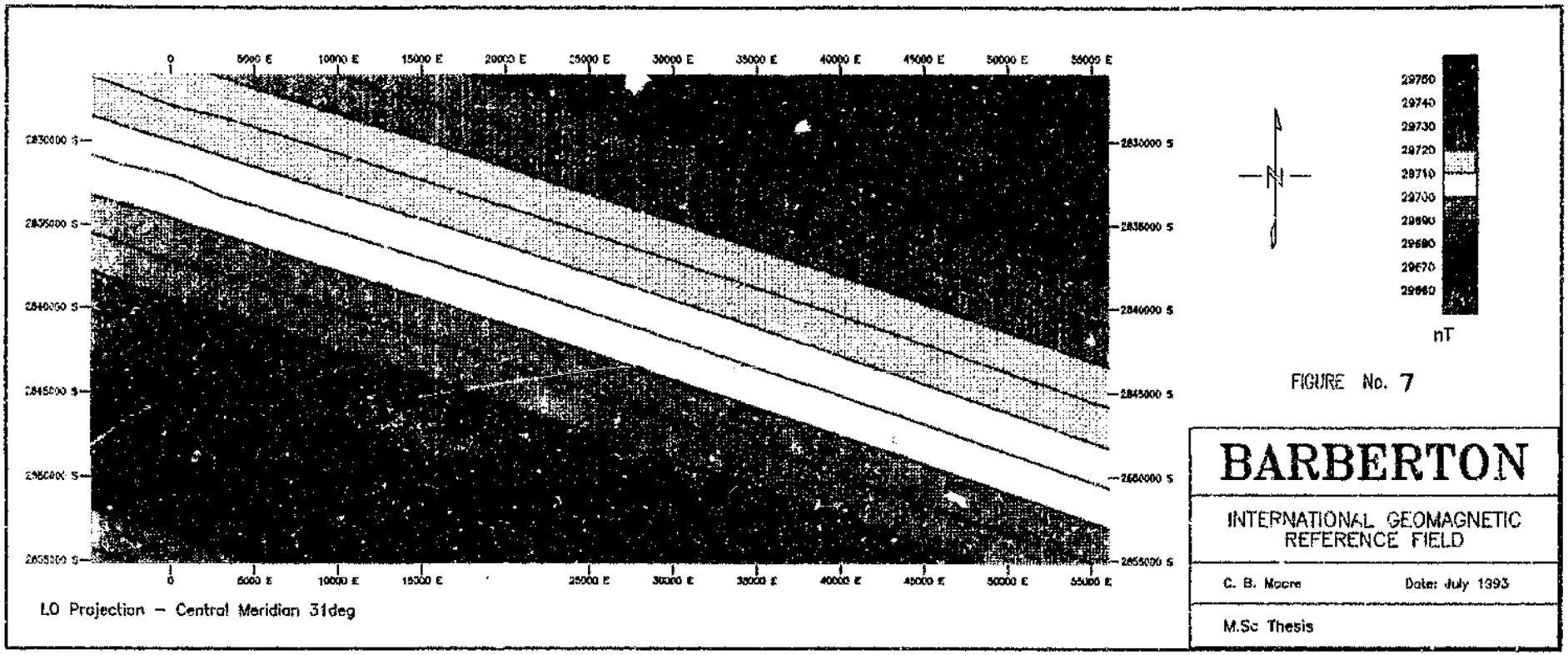


FIGURE No. 7

BARBERTON

INTERNATIONAL GEOMAGNETIC REFERENCE FIELD

C. B. Moore Date: July 1993

M.Sc Thesis

4.1.9 CONTOURING

Contour maps are commonly used to display data collected in plan over a given map area. A characteristic of geophysical data is that the information commonly has a very large dynamic range. Contouring is a useful method of presenting such data as it is able to show detail in both high and low relief areas, as well as clearly indicate the direction of relief in magnetically active areas.

The residual magnetic field is presented as a coloured contour map in plan no. 2, and as a shaded relief map in plan no. 3. Colours were added to enhance perception of trends and features. An image-processing technique termed histogram stretching was used to customise the colour scale by varying the colour intervals. The rationale being to de-emphasise the high and low extreme values whilst accentuating intermediate values to emphasize small changes and trends. Contours were also added to the relief map (plan no. 3) to further accentuate subtleties in the data.

4.1.10 REDUCTION-TO-POLE

If no remanence is present the total magnetic field is directly proportional to the magnitude of the Earth's inducing field. In the survey area, the inducing field acts at an average inclination of 60° towards the north and declination of 14° west. This means each anomaly is dipolar with the positive lobe displaced to the north of its source.

In order to minimise this dipolar distortion, a process termed reduction-to-pole (RTP) can be performed.

Reduction-to-pole re-creates the magnetic field of a body as it would appear at the magnetic pole, where the inducing field is vertical. RTP provides better correlation between individual anomalies and their sources by re-locating anomalies directly over their causative bodies. Visual recognition is also improved since total field dipoles are usually reduced to 'single-pole' anomalies.

The RTP operation is performed in the frequency domain. The following operator is used, Gunn (1975)

$$R(u,v)=\frac{\sqrt{(u^2+v^2)}}{D1} * \frac{\sqrt{(u^2+v^2)}}{D2}$$

Where: *D1* is the constant for the Earth's inducing field.
D2 is the constant for the magnetisation of the body.
u and v are wave numbers.

Since reduction-to-pole enhances high frequency noise at the expense of true signal, the data are normally low-pass filtered, at the time of the filter's application.

The form of an individual anomaly from a given source body depends on several factors:

1. The direction of the Earth's inducing field.
2. The orientation of the body.
3. The orientation of the body with respect to the aeromagnetic flight line.
4. The geometry of the body.
5. The remanent magnetisation vectors of the body.

RTP will compensate for these factors, minimising the distortion and placing anomalies over their causative bodies, with the exception of the last point mentioned (5). Remanent magnetism effects inherent in the total field data will still be present in the RTP results, unless the factor *D2* above is known.

No measurements of remanent magnetisation are available for the Barberton greenstone belt. Detailed palaeomagnetic work is required to determine the remanent magnetisation vectors for a variety of both lithologies and locations within the belt. In chapter 5, it will be shown that remanent magnetisation does indeed play a dominant role in many of the observed magnetic anomalies at Barberton. With no way to quantitatively assess remanence, it was decided that RTP would only serve to confuse the picture and it was not attempted.

4.1.11 FIRST VERTICAL DERIVATIVE

The first vertical derivative (FVD) is obtained by applying the following operator in the frequency domain, Gunn (1975).

$$F(u,v)=2\pi\sqrt{(u^2+v^2)}$$

Where: u and v are wave numbers.

Derivative filters sharpen magnetic gradients and therefore enhance the higher frequency components of anomalies associated with small shallow sources whilst reducing the effect of deep seated structures. They are especially useful for delineating faults and subtle structures. In addition, geologic contacts can be defined since the zero contour approximately defines vertical to steep magnetic boundaries.

The disadvantage of a derivative filter is that it is particularly responsive to noisy data, accentuating existing problems. For this reason the Barberton data were subjected to a further low pass filter in conjunction with the FVD filter.

Plan no. 4, illustrates the first vertical derivative for the Barberton data. As with the residual field map a customised colour scale was developed employing variable sized colour intervals for accentuating subtleties within the data.

4.1.12 UPWARD CONTINUATION

Upward Continuation filtering is performed on magnetic data to obtain a more 'regional' perspective. It is used to remove or minimise the effects of shallow sources and noise, and allows deep seated structures to be recognised more easily. For this study the magnetic residuals were of primary interest, consequently, upward continuation was of limited use. Since the long wavelength features are evident in the total field data, an upward continued plot is not included.

4.1.13 HANNING FILTER

A Hanning filter operates in the space domain, applying a 9-point smoothing filter to a grid. The filter has a minimal effect on signal content, it was used to remove high-frequency noise introduced during frequency domain processing. A further application is space domain regional-residual separation. By subtracting the filtered grid from the original, a residual is produced proportional to the curvature of the original grid. This is termed a curvature grid where the zero values indicate inflection points, it was used to locate the lateral bounds of anomalies.

4.1.14 SHADED RELIEF

The application of shading to gridded data has become a useful technique for graphically displaying two-dimensional data. A directional horizontal derivative is calculated and then overlaid onto the original grid to produce a shaded relief map. This produces a pseudo sun-shading effect that to the human eye gives an image a three-dimensional appearance. Shaded relief maps are a very effective presentation for highlighting subtle textural and linear features that are otherwise difficult to resolve. A primary application is structural mapping.

Maps shaded with a variety of apparent sun-angle inclinations and declinations were produced to aid the interpretation. Two optimal directions were selected for this study, the residual magnetic field shaded with inclination 45°, declination 0°, (plan no. 3) and the magnetic first vertical derivative with inclination 45°, declination 0°, (plan no. 4).

4.1.15 EULER DECONVOLUTION

A common procedure for magnetic data interpretation is to determine the depth and location of geologic units or structures that produce an observed anomaly.

It has been shown that simple magnetic models conform to Euler's homogeneity equation, which relates the magnetic field and its gradient components to the location of the source, (Thompson, 1982). The degree of homogeneity, N, can be expressed as a structural index (SI). The SI is a measure of the rate of fall-off with respect to distance of the potential field, ie. an inverse power of the distance.

A magnetic point dipole conforms for N=3, a magnetic pole for N=2, magnetic dyke for N=1 and a contact will yield an index of 0.

An advantage of Euler's equation is that no particular geologic model is assumed. Thus it can be applied and interpreted even when the geological geometry is not known and cannot be properly represented by an identifiable model (e.g. a prism). A further advantage of particular relevance to this study is that the equation is insensitive to magnetic inclination, declination and remanence, since these become part of the constant in the anomaly function of a given model.

The PC program 'Gridepth' was used to compute Euler solutions. The Euler equation is solved simultaneously for four unknowns - the location coordinates x, y and z and the regional value of the magnetic field, 'B'. The equation is solved simultaneously for each grid position within a windowed sub-grid of 10 by 10 grid cells by a least squares method. The window is moved along each grid row; depth solutions are output to an XYZ ascii file.

For the Barberton data a SI of 1 was found to produce results that best agreed with mapped geology, signifying a strong two-dimensionality of the geology. In several instances solutions were verified by observation in the field. Plan no. 5 is a symbol plot of the Euler solutions for SI=1. A circle is centred on each model result, the diameter of which is representative of the depth to the top of the model.

4.2 RADIOMETRIC DATA

The processing sequence adopted for the total-count radiometric data closely parallels that of the magnetic data, thus only a summary will be given.

The data were verified using preliminary grids and stacked profiles.

Minimum curvature gridding was used to grid the data with a cell size of 50m.

Due to the unlevelled nature of the radiometric data, noise levels were extremely high in the upper frequencies. A low-pass smoothing filter was used to remove the noise. An unavoidable consequence of this being the loss of high frequency signal.

The data were contoured using linear contour intervals. A colour contour plot (plan no. 7) was constructed using an equal area colour distribution.

CHAPTER 5

INTERPRETATION

It is suggested for the following discussion that whilst the interpretation maps are studied, reference be made to the image processed geophysical data plans. To facilitate comparisons between datasets, the interpretation maps are included both as coloured paper prints and transparent overlays, all maps are presented at a scale of 1:100 000. Plan no. 6 is an interpretation of the magnetic data, whilst plan no. 8 is a qualitative interpretation of the total-count radiometric data. Plan no. 9 is the culmination of this dissertation, it is a synthesis combining the interpretation of the magnetic and radiometric data with the previously mapped geology, to produce an improved regional geological map.

5.1 MAGNETICS

The inherent ambiguity of magnetic data can be reduced by an interpreter to an acceptable level, through the use of appropriate geological constraints and moderated by knowledge of the 'noise' effects produced by terrain effects and variable flight elevations. It should be noted however that a geophysical interpretation of this nature is a subjective exercise.

The total magnetic field was recorded for the Barberton survey. The total field is composed of the Earth's main inducing field, and additive to this, the effect of much smaller magnetic fields produced by crustal rocks.

The 'lithologic' fields are derived from two sources :

a) remanent magnetism, and
b) induced magnetism,

the latter being proportional to the Earth's inducing field.

The residual field magnetic maps (Plan no. 2 & 3) essentially reflect the distribution of magnetic material within the survey area. In nature, the most dominant magnetic mineral is magnetite (Fe_3O_4), other common magnetic minerals include those belonging to the titanomagnetite and haematite-ilmenite solid solution series. The susceptibility of magnetite is proportional to the intensity of the magnetising field and depends on the chemical composition of the magnetite and its grain size. Lithologies containing even minor quantities will produce characteristic magnetic signatures. Generally, mafic igneous rocks produce strong magnetic responses, whilst sedimentary sequences often depleted in magnetite elicit more subtle responses. There are many geological factors that influence magnetic properties, directly or indirectly, including: lithology, depositional environment, tectonic setting, geochemical affinities, hydrothermal alteration, metamorphic grade, structure and rock age. For this reason there is usually a broad correlation between lithology and susceptibility. Altered or mineralised lithologies may host pyrrhotite (FeS) which can also contribute to the lithological magnetic field. The presence of pyrrhotite is usually significant from a mineral exploration viewpoint.

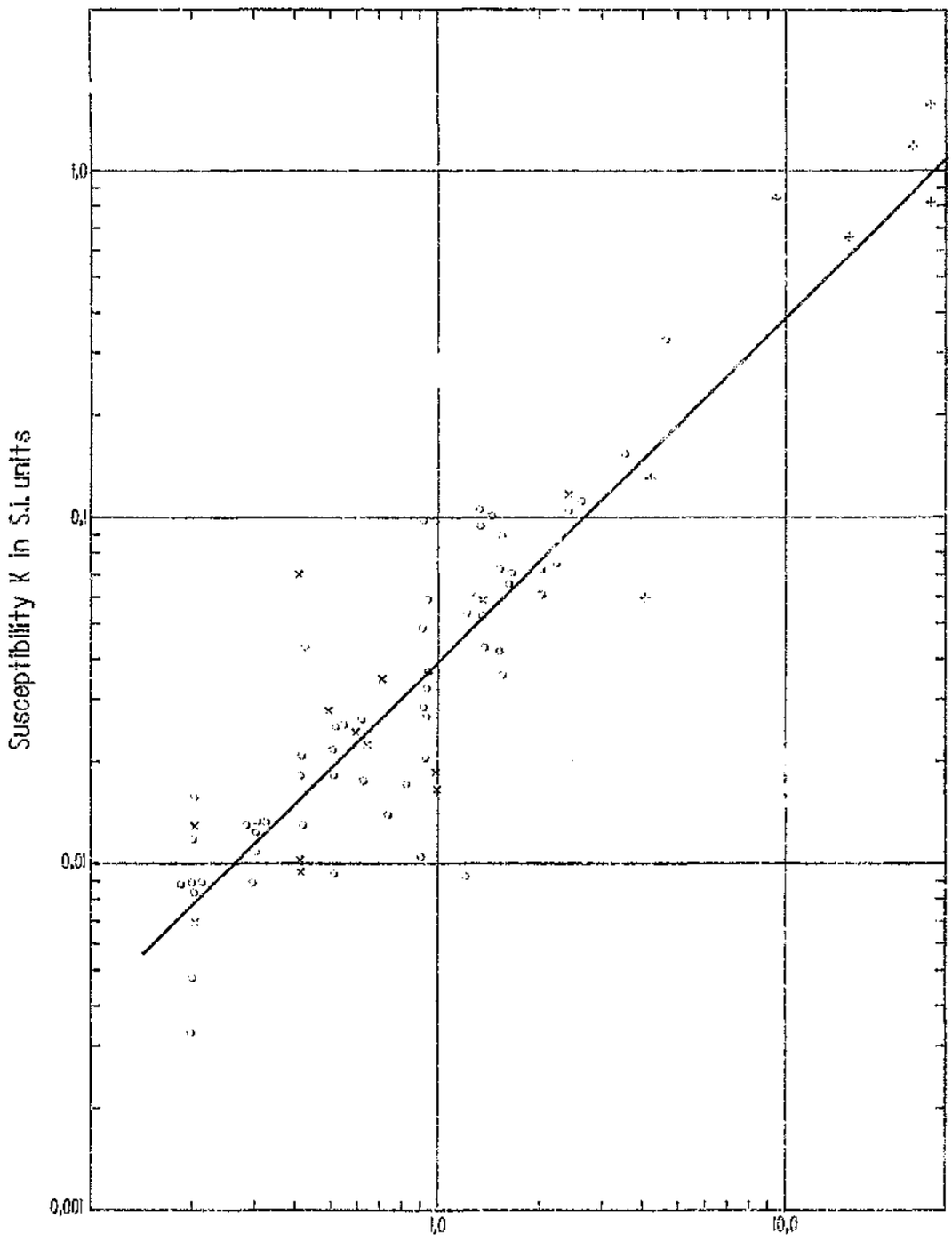
5.1.1 SUSCEPTIBILITY MEASUREMENTS

Several dozen hand specimens and sections of drill core, broadly representative of a variety of Barberton lithologies were collected in the mountain land. Susceptibility measurements were recorded using a hand held Scintrex K2 susceptibility meter. The results (tabulated in table 5.1), were used to constrain the magnetic modelling.

SAMPLE DESCRIPTION	MEAN K (SI)	MEAN K (cgs emu)	NO. OF SAMPLES
FELSIC VOLCANIC INTRUSIVE	0.040	0.0032	20
DOLERITE DYKE	0.050	0.004	20
MOODIES MAGNETIC SHALE	0.140	0.0111	15
MOODIES QUARTZITE	0.00002	0.0000016	15
MOODIES CONGLOMERATE	0.00006	0.0000048	20
FIG TREE SCHIST	0.00003	0.0000024	20
FIG TREE SHALE	0.00008	0.0000064	20

TABLE 5.1 MAGNETIC SUSCEPTIBILITY (K) MEASUREMENTS BARBERTON HAND SPECIMENS

A rough correlation has been shown to exist between susceptibility and magnetite content (Mooney and Bleifuss, 1953). The graph in figure 8, allows a volume estimate of magnetite to be made when the susceptibility is known. For example several dolerite dykes were sampled returning an average susceptibility of 0.05 SI units, this equates to 1.1% magnetite.



RELATIONSHIP OF SUSCEPTIBILITY TO MAGNETITE CONTENT

(Mooney and Bleifus 1953)

FIGURE 8

5.1.2 MODELLING OF MAGNETIC RESPONSES

For modelling of magnetic anomalies, 'MAGMOD', an inversion program allowing 2½D modelling was used. The program utilises an iterative technique based upon the algorithm of Marquardt (1963) as described by Johnson (1969). Parameters of an inductively magnetised body of simple geometry are calculated, these are iteratively adjusted to give a 'best fit' between the observed data and the calculated anomaly of the model. The fit is assessed by calculating the weighted sum of squared deviations between the observed and calculated anomalies.

The results of 10 modelling sessions are included in appendix 1, labelled A1 to A10. Profile locations for the models are shown on plan no. 6 labelled A - A' to I - I'.

5.1.3 MAGNETIC DOMAINS

The magnetic data can, by virtue of textural relationships and frequency content be divided into a number of distinct regions or domains. Three domains have been identified within the survey area, these are shown on the interpretation plan no. 6, labelled D1-D3. A brief description of each follows:

D1: This domain possesses a distinctive signature. The magnetic data are dominated by extremely high frequency, most elongate anomalies emanating from near surface sources. In places these short wavelength anomalies are superimposed over moderate wavelength anomalies that reflect deeper sources. Many of these anomalies are interpreted as originating from intrusive mafic volcanics in the form of diorite and dolerite dykes.

Magnetic gradients are very high reflecting amplitude variations of over 4000nT. A strongly defined regional magnetic fabric closely parallels lithology.

This domain includes all of the Jamestown igneous complex and much of the Moodies sediments, and Onverwacht lavas.

D2: The D2 domain can be roughly correlated with the Fig Tree sediments. The data are predominantly long wavelength giving the magnetic texture a flat appearance. This domain essentially reflects the non-magnetic character of the sediments.

D3: A small domain in the central part of the survey area. D3 possesses a distinctive texture, it consists of a cluster of subtle yet definable individually separable anomalies of moderate amplitude and high frequency. These are superimposed on the magnetically flat (long wavelength) Fig Tree sediments. D3 is interpreted as a swarm of weakly magnetic sub-cropping intrusive bodies.

5.1.4 MAGNETIC DISCONTINUITIES

Artificial sunshading of the magnetic data (plans 3 & 4), highlights discontinuities in the magnetic fabric. A total of 32 discontinuities have been identified in this survey, these are defined on plan no. 6 as straight or mildly curvilinear lines labelled DC1 to DC32. It is probable that most if not all of the discontinuities reflect structures. Two of the discontinuities reflect major breaks in the data; DC1 which can be correlated to the Albion fault in the Jamestown schist belt, and DC2, an east-west trending break in the northeast of the survey that reflects an amplitude change in the data. DC2 cannot be correlated to any known geological feature.

Several of the remaining 30 discontinuities correspond to known or inferred faults. DC26 is spatially coincident with the Barbrook fault in the Sheba hills area. DC35 lies coincident with the Scotsman fault, while DC42 is coincident with the Saddleback fault. DC20 to DC24 may reflect radial tension gashes in the Eureka syncline.

Bearing in mind the subjective nature of this interpretation, the density of discontinuities is shown as increasing over the Jamestown schist belt in the west. It is suggested that this increase is due a rise in intrusive activity in the area rather than an increase in faulting. Intrusives are usually magnetite rich and it is the disruption of an elongate intrusives continuity by a fault that creates the susceptibility contrast necessary to 'see' the fault. In other words it is not the fault itself that is viable in the magnetic data, rather it is the effect of the fault on its surroundings that is often detected.

The discontinuities possess a dominant east-northeast trend, with minor east-west and northwest-southeast trends also evident.

5.1.5 ISOLATED INTRUSIVES

A number of discrete intrusives have been interpreted in the survey area, the sub-cropping locations of which are shown on plan no. 6. The anomalies fall into two categories. first category anomalies are principally due to induced magnetisation, evidenced by prominent magnetic highs and small negative lobes toward the south.

There are five prominent anomalies in this category labelled I-1 to I-5, plus a number of smaller anomalies in the D3 domain.

Second category anomalies display evidence of strong remanent magnetisation, appearing in the dataset as distinctive magnetic lows. There are 32 of these anomalies labelled M1 to M32, the observed similarity in magnetic signatures indicate a clustering of the remanent magnetisation vectors. This may signify that the 32 interpreted intrusives were introduced within a short space of time.

A possible explanation for the intrusive magnetic signatures producing these two distinct populations is that two phases of intrusion took place, that were separated chronologically.

The majority of intrusives are found to be spatially associated with known structures. This agrees with cheory, by offering the path of least resistance, pre-existing faults are most often exploited by intrusives.

A brief description of selected intrusives follows:

I1: This anomaly lies between the Great American Syncline and Bien Venue. I1 is a 120nT magnetic high interpreted as a plug like intrusive feature. Geological field checking of the anomaly by the author revealed ultramafic float coincident with the I1 anomaly, indicating the causative body may be an ultramafic intrusive. Modelling has indicated I1 is a cylindrical body, ±100m in diameter, with a depth of burial ±200m. A susceptibility of 0.05 SI units was used for the model.

I1 has a distinctive radiometric signature, it produces a moderate response which is significantly lower than the surrounding lithologies.

I2: Located in close proximity to the Great American syncline. This is a magnetic high, interpreted as a plug-like felsic stock. Geological field checking revealed rhyolite cropping out coincidentally with the I2 anomaly, confirming that the source of the anomaly is felsic. Magnetic modelling of the I2 body is presented in Figure A8. This model indicates that the main causative body is cylindrical in shape ±700m, in diameter, with a depth of burial, some ±150m below surface. When modelling a response the anomaly responds to a magnetic pole which is within the body rather than at its surface so the 150m may be an over-estimate, alternatively the felsic outcrop may be an apophyge of the main body extending up to surface. A susceptibility of 0.04 SI units was measured in the field, the host lithology was found by measurement to be essentially non-magnetic, thus a similar susceptibility value was used to constrain the modelling. The model shown in figure A7 assumes that the measured magnetic response is due to induction. To fit the observed response requires that the intrusive be inclined at 60° to the vertical, an unlikely scenario. More realistic is the model in figure A8, where the remanent ratio was allowed to vary and a vertical body fitted. It is thus likely that the I2 intrusive has remanent magnetisation associated with it.

It should be noted that width and dip estimates vary little between the two models. Remanence principally affects dip information, so when remanence is suspected but its magnitude is unknown, it is still feasible to model the lateral extent and depth of burial for anomalies.

The radiometric count rate over I2 is raised 60% above the surrounding lithologies.

I4: This anomaly lies at the junction of two geologically inferred faults proximal to the I5 anomaly. Modelling has indicated that I4 is a cylindrical body, ±150m in diameter, with a shallow depth of burial 0m-50m.

I4 does not have a distinctive radiometric signature.

I-5: This anomaly lies at the junction of the Inyoka Fault, the Kamhlabane Fault and an unnamed north-south trending geologically mapped fault. The source of the anomaly is interpreted as a plug like felsic stock. Field checking failed to verify the existence of an intrusive. although quartz vein hosted tourmaline, talcose alteration and several breccia horizons were identified. Modelling has indicated the I5 anomaly to be a cylindrical body ±100m in diameter, with a depth of burial of some 110m.

I5 does not have a distinctive radiometric signature.

Pemanently magnetised intrusives: Remanence adds a vector of independent amplitude and direction to the induced field vector. In general if the south-side low alignment is not positioned close to the line of declination, some remanence effect may be suspected. Anomalies M1 - M32 fall into this category. In some cases, remanence where suspected can be factored into the interpretation process but this generally minimises quantitative analysis. In general however even for moderate remanent effects, definition is unlikely without orientated samples being taken and analysed. For these anomalies the orientation of the dipolar alignment was measured and input into the modelling as the remanent declination.

The inclination vector was allowed to vary in order to fit the anomaly. Appendix 1 includes models of anomalies M11, M26 and M28. In all cases vertical cylindrical bodies were fitted, depths were always in the order of 100m and lateral dimensions from 300m to 500m.

5.1.5 ELONGATE MAGNETIC UNITS

A number of elongate magnetic responses are found in the data set, labelled E1 etc. on plan no. 6. The high frequency of the anomalies suggests the causative bodies are narrow with a shallow depth of burial.

Anomalies E1 to E5 display remanent magnetisation, appearing in the data as magnetic lows which are not conformable with geologic strike. Anomalies E23 to E29 are extremely high amplitude responses, conformable with the Moodies meta-sediments of the Eureka syncline, they cannot be ascribed to intrusive activity. The magnetic anomaly generated by these units outlines the Eureka synform and dominates the data to such an extent that the syncline is highly visible even in the government regional aeromagnetic data. The remainder of the elongate responses are normally magnetised and cross-cut geologic strike. It is difficult to ascertain whether they should be classified as dykes or structures, many of the structures in the mountain land are thought to have been reactivated on numerous occasions and may been in-filled by mafic material during periods of relaxation.

Euler deconvolution (plan no. 5) was of particular use in locating elongate units. Several Euler solutions were field checked, lateral location was found to be extremely good, within the locational accuracy of the survey.

This was not the case for the Euler depth solutions as many outcropping dykes had depth solutions of 100m or more generated over them. The minimum depth that the program can resolve is one grid cell or 50m.

5.2 RADIOMETRICS

As discussed in chapter 3, the radiometric results discussed in this interpretation are only the partially corrected total-count data.

Due to the nature of radiometric data the interpretation of an airborne survey is qualitative. This is due to the extremely small depth of penetration and the inherently complex nature of the gamma-ray spectra. Approximately 30cm of rock, 60cm of soil or 1m of water effectively obscures underlying radiation sources no matter how intense. The colour contour map of the total-count plan no. 7, is thus a reflection of lithological variations at surface. A mean total-count rate of 650cps was recorded for the survey. Statistically this figure allows reasonable lithologic discrimination. A qualitative interpretation of the radiometric data is presented in plan no. 8.

All of the major lithological constituents of the Barberton mountain land display distinctive and diagnostic radiometric signatures allowing accurate discrimination and mapping. The Nelspruit granite has an extremely high count rate associated with it allowing highly accurate placement of the granite/greenstone contact. The response of the Kaap valley granite differs significantly from the Nelspruit granite. The Moodies sediments display extremely high count rates, Fig Tree sediments intermediate rates, Onverwacht lavas low count rates and the Jamestown Igneous Complex extremely low rates.

Several of the larger dykes can be distinguished within the radiometric data. They appear as either positive responses displaying increased count rates, or b[illegible] in the data evidenced by DL9 and DL10.

Lithologic fabric is visible within the radiometric data throughout the survey area and this fabric has been used to delineate a number of synclinal structures. A total of eight previously unmapped synclines have been interpreted, the fold axes for these are shown on plan no. 9. Included are:

A small northeast plunging syncline labelled R12 on plan no. 8. The signature closely resembles that of the Great American syncline (R10), which lies 12km to the southwest. The limbs of the Great American syncline are clearly visible in the radiometric data.

An east-west trending, east plunging syncline developed south of the Ulundi syncline and separated by an interpreted structure termed the Alfstrom thrust.

Onverwacht volcanics are interpreted to be imbricated within the Fig Tree sediments.

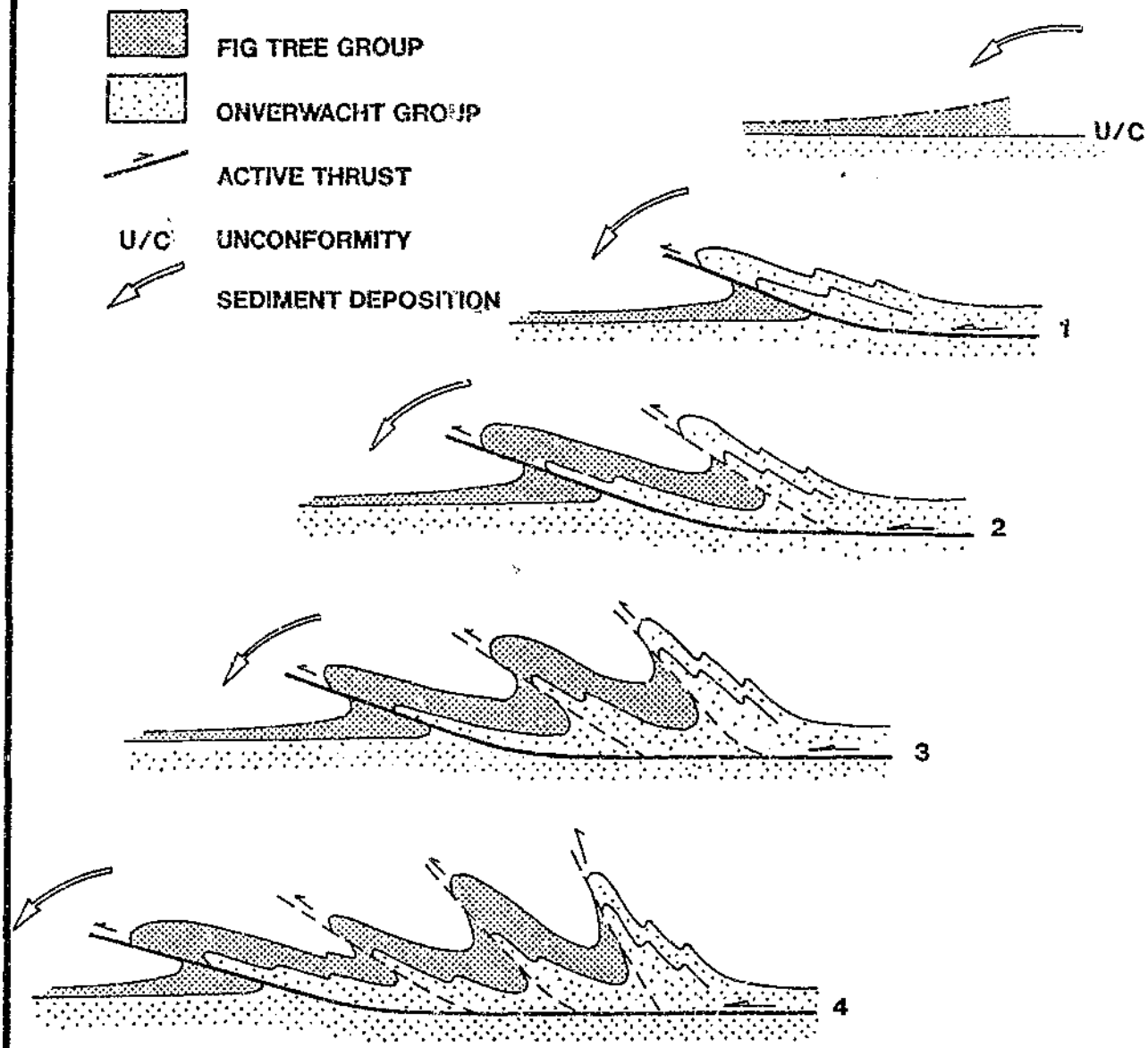
Alluvium has been mapped in numerous locations within the survey area. Indications are that the Jamestown Igneous Complex, Nelspruit granite and Fig Tree sediments all sub-crop beneath isolated alluvium occurrences. An unusual feature of note is that the alluvium does not display a recognisable signature in the radiometric data. Indeed the radiometric signature of the subcropping lithology does not seem to be affected by the alluvium cover, continuing unabated beneath the cover. Field checking confirmed the presence of alluvium like material in several locations.

Although the depth could not be established the extent of the coverage would indicate that greater than 60cm is probable. A likely explanation for the observed radiometric response is that the cover is not alluvium in the strict sense of the word, but rather in situ 'soil', ie. the weathered product of the bedrock.

5.3 DISCUSSION

In developing a structural model for the tectonic evolution of the northern mountain land the Barbrook fault is interpreted as representing a thrust detachment zone that together with a series of associated sub-parallel thrust faults emplaced Onverwacht Group lithologies over Fig Tree Group sediments. The thrust sheets form an emergent imbricate stack that developed by footwall propagation towards the north. A schematic thrust development sequence for the Barbrook (E40) package, including the Saddleback (E42), Inyoka (E78), Alfstrom (E36) and other faults, is shown in figure 9. In like manner the Lily, Scotsman and Sheba faults are interpreted as a thrust sequence.

There is evidence in the radiometric data to suggest that the L1 radiometric contact (see plan no. 8) is of great significance to the regional structure of the Barberton Greenstone Belt. L1 is spatially coincident with the Scotsman fault (which laterally passes into the Woodstock fault) in the east and the Lily fault in the west. The Moodies sediments, Fig Tree sediments and Onverwacht lavas mapped to the north of L1 display a fundamentally different radiometric signature from those mapped south of the contact. L1 may represent a major detachment zone in the northern mountain land.



(1–4 THRUST DEVELOPMENT SEQUENCE)

BARBROOK FAULT THRUST DEVELOPMENT SEQUENCE

FIGURE 9

De Wit and Roering (1990) suggest that The Scotsman fault is a terrane boundary, possibly a suture zone, separating two distinct greenstone successions. The geophysical data would support this hypothesis. It is postulated by the author that the entire stratigraphic package was accreted onto the Jamestown Igneous Complex.

In the south of the survey the L2 radiometric contact trends sub-parallel to the L1 contact. It is also interpreted as significant boundary and will be discussed further in section 5.3.1.

5.3.1 BARBROOK FAULT

The Barbrook fault is mapped as a regional east-northeast/west-southwest trending south dipping thrust fault. In the west, it emplaces Onverwacht lithologies over Fig Tree sediments of the Alfstrom syncline. Moving eastward, the Barbrook fault imbricates Swartkoppie lithologies into the Ulundi syncline Fig Tree succession. Up to six imbricate thrusts that detach from the Barbrook thrust in the region of the Barbrook mine have been identified, Houston (1984).

The major radiometric contact L2 is spatially coincident with the previously mapped location of the Barbrook fault for most of its length, but divergence occurs in the extreme east of the survey. The present study suggests that the Barbrook fault can be mapped in the extreme east using the radiometric data.

No single magnetic anomaly is coincident with the Barbrook fault for most of its length. A number of parallel trending, elongate magnetic horizons are clearly visible.

Blackwell (1990) recognised that in the Florence and Devonian mine area, gold is hosted in shear zones trending parallel to the Barbrook fault, located in steeply south dipping attenuated fold limbs in the footwall of the fault. The Barbrook mine is located in the footwall of the Barbrook fault. Here again the gold is hosted by shear zones that trend parallel to the footwall of the Barbrook fault and dip steeply south, cutting through overturned tight to isoclinal fold hinges. In both these cases, the mineralised shears are spatially related to the above-mentioned magnetic anomalies located south of M-5. It thus seems probable that the magnetic method is delineating the mineralised shears.

The importance of the Barbrook Fault in relation to mineralisation is illustrated by the considerable number of shear hosted gold deposits located along its entire mapped extent, from the Florence and Devonian mine area in the west to the Aurora mine at its eastern extent. The fault almost certainly acted as a major conduit for mineralising fluids.

5.3.2 SHEBA FAULT

The Sheba Fault is a major structural feature, serving to separate the Eureka and Ulundi Synclines in the central portion of the greenstone belt. It is mapped as a strike extensive thrust fault which imbricates thin sheets of the Onverwacht Group into the Ulundi syncline. This fault is known to have played a significant role in channelling mineralising fluids and is intimately associated with some of the largest gold deposits in the greenstone belt.

The Sheba fault is defined clearly in the geophysical data. Interpretation suggests that the fault continues uninterrupted eastward well beyond its mapped extent, where it passes laterally into the Scotsman fault. This eastward continuance is termed the 'Sheba extension' on plan no. 9. In the magnetic data the Sheba fault including its eastern extension, is defined by the E30 anomaly (plan no. 6). The L1 radiometric anomaly (plan no. 7) can be spatially correlated to the eastward extension of the Sheba fault.

5.3.3 EUREKA SYNCLINE

The Eureka syncline is an exceedingly dominant feature in the magnetic data set, indeed the syncline is clearly visible even in the regional government airborne magnetic data. The intense magnetic anomaly centred over the Eureka syncline is not generated as has been previously supposed by a single large body at considerable depth. Signal processing and modelling of the data has shown that the source is in fact a number of thin narrow bands of extremely magnetic material (anomalies E23 to E29 on plan no. 6) that extend upward to near surface. These anomalies are interpreted as multiple small, steeply dipping, narrow bands of ferruginous highly magnetic shale and slate, within the Moodies sediments. These shale bands are only a few ten's of metres wide and extend to surface.

Resolution is defined as the ability to identify small features that make up larger composite anomalies. Resolution of small anomalies is significantly affected by flying height. As a rule of thumb multiple small, shallow bodies cannot be discerned where the flying height exceeds the separation between the bodies. In the case of the Eureka syncline, separation between shale bands is approximately 250m.

Therefore a regional survey exceeding 250m terrain clearance will be unable to discriminate individual anomalies within the Eureka syncline, a singly broad anomaly will be observed. The magnetic model shown in figure A3 demonstrates this problem. Without high resolution magnetic data or knowledge of the multiple body geology, interpretation of regional airborne data results in a vastly different scenario. The model that most satisfactorily fits the Eureka syncline data is an 1800m wide, highly magnetic body, buried to a depth of 500m. Figure A4 is a model produced for a single magnetic shale band.

5.3.4 JAMESTOWN IGNEOUS COMPLEX

The geophysical data indicate that the Jamestown Igneous Complex is more extensive in the north of the mountain land than has previously been mapped. In particular west of the Great American syncline mapped as Onverwacht Group. The northern margins of the Fig Tree Group. and extending 500m or more into the Nelspruit granite.

5.3.5 DYKES

Units labelled E1 to E5 on plan no. 6 are interpreted as remanently magnetised dolerite dykes. Units E100 to E123 are interpreted as diorite dykes. Several of these magnetic responses can be spatially correlated to geologically mapped dykes. In a number of cases the lateral extent of a known dyke is able to be significantly extended. In several locations where a single dyke has been mapped it is now interpreted that two unrelated dykes are present. Several of the dykes produce an interpretable response in the radiometric data, evidenced by DL9 and DL10 plan no. 8.

At regional scales each of the interpreted dykes appears to represent a single elongate intrusive body. A detailed inspection reveals the dykes are composed of a number of narrow, discontinuous mafic bodies, highly disrupted by small scale faults, forming anastomosing patterns. In many cases the ultramafic rocks have intruded along fault planes. Intense shearing along individual faults may have generated sub-parallel zones of weakness, allowing each dyke to intrude syntectonically as a number of narrow bands.

5.4 MINERALISATION

This section is purposefully cursory due to company confidentiality.

The Onverwacht Group assemblages are considered to be the primary source of most of the gold and sulphide mineralisation in the mountain land. Mineralisation is well known to be largely confined to a broad zone adjacent to the periphery of the greenstone belt and to decrease progressively toward the central areas. The influence of intrusive granites was minimal away from the greenstone belt contacts, thus reducing the influence of hydrothermal fluids and contact metamorphic effects. Structures also played a major role in channelling and confining mineralisation. Away from the sphere of influence of the major planes of weakness, the incidence of gold mineralisation decreases.

In the context of this survey known mineralisation occurrences are almost invariably found spatially associated with interpreted structures. Interpreted structural junctions in particular, are often found coincident with known deposits.

CHAPTER 6

CONCLUSIONS

6.1 SUMMARY OF CONCLUSIONS

Plan no. 9 is a geological map derived from the interpretation of the airborne magnetic/radiometric survey. It differs significantly from the published geological map, particularly in the eastern area of the survey. The major conclusions that have been derived from this map are enumerated below:

1. The airborne magnetic data contain detailed lithologic and structural information. Several prominent lineaments have been defined that may reflect previously unknown faults. In several cases known faults have been extended beyond their mapped limits.

2 The radiometric data suggest that the L1 radiometric contact is of great significance to the regional structure of the Barberton Greenstone Belt. Moodies sediments, Fig Tree sediments and Onverwacht lavas mapped to the north of this contact display a fundamentally different radiometric signature from those mapped south of the contact.

3 The northern mountain land succession is interpreted as a northward verging imbricate thrust stack that has been accreted onto the Jamestown Igneous Complex.

4 The magnetic and radiometric data suggest that the Jamestown Igneous Complex is more extensive than suggested by the geological mapping.

5 The intense magnetic anomaly centred over the Eureka syncline is not generated as has been previously supposed by a single large body at considerable depth. Signal processing and modelling of the data have shown that the source is in fact multiple small, steeply dipping, narrow bands of ferruginous highly magnetic shale and slate, within the Moodies sediments. These shale bands are only a few ten's of metres wide and extend to surface.

6 Intrusives, both mafic and felsic, are accurately defined by the magnetic, and to a lesser degree, by the total-count radiometric data. Moreover within the survey area diorite can be differentiated from dolerite due to remanent magnetisation effects.

7 Remanent magnetisation is interpreted to be prevalent in the belt. Magnetically derived dip information is thus unreliable.

8 There is no evidence contained within the geophysical data herein presented, to suggest the greenstone belt extends to a depth greater than 3km.

9 The major geological constituents of the Barberton mountain land display distinctive and diagnostic radiometric signatures, enabling accurate lithologic discrimination. Mapped alluvial cover does not mask the response of the underlying lithologies.

10 The radiometric data have revealed a number of intricate east-west trending, synclinal structures within sediments of the Fig Tree Group.

11 In the central section of the survey area thin bands of the Onverwacht Group are interpreted as being imbricated within the Fig Tree sediments.

12 Interpretation suggests that the Sheba fault extends eastward, beyond its currently mapped extent. The Barbrook fault is interpreted as diverging from its mapped location in the extreme east of the survey.

13 Mineralisation in the mountain land is often spatially associated with interpreted structural junctions.

6.2 SCOPE FOR FURTHER RESEARCH

The research work so far conducted has been constrained in a number of instances due to budgetary restrictions. This study suggests that the following additional aspects of research could further enhance the geophysical interpretation of the Barberton mountain land.

1 A palaeomagnetic study of the Barberton lithologies in order to resolve the remanent magnetisation vectors. This would allow more accurate quantitative modelling of magnetic anomalies.

2 Additional processing of the radiometric data to discriminate the component responses contributed by isotopes of potassium, thorium and uranium. The resulting elemental distribution maps would benefit lithologic discrimination, particularly in the greenstone belt's northeast extreme.

BIBLIOGRAPHY

ANHAEUSSER, C R (1966).
Facets of the Granitic Assemblages on the Northwest Flank of the Barberton Mountain Land.
Inform. Circ. No. 32, Econ. Geol. Res. Unit. Univ. of the Witswatersrand, Johannesburg.

ANHAEUSSER, C R; ROERING, C; VILJOEN, M J AND VILJOEN, R P (1968).
The Barberton Mountain Land: a Model of the Elements and Evolution of an Archaean Fold Belt.
Annex. Trans. Geol. Soc. S. Afr. V. 71, pp 225 - 254.

ANHAEUSSER, C R; MASON, C R; VILJOEN, M J AND VILJOEN, R P (1969).
A Re-Appraisal of some aspects of Precambrian Shield Geology. Geol. Soc. Amer. Bull. 80, pp 2175 - 2200.

ANHAEUSSER, C R (1973).
The Evolution of the Early Precambrian Crust of Southern Africa. Phil. Trans. Roy. Soc. London. Ser. A, 273, pp 359 - 388.

ANHAEUSSER, C R (1975).
Precambrian Tectonic Environments.
Ann. Rev. Earth Planet. Sci., 3, pp 31 - 53.

ANHAEUSSER, C R AND ROBB, L J (1981).
Magmatic Cycles and the Evolution of the Archaean Granitic Crust in the Eastern Transvaal and Swaziland.
Spec. Publ. Geol. Soc. Aust., 7, pp 457 - 467.

ANHAEUSSER, C R (1984).
Structural Elements of Archaean Granite-Greenstone Terranes as Exemplified by the Barberton Mountain Land, southern Africa, 57-78.
In: Kroner and Greiling, Eds., Precambrian Tectonics Illustrated. E Schweizerbart'sche Verlagsbuchhandlung, Stuttgart, pp 57 - 78 419pp.

ANHAEUSSER, C R (1986).
Archaean gold mineralisation in the Barberton Mountain Land.
Anhaeusser, C R and Maske, S, Eds., Mineral Deposits of S. Afr., I., pp 113-154 1020pp

BARTON, C M (1982).
Geology and Mineral Resources of Northwest Swaziland (Barberton Greenstone Belt).
Geol. Surv. Swaziland, Bull. 10, 97pp.

BLACKMAN, R B AND TUKEY, J W (1959).
The Measurement of Power Spectra.
New York, Dover Publications.

BLACKWELL, M (1990).
Florence and Devonian - Project Summary and drilling report.
Genmin Bull. No. 44, in-house rpt.

BRIGGS, I C (1974).
Machine Contouring using Minimum Curvature.
Geophysics, V. 39, No. 1, pp 39 - 48.

BURLEY, A J; EVANS, R B; GILLINGHAM, J M AND SMITH, D (1970).
Gravity Anomalies in Swaziland.
Swaziland Geol. Surv. Mines Dep., Bull. 7, pp 4 - 16.

CLARKE, D A AND EMERSON, D W (1991).
Notes on Rock Magnetization Characteristics in Applied Geophysical Studies.
Exploration Geophysics, V. 22, pp 547 - 555.

CORDELL, L AND GRAUCH, V J S, (1982).
Reconciliation of the Discrete and Integral Fourier Transforms. Geophysics, V. 47, No. 2.

CORDELL, L; PHILLIPS, J D AND GODSON R H (1992).
USGS Potential Field Geophysical Software . 2.0, Open file Rpt. 92 No. 18.

DARRACOTT, B W (1975).
The Interpretation of the Gravity Anomaly Over the Barberton Mountain Land, South Africa.
Trans. Geol. Soc. S. Afr., No.78, pp 123 - 128.

DE BEER, J H; STETTLER, E H; dU PLESSIS, J G AND BLUME, J (1988).
The deep structure of the Barberton greenstone belt: a geophysical study.
S. Afr. Tydskr. Geol., 1988,91(2), pp 184-197.

DE WIT, M J; HART, R; MARTIN, A AND ABBOTT, P (1982).
Archaean biogenic and Probable Biogenic Structures Associated with Mineralised Hydrothermal Vent Systems and Regional
Metasomatism, with Implications for Greenstone Belt Studies. Studies Econ. Geol. 77, pp 1783 - 1802.

DE WIT, M J; FRIPP, R E P AND STANISTREET, I J (1983).
Tectonic and Stratigraphic Implications of New Field Observations Along the Southern Part of the Barberton Greenstone Belt.
In Geol. Soc. S. Afr. Spec. Publ. No.9, pp 21 - 29.

DE WIT, M J AND ASHWAL, L D (1986).
Workshop on Tectonic Evolution of Greenstone Belts.
LPI Tech. Rep. 86-10. Lunar and Planetary Institute, Houston, 227pp.

DE WIT, M J AND ARMSTRONG, R (1987).
Felsic Igneous Rocks Within the 3.3-3.5Ga Barberton Greenstone Belt: High Crustal Level Equivalents of the Surrounding Tonalite-Trondhjemite Terrane, Emplaced during Thrusting.
Tectonics V6 No.5, pp 529 - 549.

DE WIT, M J AND ROERING, C (1990).
Episodes of Formation and Stabilisation of the Kaapvaal Craton in the Archaean: An overview based on some Selected Recent Data.
In Barton, J M (ed.) Extended Abstracts the Limpopo Belt: A Field Workshop on Granulites and Deep Crustal Tectonics, Dept. of Geol. Rand Afrikaans Univ. Johb., 160pp.

FRIPP, R E P; VAN NIEKOP, D A; CALLOW, M J; LILLY. P A AND DU PLESSIS, L U, (1980).
Deformation in Part of the Archaean Kaapvaal Craton, South Africa.
Precambrian Res. No. 13, pp 241 - 251.

GOLDIE, R (1985).
The Sinters of the Ohaki and Champagne Pools, New Zealand : Possible Modern Analogues of the Hemlo Gold Deposit, Northern Ontario.
Geoscience Canada, V. 12, pt. 2, pp 60 - 64.

GROENEVELD, D (Compiler), (1973).
The Economic Mineral Deposits in the Archaean Complex of the Barberton Area.
Unpubl. Rep. Geol. Surv. S. Afr., 353pp.

GUNN, P J, (1975).
Linear Transformations of Gravity and Magnetic Fields.
Geophysical Prospecting, V. 23, pp 300 - 312.

HALL, A L (1918).
The Geology of the Barberton Gold Mining District.
Mem. Geol. Surv. S. Afr., No. 9, 347pp.

HANSEN, D A (1992).
Geological Applications for Portable Gamma Ray Spectrometers.
In Van Blaricom, D, Ed., Practical Geophysics II, NW. Mining Assoc. USA., pp 2 - 38.

HOOD, P J; HOLROYD, M T AND McGARTH, P H (1979).
Magnetic Methods Applied to Base Metal Exploration.
Geol. Survey of Canada, Economic Geol. Rpt. No. 31.

HOUSTON, S (1984).
First Ph.D Field Report to Barbrook Mine Ltd, South Afr., 24pp.

HUGON, H (1984).
The Hemlo Deposit : Gold mineralisation within a Dextral Shear Zone : In Summary of Fieldwork 1984, Ontario
Geol. Survey, Misc. Pub. : 212 - 217.

HUNTER, D R (1974).
Crustal Development in the Kaapvaal Region, I. the Archaean.
Precambrian Res. 1, pp 259 - 294

JOHNSON, W W (1969).
A Least-Squares Method of Interpreting Magnetic Anomalies Caused by Two-Dimensional Structures.
Geophysics V. 11, pp 65 - 74.

JONES, D H (1969).
Geology and Gold Mineralization of the Hhohho Area, Northwestern Swaziland.
M.Sc. Thesis (Unpubl.) Univ. Witwatersrand, Johannesburg, 165pp.

KRONER, A et al (1991).
Chronology of early Archeaean Granite-Greenstone Evolution in the Barberton Mountain Land, South Africa, based on precise dating by single zircon evaporation.
Earth and Planetary Science Letters 103, pp 41-54

LEINSTER, R C (1992).
Shear Zones and Tectonics of the Barberton Mountain Land, South Africa.
Ph.D Trans. rpt. (Unpubl) dept. geol. Imperial col. London.

LAMB, S H AND PARIS, I A (1988).
Post-Onverwacht Group Stratigraphy in the SE part of the Archaean Barberton Greenstone Belt.
J. Afr. Earth sciences V. 7 No. 1, pp 285 - 306.

LOWE, D R (1991).
Geology of the Barberton Greenstone Belt, South Africa, pp 47-58.
In ASHWEL, L D (ed.), Two Cratons and an Orogen - Excursion Guidebook and review Articles for a Field Workshop through selected Terranes of Swaziland, South Africa and Zimbabwe. IGCP Project 280, Dept. of Geol. Univ. of the Witswatersrand, Johannesburg, pp 311.

MARQUARDT, D W (1963).
An algorithm for Least-Squares Estimation of Non-Linear Parameters.
Joul. of Soc. Industrial Applied M[illegible]. V. 11, pp 431 - 441.

MOONEY, H M AND BLEIFUSS, R (1953).
Magnetic Susceptibility Measurements in Minnesota.
Geophysics, V. 18 No. 2.

MOORE, C B (1991).
Interim Report on the Barberton Mountain Land Airborne Magnetic Survey, Eastern Transvaal
Genmin Bull. No., 2882, in-house rpt.

MOORE, C B (1991).
Aeromagnetic Interpretation of the Fairview Top Prospect, Eastern Transvaal.
Genmin Bull. No. 2883, in-house rpt.

PARIS, I A (1987).
The 3.5Ga Barberton Greenstone Succession, South Africa: implications for Modelling the Evolution of Archaean Crust.
Geol. Joul. No. 22, Thematic Issue, pp 5 - 24.

PATTERSON, G C (1984).
Exploration History and Field Stop Descriptions of the Hemlo Area.
Ontario Geological Survey Information Package on Hemlo,
pp H1 - 44.

POOLE, E J (1964).
Structural Control of Mineralization in the Agnes Gold Mine, Barberton Mountain Land.
Inform. Circ. No. 22, Econ. Geol. Res. Unit. Univ. of the Witwatersrand, Johannesburg.

RAMSAY, J G (1963).
Structural investigations in the Barberton mountain land, Eastern Transvaal.
Inform. Circ. No. 14, Econ. Geol. Res. Unit. Univ. of the Witswatersrand, Johannesburg.

REID, A B (1980).
Aeromagnetic Survey Design, Short Note
Geophysics, V. 45 No. 5, pp 973 - 976.

ROERING, C (1965).
The Tectonics of the Main Gold Producing Area of the Barberton Mountain Land.
Inform. Circ. No. 23, Econ. Geol. Res. Unit, Univ. of the Witwatersrand, Johannesburg.

SACS (1980).
Barberton Sequence.
In: Stratigraphy of Southern Africa, Handbook No. 8, Part 1, Geol. Surv. S. Afr.. pp. 29 - 44

SPECTOR, A, (1968).
Spectral Analysis of Aeromagnetic Data.
Unpub. Ph.D. Thesis, Dept. of Physics, Univ. of Toronto.

SPECTOR, A; AND GRANT, F S (1970).
Statistical models for interpreting aeromagnetic data.
Geophysics, V. 35, No.2, pp. 293-302

STEYN, M V R (1976).
Basal Rocks of the Swaziland System in the Steynsdorp Valley and Fairview areas of the Barberton Mountain Land.
Geol. Soc. S. Afr., pp 37.

TELFORD, W M; GELDART, L P AND SHERIFF R E (1976).
Applied Geophysics.
Cambridge Univ. Press Publ., pp 133 - 139.

THOMKINSON, M J AND KING, V J (1991).
The Tectonics of the Barberton Greenstone Belt - An Overview, pp 69 - 83.
In ASHWEL, L D (ed.), Two Cratons and an Orogen - Excursion Guidebook and review Articles for a Field Workshop through selected Terranes of Swaziland, South Africa and Zimbabwe. IGCP Project 280, Dept. of Geol. Univ. of the Witswatersrand, Johannesburg, pp 311.

THOMPSON, D T (1982).
EULDEPH: A new Technique for making Computer-Assisted Depth Estimates from Magnetic Data.
Geophysics, V. 47, pp 31 - 37.

TINTOR, N (1986).
Who Really Knows?
The Northern Miner Magazine, #1 Issue, pp 39 - 43.

URIE, J G AND JONES, D H (1965).
Metamorphic Zones of the Archaean Fold Belt in Northwestern Swaziland.
Unpubl. Report Prepared for Submission to the Geological Society of South Africa. (8th Ann. Congr.).

VALLIENT, R I; GUTHRIE, A; BRADBROOK, C; MOTZOK, A; McLLVEEN, D; KENT, J' MacMILLAN, G; SKRECKY, G' WINGFIELD, T AND SHEEHAN, D G (1984).
Field Guide to Geological Setting of Lac Minerals Ltd., Pyritic Gold Orebodies, Hemlo, Ontario.
In McMillan, R H and Robinson, D J, Eds., Gold and Copper-Zinc Metallogeny Hemlo-Manitouwadge-Winston Lake, Ontario, Canada. Geol. Ass. of Canada, Canadian Inst. of Mining and Metallurgy Joint Publ., pp 47 - 57.

VILJOEN, M J AND VILJOEN, R P (1969a).
A Proposed New Classification of the Granite Rocks of the Barberton Region.
Geol. Soc. S. Afr. Spec. Publ. No. 2, pp 153 - 179.

VILJOEN, M J AND VILJOEN, R P (1969b).
An introduction to the Geology of the Barberton Granite-Greenstone Terrane.
Upper Mantle Proj. Geol. Soc. S. Afr. Spec. Publ. No. 2, pp 9-28.

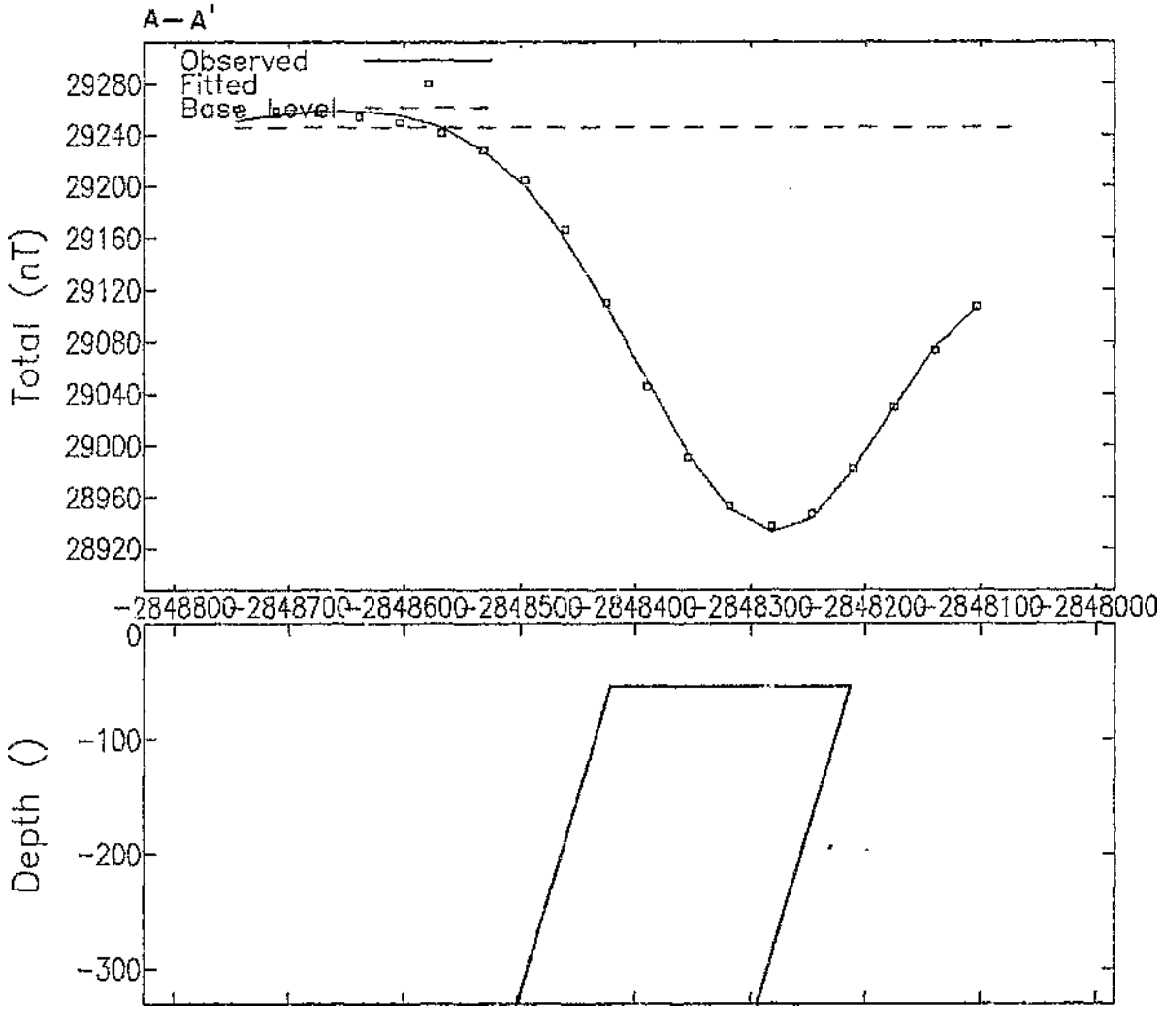
VILJOEN, M J AND VILJOEN, R P (1969c).
The Geological and Geochemical Significance of the Upper Formations of the Onverwacht Group.
Upper Mantle Proj. Geol. Soc. S. Afr. Spec. Publ. No. 2, pp 113 - 152.

VILJOEN, M J AND VILJOEN, R P (1970).
The geology and Geochemistry of the Layered Ultramafic Bodies of the Kaapmuiden area, Barberton Mountain Land.
Geol. Soc. S. Afr. Spec. Publ. No. 1, pp 661 - 688.

APPENDIX 1

MAGNETIC MODELLING RESULTS

E2 ANOMALY JAMESTOWN SCHIST BELT



MODEL PARAMETERS:

Model Type		Tabular
Depth	F	54.3
Half Width	F	104
Dip	F	106 deg
Susceptibility	X	0.00400 emu
Remnance Ratio	X	2
Remnance Incl	F	118 deg
Remnance Decl	X	−3 deg
Main Position	F	−2848318
Cross Position	X	5552.206
Base Level	F	29245.67 nT
Base Slope	X	0 nT/

(F–fitted, X–fixed, L–limit)

GEOMAGNETIC FIELD:

Field Strength	29000 nT
Inclination	−60 deg
Declination	−14 deg

COORDINATES:

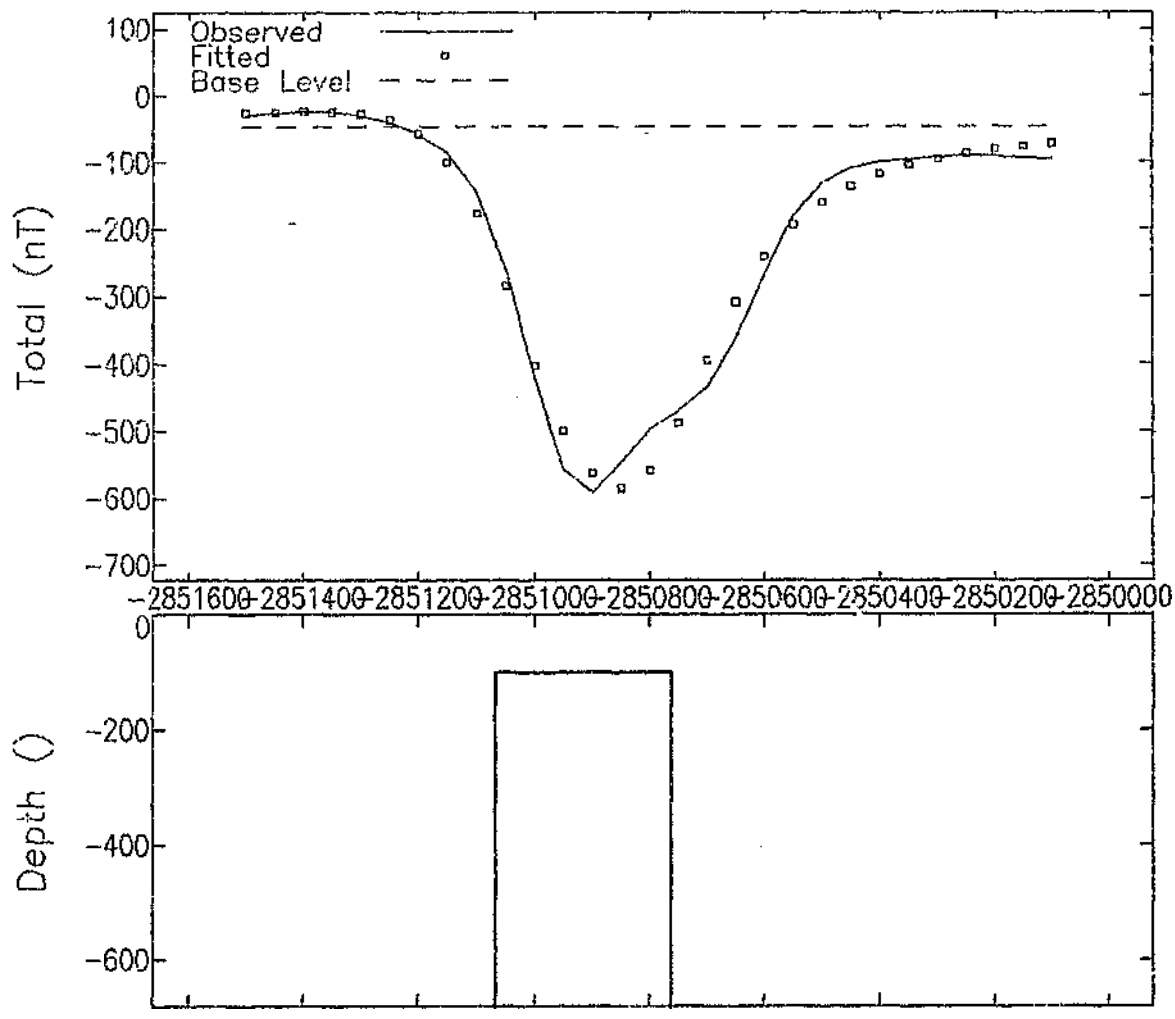
Sensor Height	45
Strike Perp	45 deg
Line Direction	45 deg
Main Direction	45 deg
Main Offset	
Cross Direction	
Cross Offset	

FIGURE A1

Geosoft MAGMOD–3 Modeling Result 93/12/15

M II ANOMALY ULUNDI SYNCLINE

B - B'



MODEL PARAMETERS:

Model Type		Tabular2
Depth	F	103
Half Width	F	153
Half Length	X	160
Offset	X	0
Dip	X	90 deg
Thickness	F	10000
Susceptibility	X	0.00600 emu
Remnance Ratio	X	2.5
Remnance Incl	F	77 deg
Remnance Decl	F	162 deg
Main Position	F	-2850915
Cross Position	X	10994.12
Base Level	F	-46.89026 nT
Base Slope	X	0 nT/

GEOMAGNETIC FIELD:

Field Strength	29000 nT
Inclination	-60 deg
Declination	-14 deg

COORDINATES:

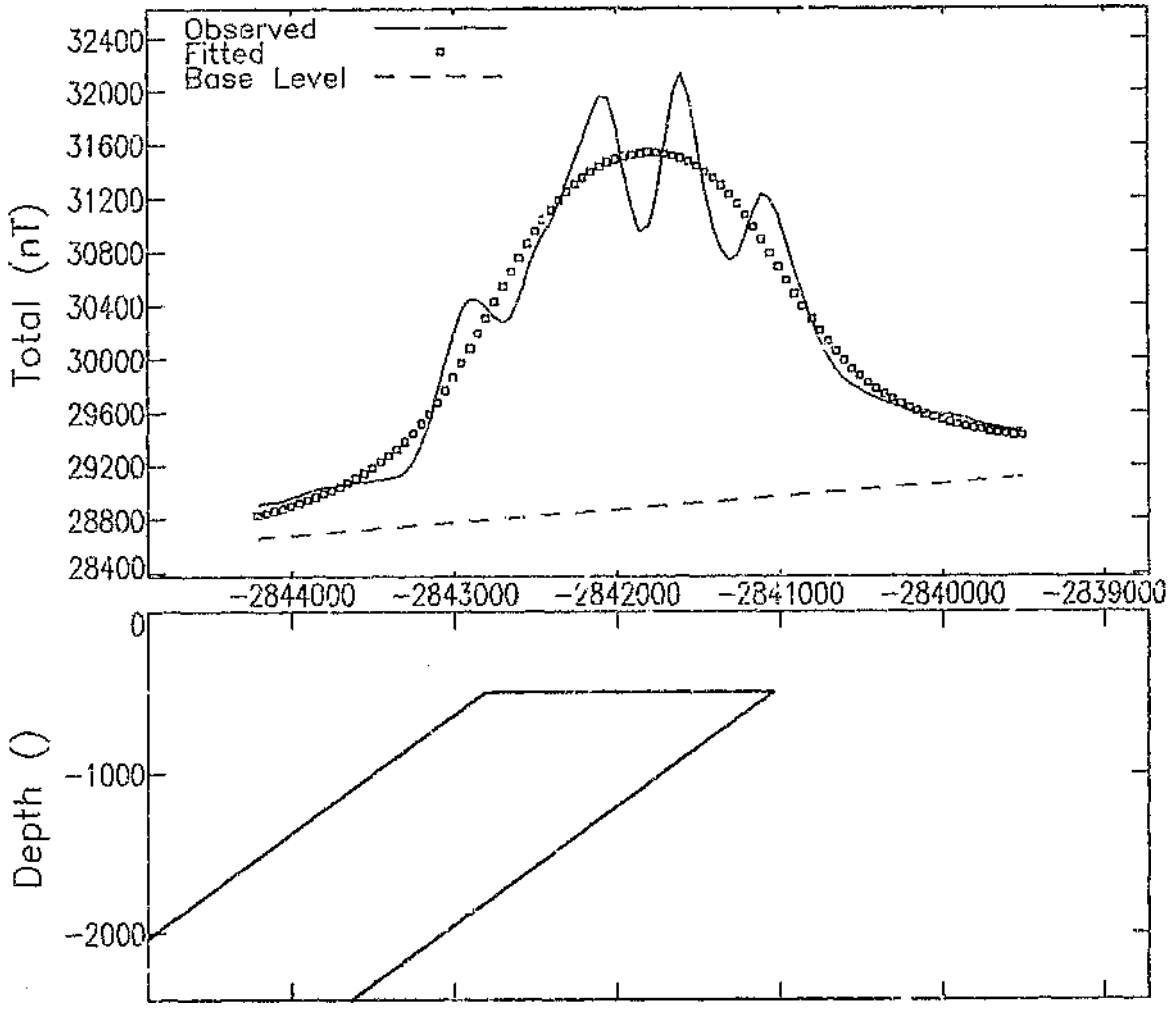
Sensor Height	50
Strike Perp	0 deg
Line Direction	0 deg
Main Direction	0 deg
Main Offset	
Cross Direction	
Cross Offset	

FIGURE A2

Geosoft MAGMOD-3 Modeling Result 93/12/15

E24, E25,E28,E29 ANOMALIES EUREKA SYNCLINE

C-C'



MODEL PARAMETERS:

Model Type		Tabular
Depth	F	490
Half Width	F	886
Dip	F	143 deg
Susceptibility	F	0.036 emu
Remnance Ratio	X	0
Remnance Incl	X	0 deg
Remnance Decl	X	0 deg
Main Position	F	-2841925
Cross Position	X	13785.32
Base Level	F	28880.4 nT
Base Slope	F	.0956086 nT/

(F-fitted, X-fixed, L-limit)

GEOMAGNETIC FIELD:

Field Strength	29000 nT
Inclination	-60 deg
Declination	-14 deg

COORDINATES:

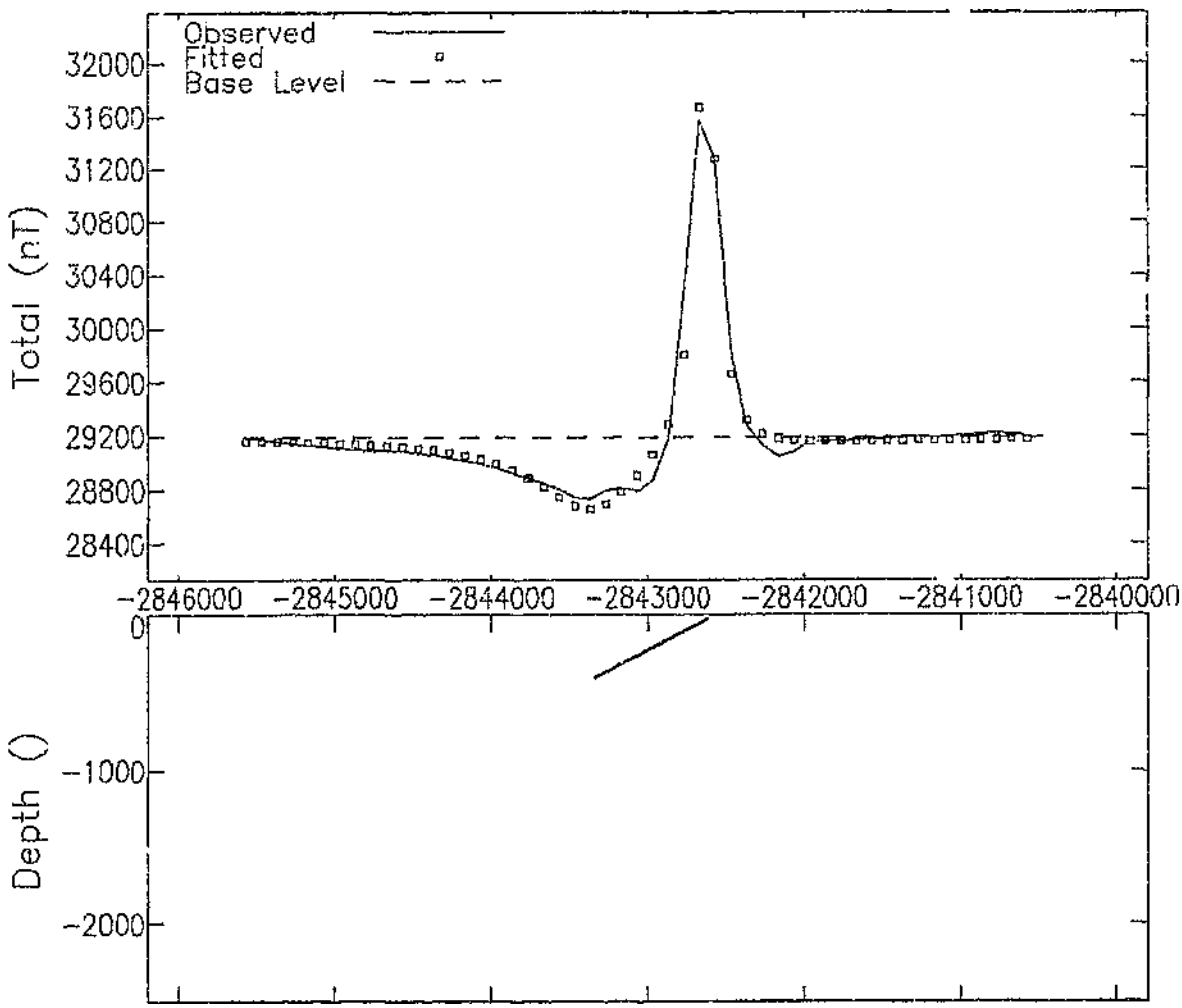
Sensor Height	50
Strike Perp	0 deg
Line Direction	0 deg
Main Direction	
Main Offset	
Cross Direction	
Cross Offset	

FIGURE A3

Geosoft MAGMOD-3 Modeling Result 93/12/13

E24 ANOMALY EUREKA SYNCLINE MAGNETIC SHALE

D - D'



MODEL PARAMETERS:

Model Type		Ribbon
Depth	F	25.0
Width	F	809
Dip	F	152 deg
Suscep x Thick	F	4.63 emu-
Remnance Ratio	X	0
Remnance Incl	X	0 d--
Remnance Decl	X	0 deg
Main Position	F	-2842622
Cross Position	X	19791.44
Base Level	F	29186.3 nT
Base Slope	X	0 nT/

(F--fitted, X--fixed, L--limit)

GEOMAGNETIC FIELD:

Field Strength	29000 nT
Inclination	-60 deg
Declination	deg

COORDINATES:

Sensor Height	50
Strike Perp	0 deg
Line Direction	0 deg
Main Direction	
Main Offset	
Cross Direction	
Cross Offset	

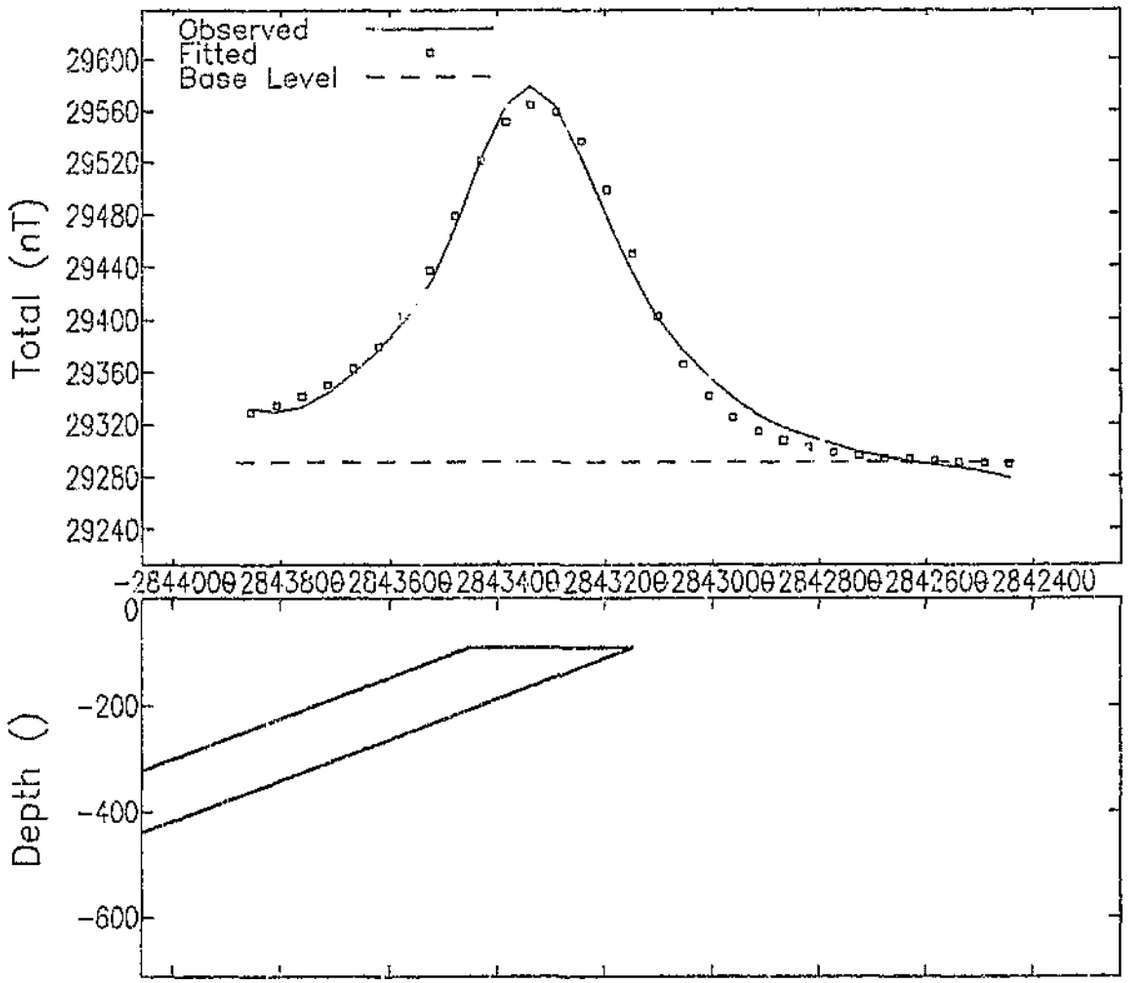
FIGURE A4

Geosoft MAGMOD-3 Modeling Resul

93/12/13

ANOMALY E40 BARBROOK FAULT

E – E'



MODEL PARAMETERS:

Model Type		Tabular
Depth	F	91.0
Half Width	F	152
Dip	F	159 deg
Susceptibility	F	0.00799 emu
Remnance Ratio	X	0
Remnance Incl	X	0 deg
Remnance Decl	X	0 deg
Main Position	F	-2843300
Cross Position	X	37549.52
Base Level	F	29291.13 nT
Base Slope	X	0 nT/

(F–fitted, X–fixed, L–limit)

GEOMAGNETIC FIELD:

Field Strength	29000 nT
Inclination	-60 deg
Declination	-14 deg

COORDINATES:

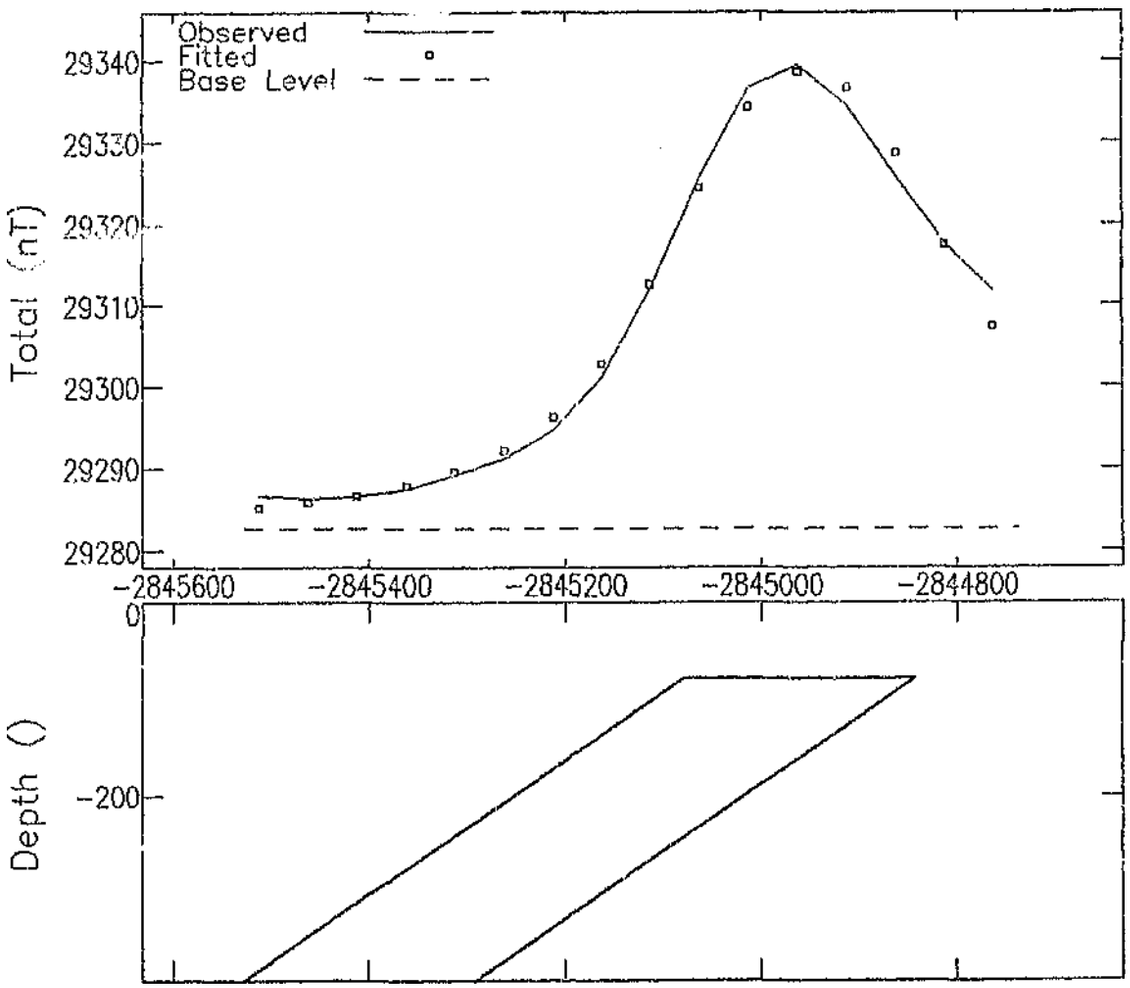
Sensor Height	45
Strike Perp	0 deg
Line Direction	0 deg
Main Direction	
Main Offset	
Cross Direction	
Cross Offset	

FIGURE A5

Geosoft MAGMOD-3 Modeling Result 93/12/17

E77 ANOMALY INYOKA FAULT

F – F'



MODEL PARAMETERS:

Model Type		Tabular
Depth	F	77.7
Half Width	F	118
Dip	F	145 deg
Susceptibility	F	0.00112 emu
Remnance Ratio	X	0
Remnance Incl	X	0 deg
Remnance Decl	X	0 deg
Main Position	F	-2844961
Cross Position	X	38285.72
Base Level	F	29282.66 nT
Base Slope	X	0 nT/

(F–fitted, X–fixed, L–limit)

GEOMAGNETIC FIELD:

Field Strength	29000 nT
Inclination	-60 deg
Declination	-14 deg

COORDINATES:

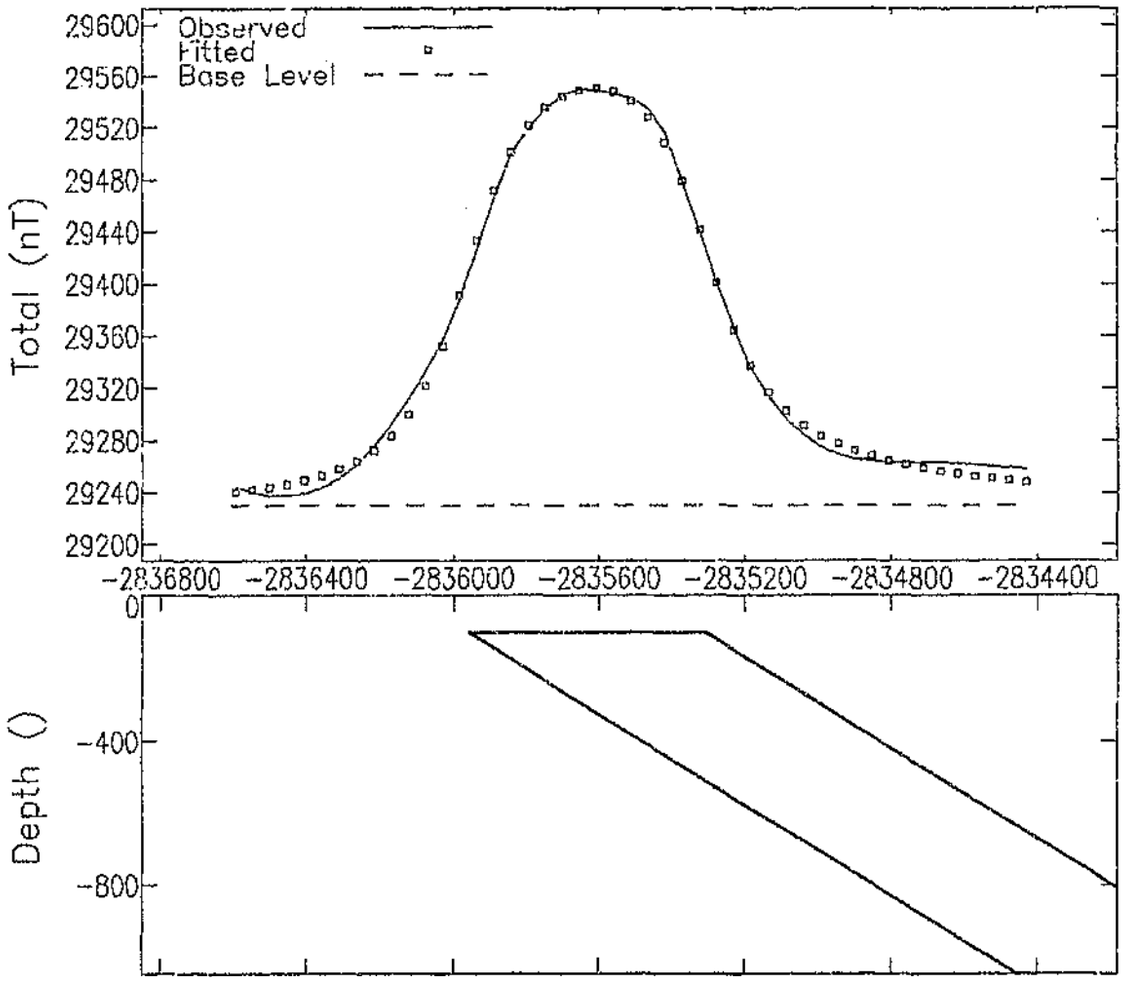
Sensor Height	45
Strike Perp	0 deg
Line Direction	0 deg
Main Direction	
Main Offset	
Cross Direction	
Cross Offset	

FIGURE A6

Geosoft MAGMOD–3 Modeling Result 93/12/17

I2 ANOMALY BIEN VENUE INDUCED MAGNETISATION

G – G'



MODEL PARAMETERS:

Model Type		Tabular2
Depth	F	100
Half Width	F	325
Half Length	X	350
Offset	X	0
Dip	F	32 deg
Thickness	X	2500
Susceptibility	F	0.00467 emu
Remnance Ratio	X	0
Remnance Incl	X	0 deg
Remn nce Decl	X	0 deg
Main ı osition	F	-2835633
Cross Position	X	36326.81
Base Level	F	29229.99 nT
Base Slope	X	0 nT/

GEOMAGNETIC FIELD:

Field Strength	29000 nT
Inclination	-60 deg
Declination	-14 deg

COORDINATES:

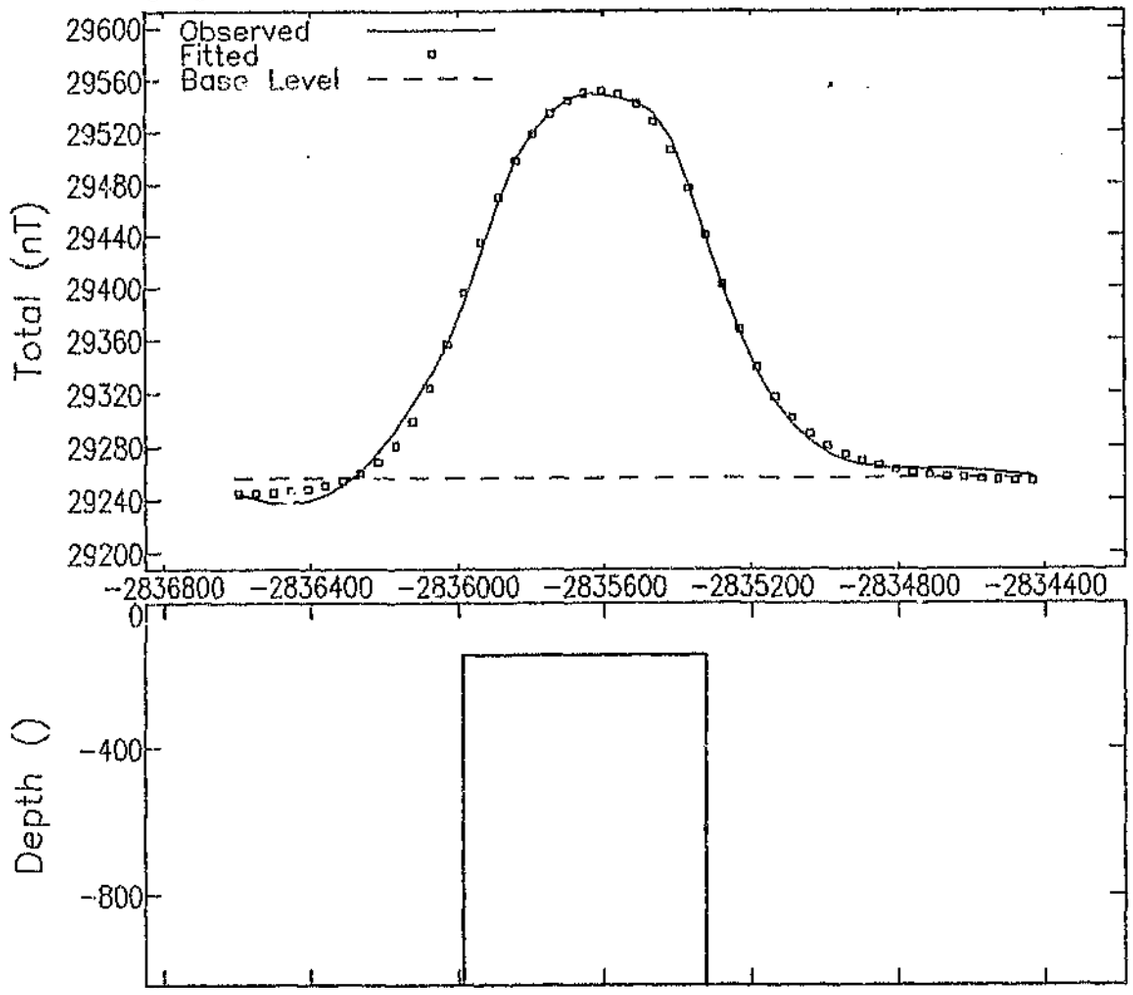
Sensor Height	50
Strike Perp	160 deg
' ine Direction	160 deg
Main Direction	160 deg
Main Offset	
Cross Direction	
Cross Offset	

FIGURE A7

Geosoft MAGMOD-3 Modeling Result 93/12/13

I2 ANOMALY BIEN VENUE REMANENT MAGNETISATION

G - G'



MODEL PARAMETERS:

Model Type		Tabular2
Depth	F	142
Half Width	F	332
Half Length	X	350
Offset	X	0
Dip	X	90 deg
Thickness	X	2500
Susceptibility	F	0.00322 emu
Remnance Ratio	F	-1.241406
Remnance Incl	X	0 deg
Remnance Decl	X	0 deg
Main Position	F	-2835656
Cross Position	X	36326.8!
Base Level	F	29256.18 nT
Base Slope	X	0 nT/

GEOMAGNETIC FIELD:

Field Strength	29000 nT
Inclination	-60 deg
Declination	-14 deg

COORDINATES:

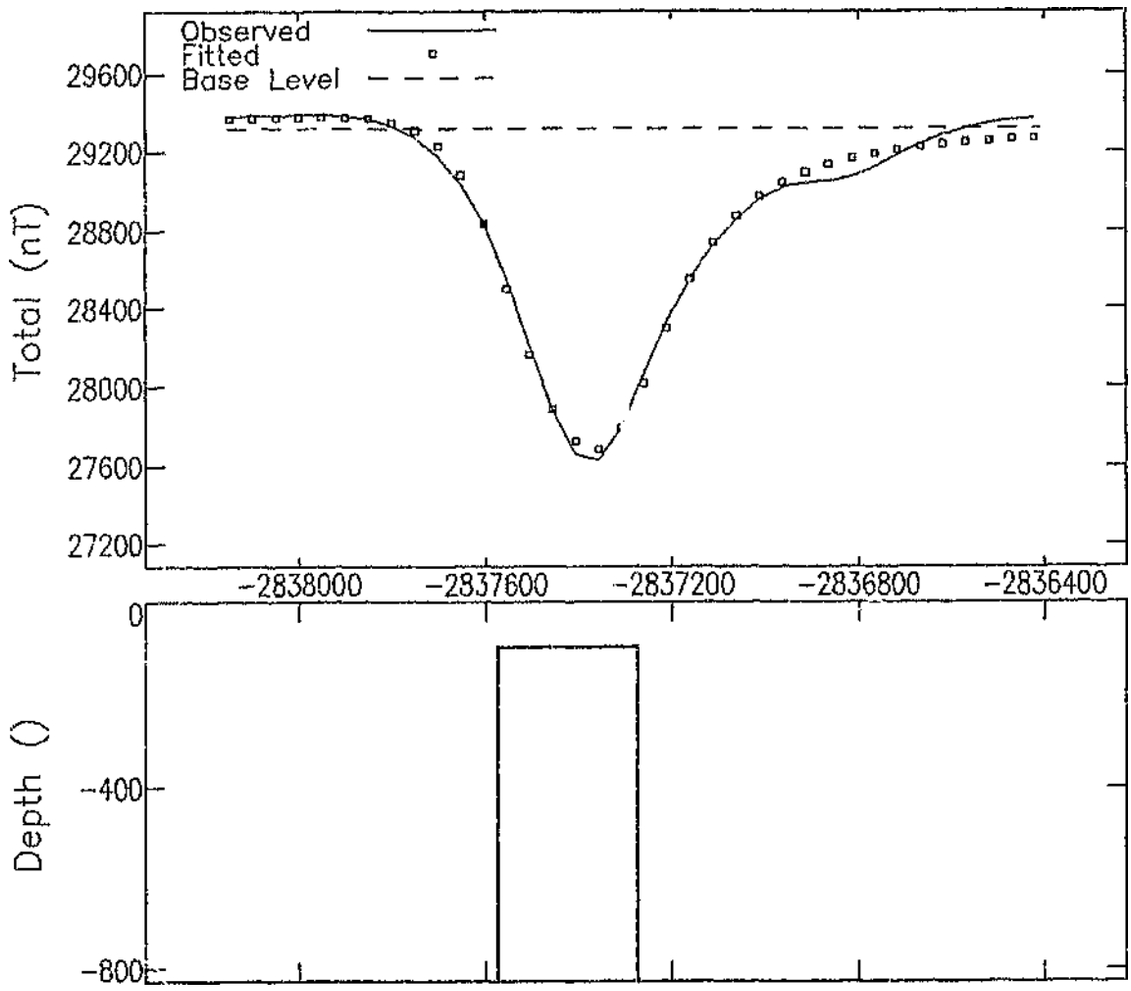
Sensor Height	50
Strike Perp	160 deg
Line Direction	160 deg
Main Direction	160 deg
Main Offset	
Cross Direction	
Cross Offset	

FIGURE A8

Geosoft MAGMOD-3 Modeling Result 93/12/13

M28 ANOMALY THREE SISTERS

H – H'



MODEL PARAMETERS:

Model Type		Tabular2
Depth	F	95.5
Half Width	F	151
Half Length	X	300
Offset	X	0
Dip	X	90 deg
Thickness	F	6327
Susceptibility	X	0.00500 emu
Remnance Ratio	X	5
Remnance Incl	F	89 deg
Remnance Decl	X	190 deg
Main Position	F	-2837423
Cross Position	X	38060.66
Base Level	F	29316.35 nT
Base Slope	X	0 nT/

GEOMAGNETIC FIELD:

Field Strength	29000 nT
Inclination	-60 deg
Declination	-14 deg

COORDINATES:

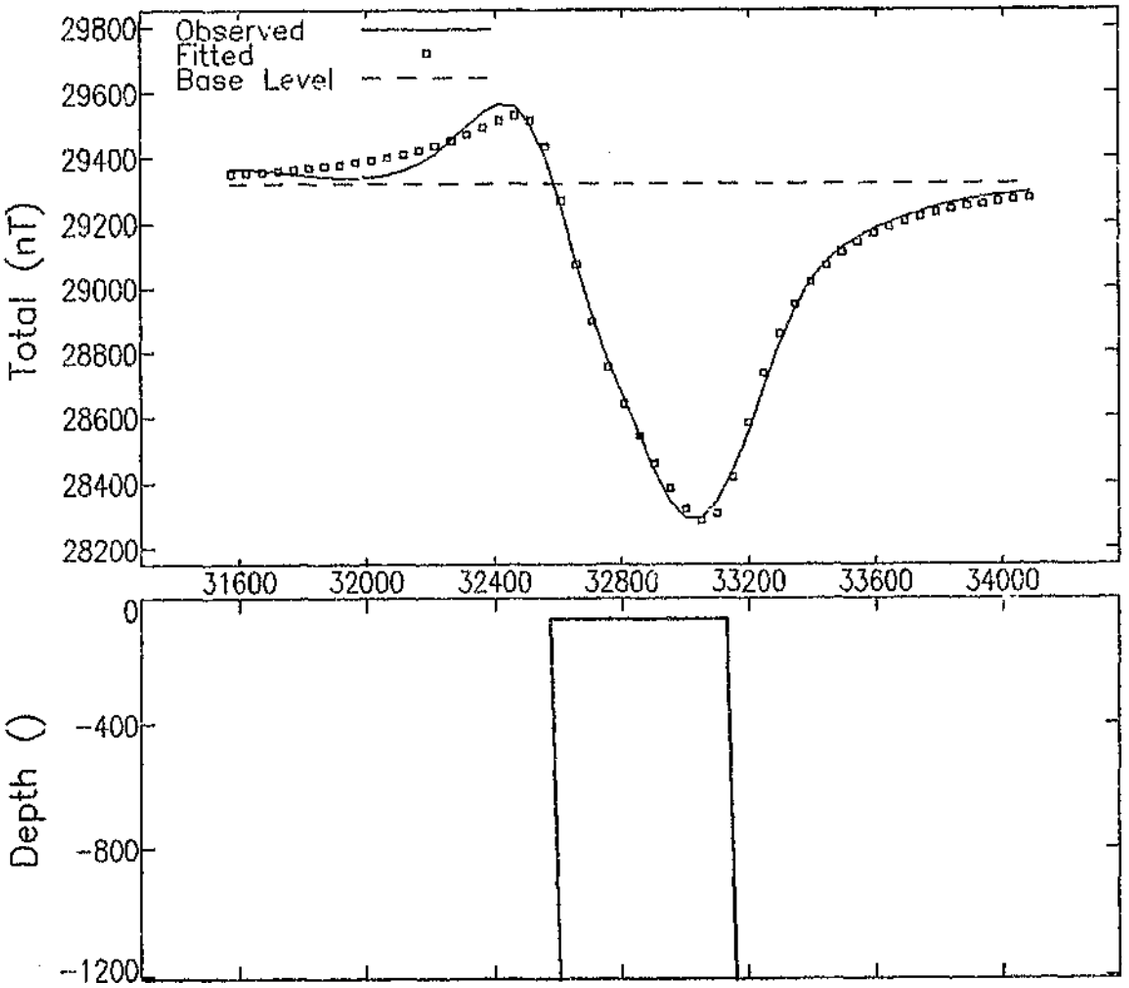
Sensor Height	45
Strike Perp	0 deg
Line Direction	0 deg
Main Direction	
Main Offset	
Cross Direction	
Cross Offset	

FIGURE A 9

Geosoft MAGMOD-3 Modeling Result 93/12/15

M26 ANOMALY

I - I'



MODEL PARAMETERS:

Model Type		Tabular2
Depth	F	66.4
Half Width	F	278
Half Length	X	271
Offset	X	0
Dip	F	88 deg
Thickness	F	2139
Susceptibility	F	0.00786 emu
Remnance Ratio	X	2
Remnance Incl	F	123 deg
Remnance Decl	X	80 deg
Main Position	F	32853.06
Cross Position	X	-2838747
Base Level	F	29318.65 nT
Base Slope	X	0 nT/

GEOMAGNETIC FIELD:

Field Strength	29000 nT
Inclination	-60 deg
Declination	-14 deg

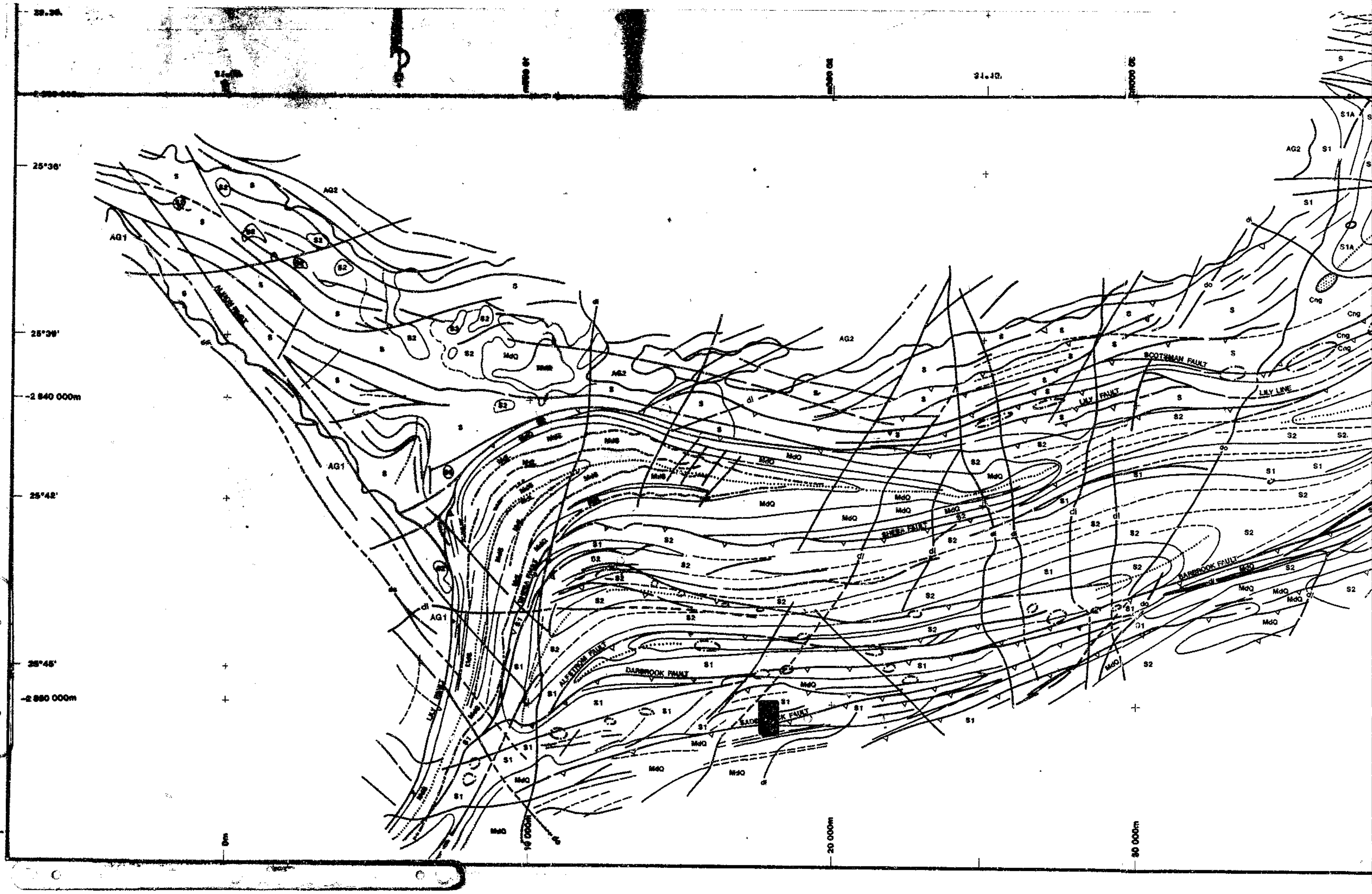
COORDINATES:

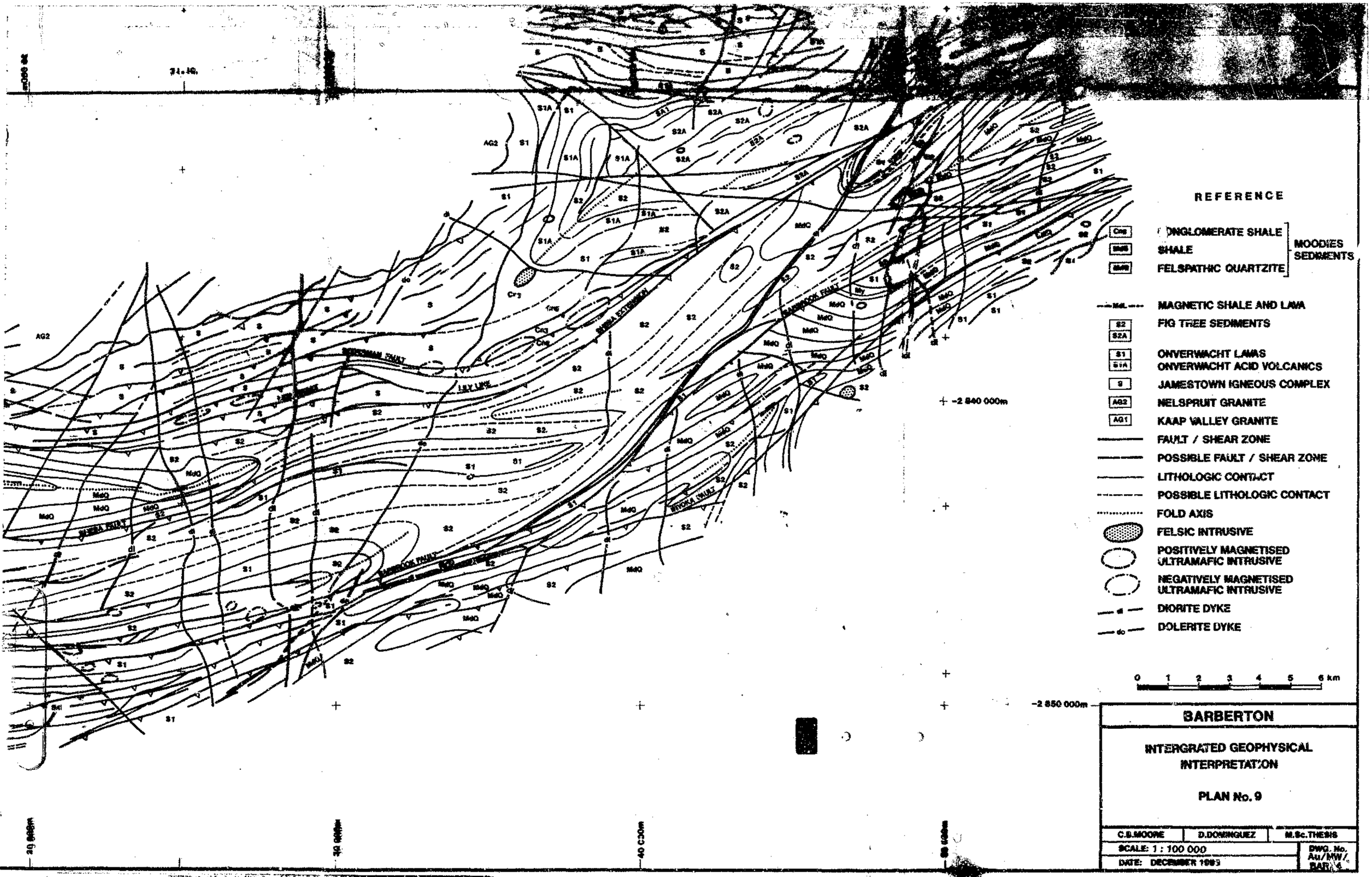
Sensor Height	45
Strike Perp	80 deg
Line Direction	80 deg
Main Direction	80 deg
Main Offset	
Cross Direction	
Cross Offset	

FIGURE A 10

Geosoft MAGMOD-3 Modeling Result 93/12/15

ATTACHMENTS


25°36'
25°39'
-2 840 000m
25°42'
25°45'
-2 860 000m
AG1
AG2
S1
S1A
S2
MdQ
Cng
dl
do
ALESTRONE FAULT
DARBROOK FAULT
SCOTSMAN FAULT
LILY FAULT
LILY LINE
SHEBA FAULT
10 000m
20 000m
30 000m



REFERENCE

- Cng — CONGLOMERATE SHALE
- MdS — SHALE
- MdQ — FELSPATHIC QUARTZITE

MOODIES SEDIMENTS

- MdL — MAGNETIC SHALE AND LAVA
- S2 / S2A — FIG TREE SEDIMENTS
- S1 / S1A — ONVERWACHT LAVAS / ONVERWACHT ACID VOLCANICS
- S — JAMESTOWN IGNEOUS COMPLEX
- AG2 — NELSPRUIT GRANITE
- AG1 — KAAP VALLEY GRANITE
- FAULT / SHEAR ZONE
- POSSIBLE FAULT / SHEAR ZONE
- LITHOLOGIC CONTACT
- POSSIBLE LITHOLOGIC CONTACT
- FOLD AXIS
- FELSIC INTRUSIVE
- POSITIVELY MAGNETISED ULTRAMAFIC INTRUSIVE
- NEGATIVELY MAGNETISED ULTRAMAFIC INTRUSIVE
- di — DIORITE DYKE
- do — DOLERITE DYKE

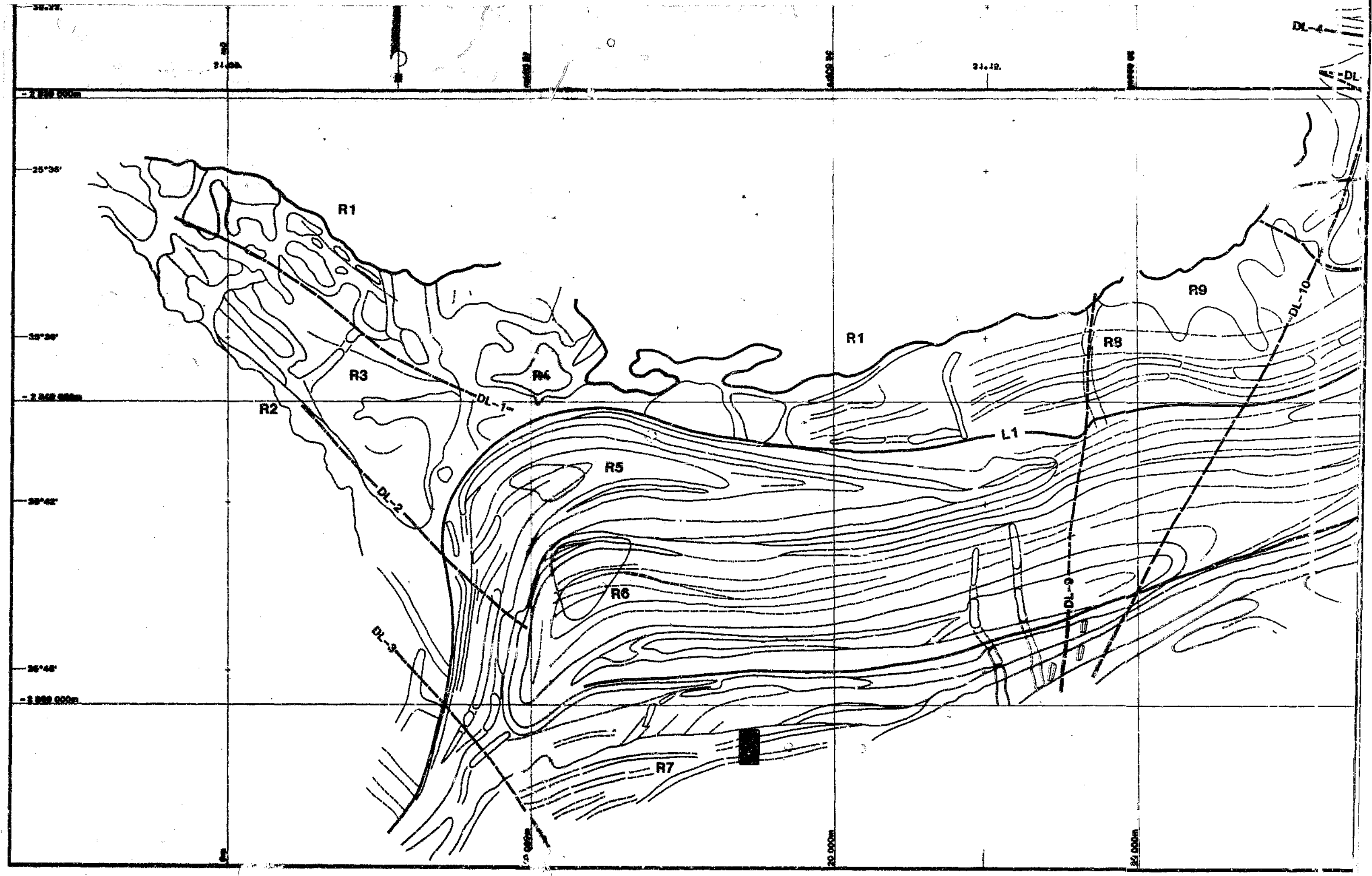
0 1 2 3 4 5 6 km

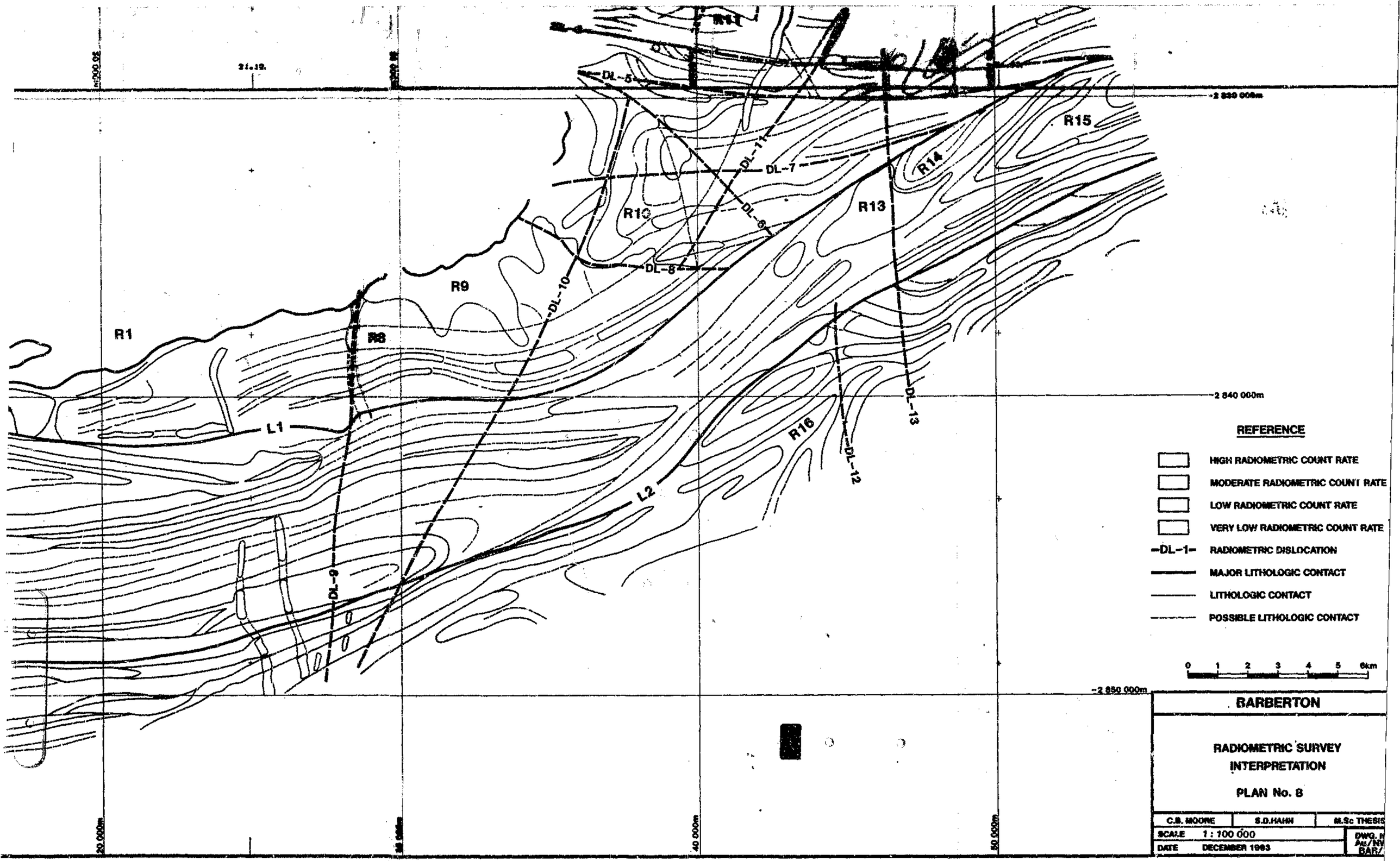
BARBERTON

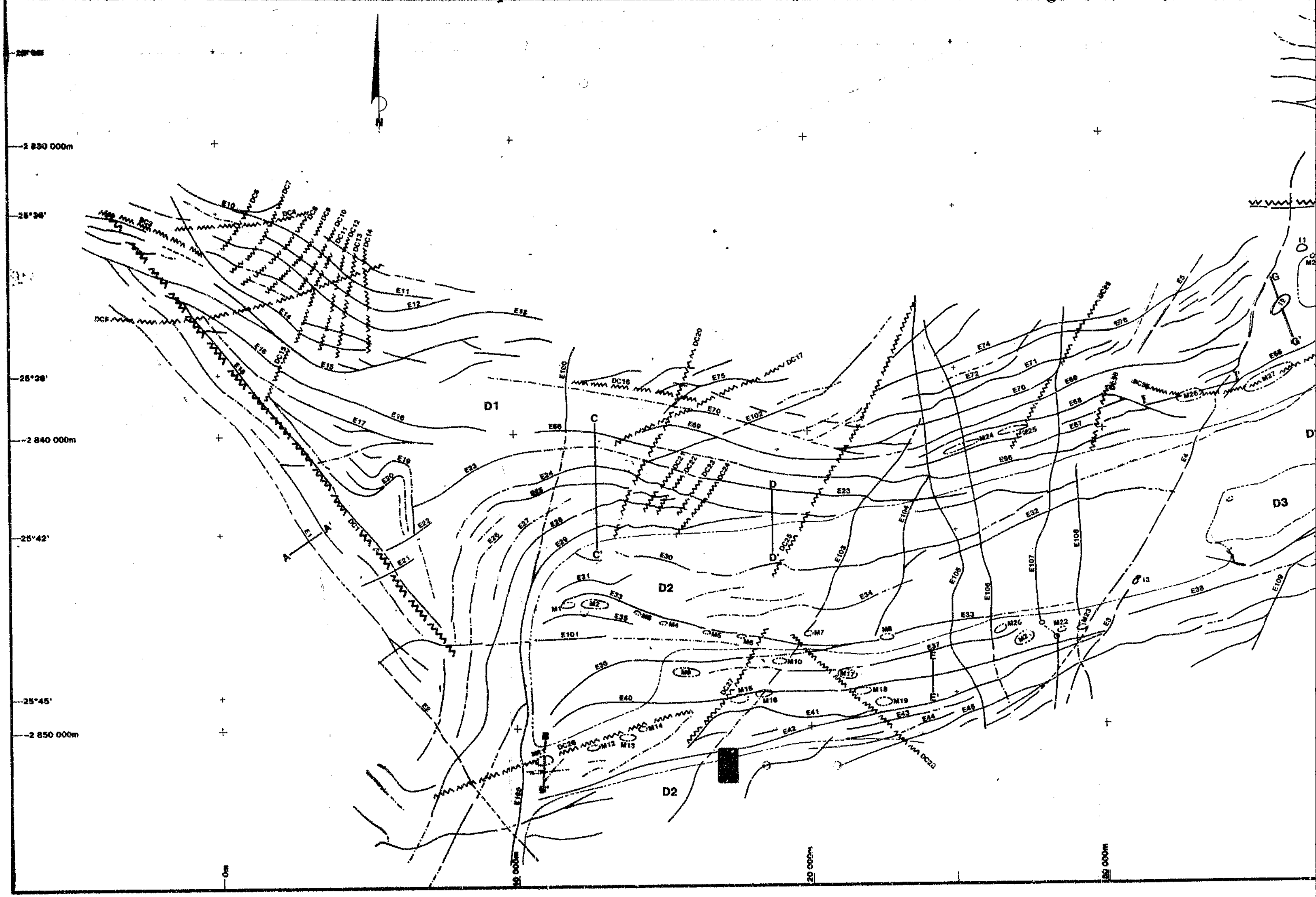
INTERGRATED GEOPHYSICAL INTERPRETATION

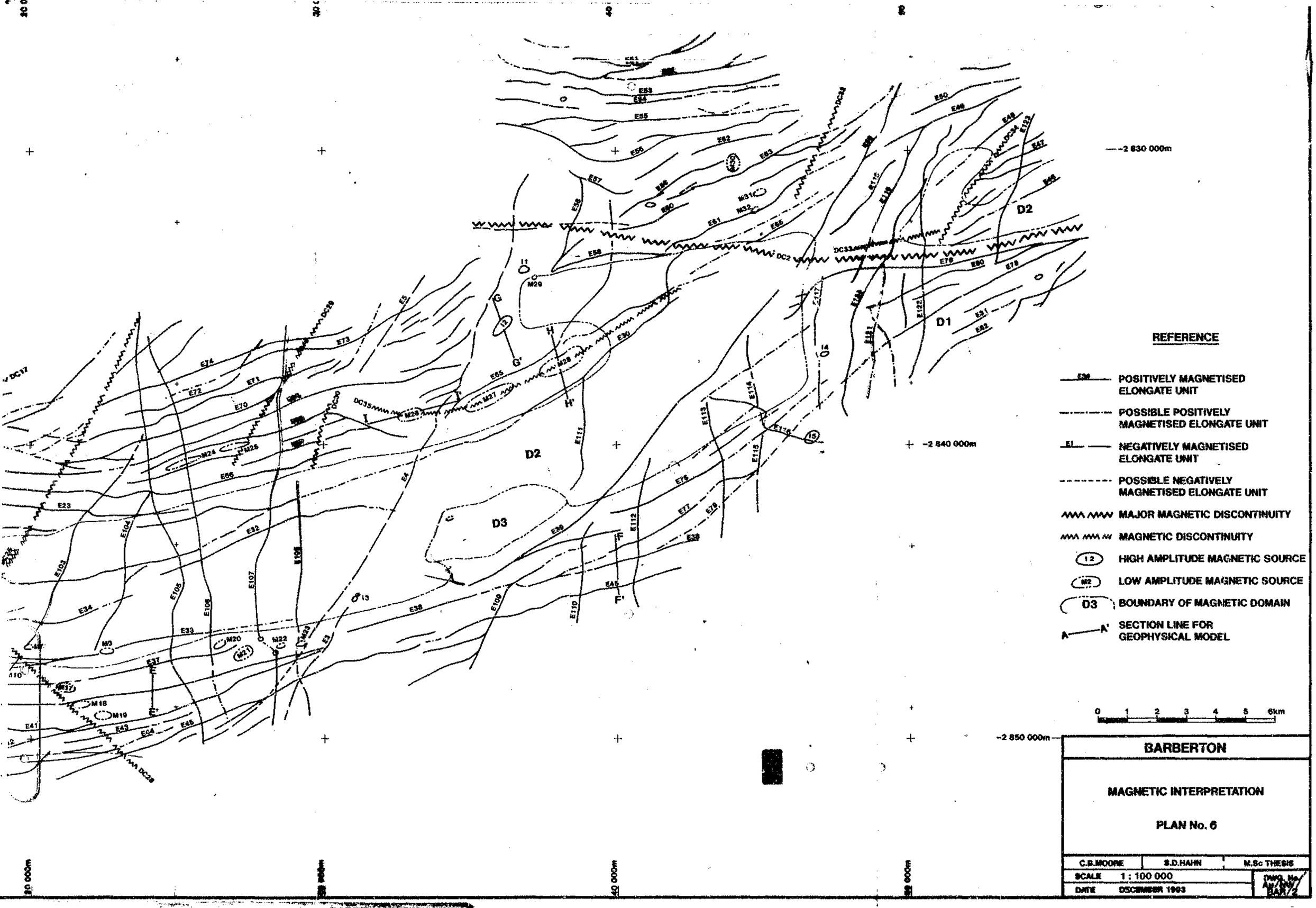
PLAN No. 9

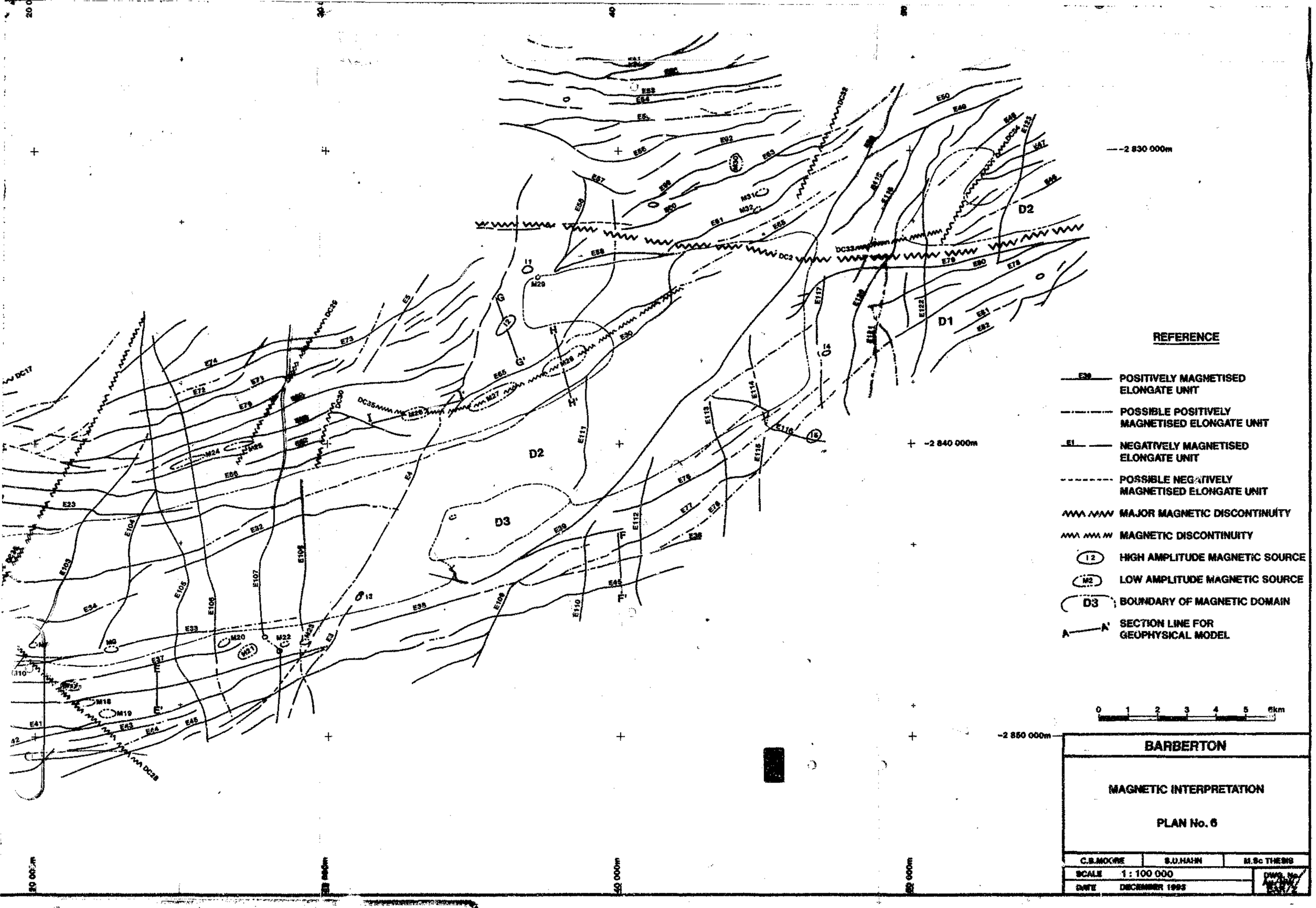
C.B.MOORE	D.DOMINGUEZ	M.Sc.THESIS
SCALE: 1 : 100 000		DWG. No. Au/MW/BAR/9
DATE: DECEMBER 1993		


DL-4
DL-
25°36'
R1
R3
R4
R2
DL-1
R1
R9
R8
DL-10
L1
R5
DL-2
R6
DL-9
DL-3
R7


R11
DL-5
DL-11
DL-7
R15
R14
R10
DL-6
R13
DL-8
DL-10
R9
R1
R8
L1
DL-13
R16
DL-12
L2
DL-9
2 840 000m
2 850 000m
20 000m
30 000m
40 000m
50 000m
REFERENCE
HIGH RADIOMETRIC COUNT RATE
MODERATE RADIOMETRIC COUNT RATE
LOW RADIOMETRIC COUNT RATE
VERY LOW RADIOMETRIC COUNT RATE
DL-1 RADIOMETRIC DISLOCATION
MAJOR LITHOLOGIC CONTACT
LITHOLOGIC CONTACT
POSSIBLE LITHOLOGIC CONTACT
0 1 2 3 4 5 6km
BARBERTON
RADIOMETRIC SURVEY
INTERPRETATION
PLAN No. 8
C.B. MOORE
S.D.HAHN
M.Sc THESIS
SCALE 1 : 100 000
DATE DECEMBER 1983


2 830 000m
25°36'
25°39'
2 840 000m
25°42'
25°45'
2 850 000m
N
A
A'
B
B'
C
C'
D
D'
E
E'
D1
D2
D3
0m
20 000m
E1
E2
E3
E4
E5
E6
E7
E8
E9
E10
E11
E12
E13
E14
E15
E16
E17
E18
E19
E20
E21
E22
E23
E24
E25
E26
E27
E28
E29
E30
E31
E32
E33
E34
E35
E36
E37
E38
E39
E40
E41
E42
E43
E44
E45
E46
E47
E48
E49
E50
E51
E52
E53
E54
E55
E56
E57
E58
E59
E60
E61
E62
E63
E64
E65
E66
E67
E68
E69
E70
E71
E72
E73
E74
E75
E76
E77
E78
E79
E80
E81
E82
E83
E84
E85
E86
E87
E88
E89
E90
E91
E92
E93
E94
E95
E96
E97
E98
E99
E100
E101
E102
E103
E104
E105
E106
E107
E108
E109
DC1
DC2
DC3
DC4
DC5
DC6
DC7
DC8
DC9
DC10
DC11
DC12
DC13
DC14
DC15
DC16
DC17
DC18
DC19
DC20
DC21
DC22
DC23
DC24
DC25
DC26
DC27
DC28
M1
M2
M3
M4
M5
M6
M7
M8
M9
M10
M11
M12
M13
M14
M15
M16
M17
M18
M19
M20
M21
M22
M23
M24
M25
M26
M27


-2 830 000m
-2 840 000m
-2 850 000m
D1
D2
D2
D3
G
G'
H
H'
F
F'
E'
REFERENCE
POSITIVELY MAGNETISED ELONGATE UNIT
POSSIBLE POSITIVELY MAGNETISED ELONGATE UNIT
NEGATIVELY MAGNETISED ELONGATE UNIT
POSSIBLE NEGATIVELY MAGNETISED ELONGATE UNIT
MAJOR MAGNETIC DISCONTINUITY
MAGNETIC DISCONTINUITY
HIGH AMPLITUDE MAGNETIC SOURCE
LOW AMPLITUDE MAGNETIC SOURCE
BOUNDARY OF MAGNETIC DOMAIN
SECTION LINE FOR GEOPHYSICAL MODEL
0 1 2 3 4 5 6km
BARBERTON
MAGNETIC INTERPRETATION
PLAN No. 6
C.B.MOORE
S.D.HAHN
M.Sc THESIS
SCALE 1 : 100 000
DATE DECEMBER 1993
DWG. No AM/BAR/7 BAR/2


-2 830 000m
-2 840 000m
-2 850 000m
D1
D2
D3
REFERENCE
POSITIVELY MAGNETISED ELONGATE UNIT
POSSIBLE POSITIVELY MAGNETISED ELONGATE UNIT
NEGATIVELY MAGNETISED ELONGATE UNIT
POSSIBLE NEGATIVELY MAGNETISED ELONGATE UNIT
MAJOR MAGNETIC DISCONTINUITY
MAGNETIC DISCONTINUITY
HIGH AMPLITUDE MAGNETIC SOURCE
LOW AMPLITUDE MAGNETIC SOURCE
BOUNDARY OF MAGNETIC DOMAIN
SECTION LINE FOR GEOPHYSICAL MODEL
0 1 2 3 4 5 6km
BARBERTON
MAGNETIC INTERPRETATION
PLAN No. 6
C.B.MOORE
S.U.HAHN
M.Sc THESIS
SCALE 1 : 100 000
DATE DECEMBER 1993

-2 850 000m

25°45'

25°42'

-2 840 000m

25°39'

25°36'

-2 830 000m

0m

20 000m

30 000m

N

20 000m

31°15'

40 000m

31°45'

50 000m

-2 850 000m

REFERENCE

	ALLUVIUM	
MdSs	SANDY SHALE, LOCALLY MAGNETIC	MOODIES SYSTEM (ARCHAEOZOIC)
MdGs	GRITTY, FELSPATHIC QUARTZITE	
MdSs	SHALE WITH BANDS OF CONGLOMERATE AND LAVA (Mdl.)	
Mdqz	FELSPATHIC QUARTZITE	
Mdsh	SHALE WITH BANDS OF QUARTZYTE: MAGNETIC SHALE (Mdl)	
Mdfs	FELSPATHIC QUARTZITE	
MdC Mdl	CALCAREOUS QUARTZITE WITH LIMESTONE AND MARBLE	
Kpc	SHALE WITH GREYWACKE	Fig-tree Series / Onverwacht Series — SWAZILAND SYSTEM (ARCHAEOZOIC)
Kpv	LAVA, FELSPAR PORPHYRY	
Kpb	SHALE WITH BANDED IRONSTONE	
Kpsc	CARBONATE SCHISTS, ZWARTKOPPIE HORIZON	
Kfp	QUARTZ AND FELSPAR PORPHYRY, WITH BASIC LAVA	
Kbv	BASIC LAVA	
Kdo	DOLERITE DYKE	
Kqd	QUARTZ DYKE	
Abg	NELSPRUIT GRANITE	POST JAMESTOWN
Agn	KAAP VALLEY GRANITE	JAMESTOWN IGNEOUS COMPLEX
Sp	SERPENTINITE	
Sa	SERPENTINITE, CARBONATE SCHIST, AMPHIBOLE SCHIST	
	MYLONITE	
	FAULT	
	FAULT NOT ACCURATELY LOCATED	
	RIVER	
	MINE	

0 1 2 3 4 5 6km

*SOURCE GOVERNMENT 1:50 000 GEOLOGICAL

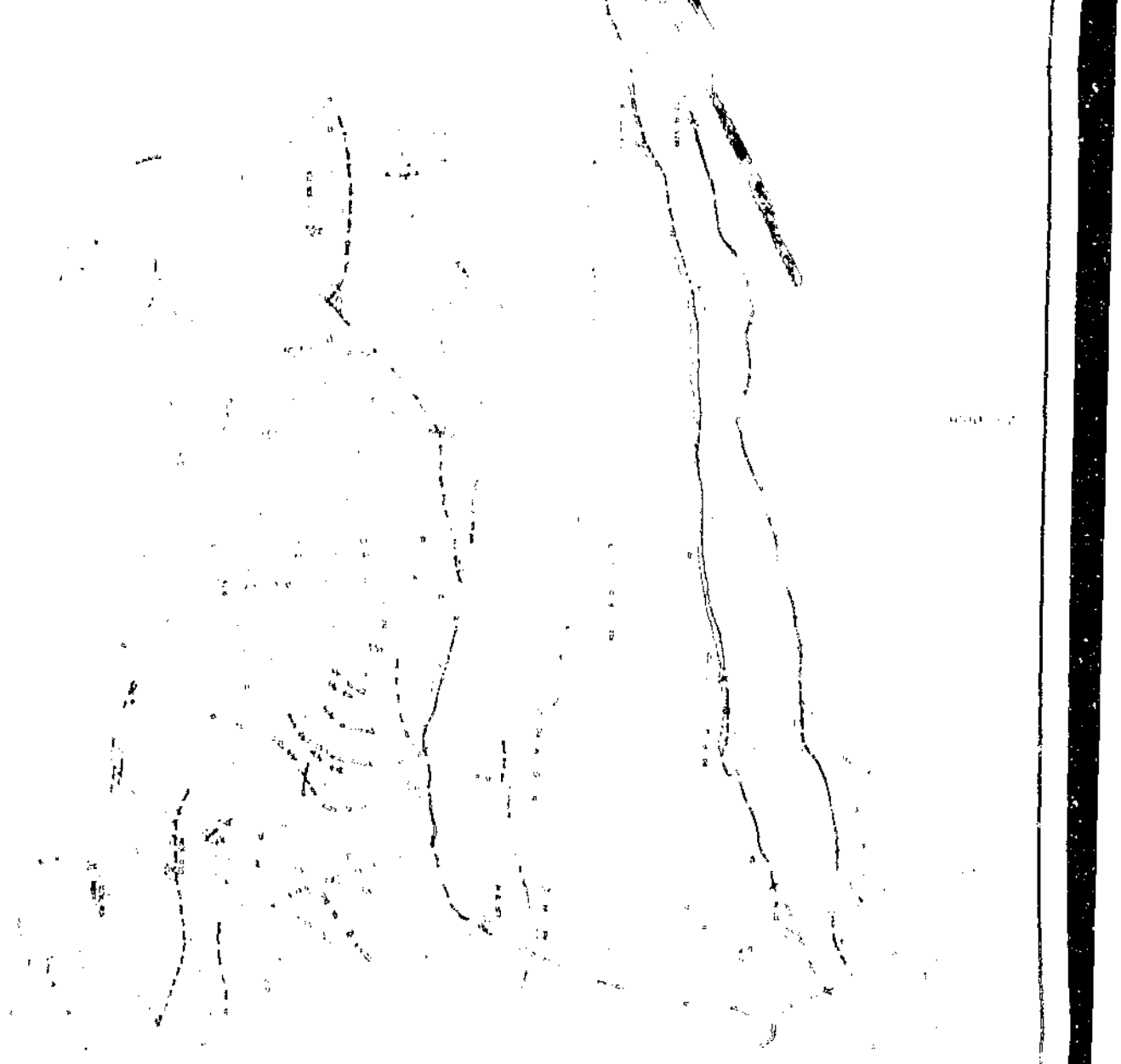
BARBERTON

NORTHERN MOUNTAIN LAND

REGIONAL GEOLOGY

PLAN No. 1

C.B. MOORE	M.KEMPEN	M.Sc THESIS
SCALE 1 : 100 000		Drwg. No. Ag/NW/ BAR/1
DATE DECEMBER 1982		



REFERENCE

MOUNTAIN SYSTEM ARCHAEAN

SWAZILAND SYSTEM ARCHAEAN

POST JAMESTOWN

JAMESTOWN IGNEOUS COMPLEX

FAULT

FAULT NOT ACCURATELY LOCATED

RIVER

MINE

0 1 2 3 4 5 6km

+2 850 000m

* SOUTH AFRICAN GOVERNMENT 1:250 000 GEOLOGICAL MAP

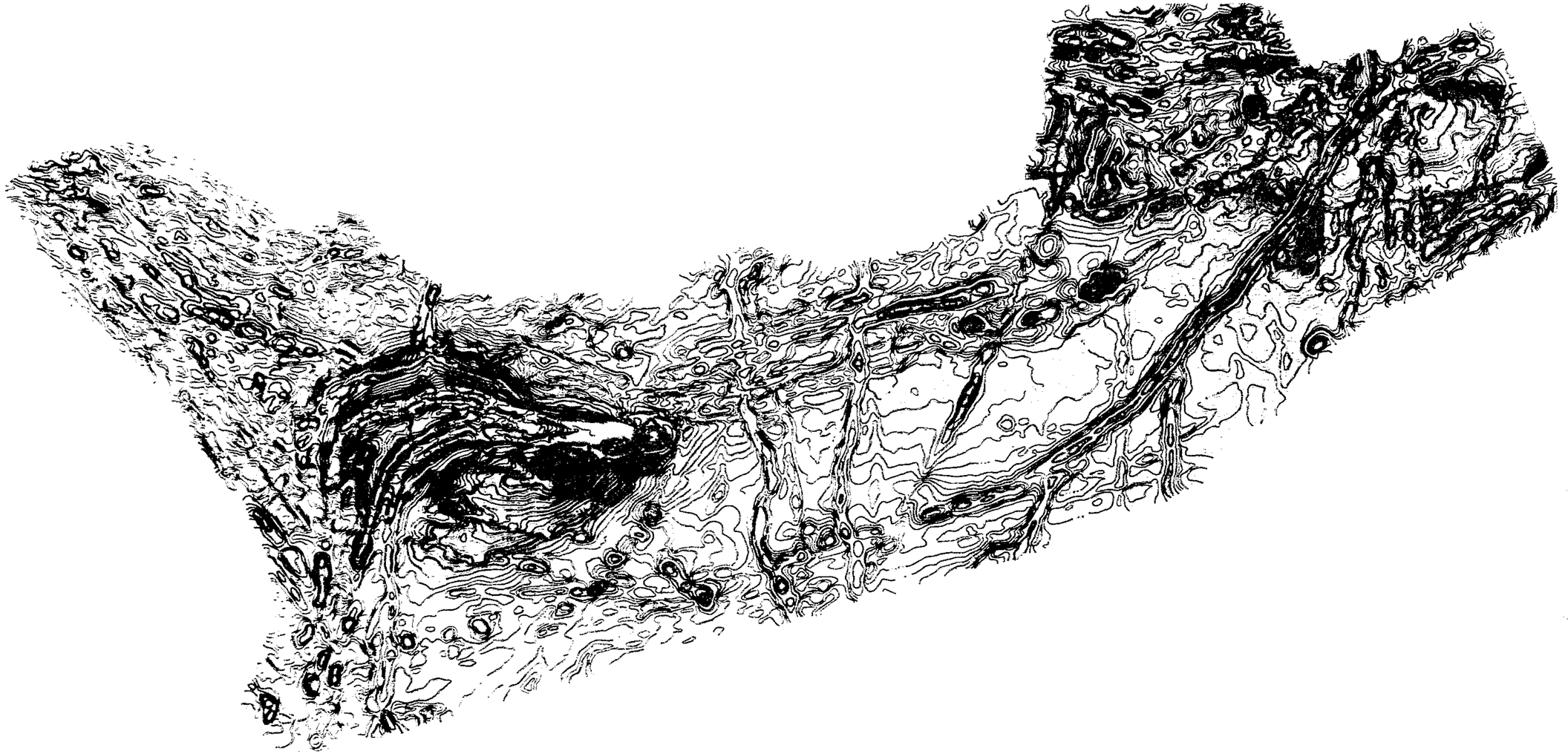
BARBERTON

NORTHERN MOUNTAIN LAND

REGIONAL GEOLOGY

PLAN No 1

C B MOORE	M KEMPEN	M.Sc THESIS
SCALE 1 : 100 000		DWG. No. Au. NW. BAR. 1
DATE DECEMBER 1993		



BARBERTON

RESIDUAL MAGNETIC FIELD
CONTOUR MAP

2

M.Sc Thesis



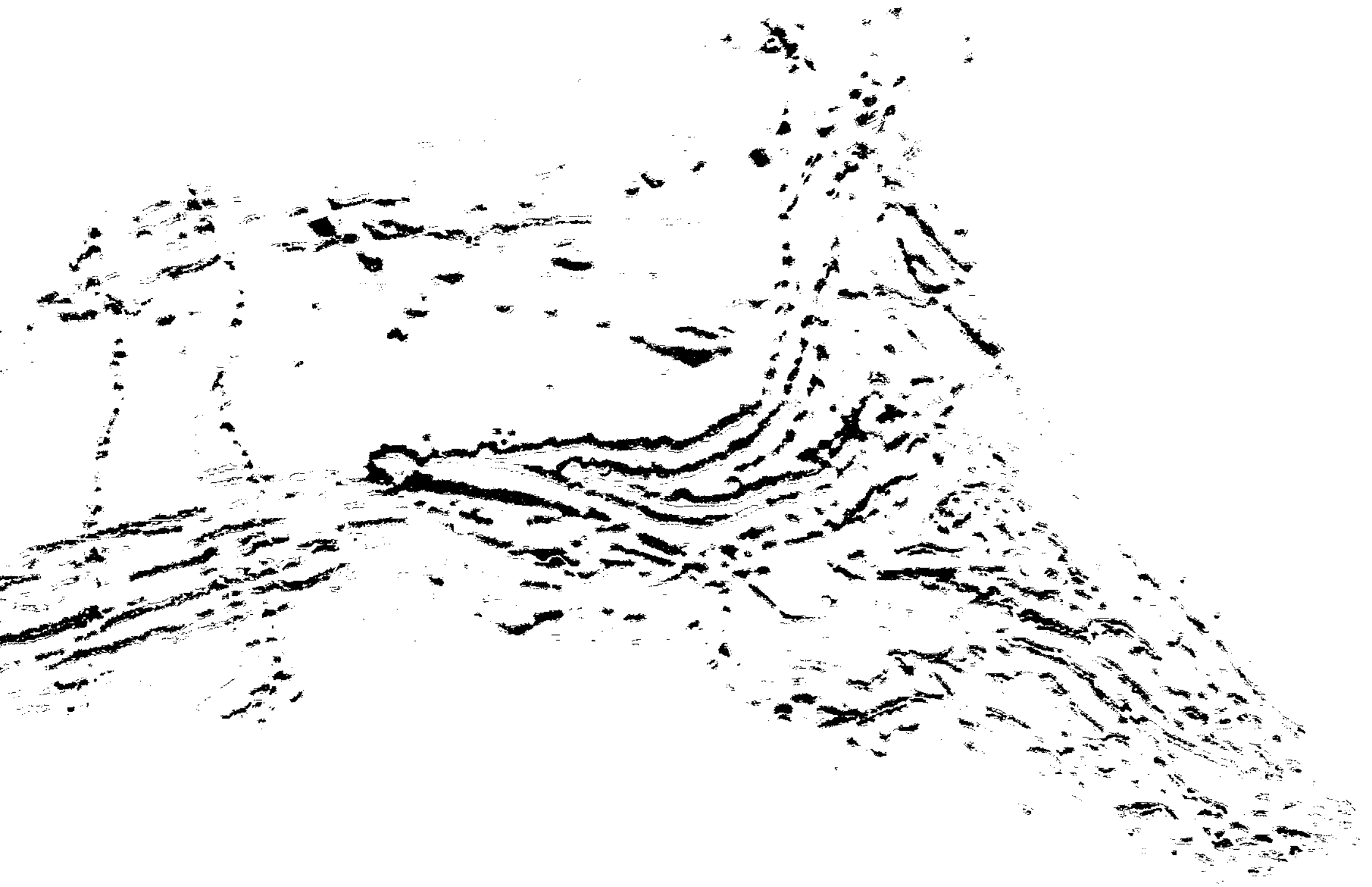


BARBERTON

REGIDUAL MAGNETIC FIELD
CONTOURED RELIEF MAP

3

M.Sc Thesis





N

BARBERTON

MAGNETIC 1ST VERTICAL DERIVATIVE
SHADED RELIEF MAP

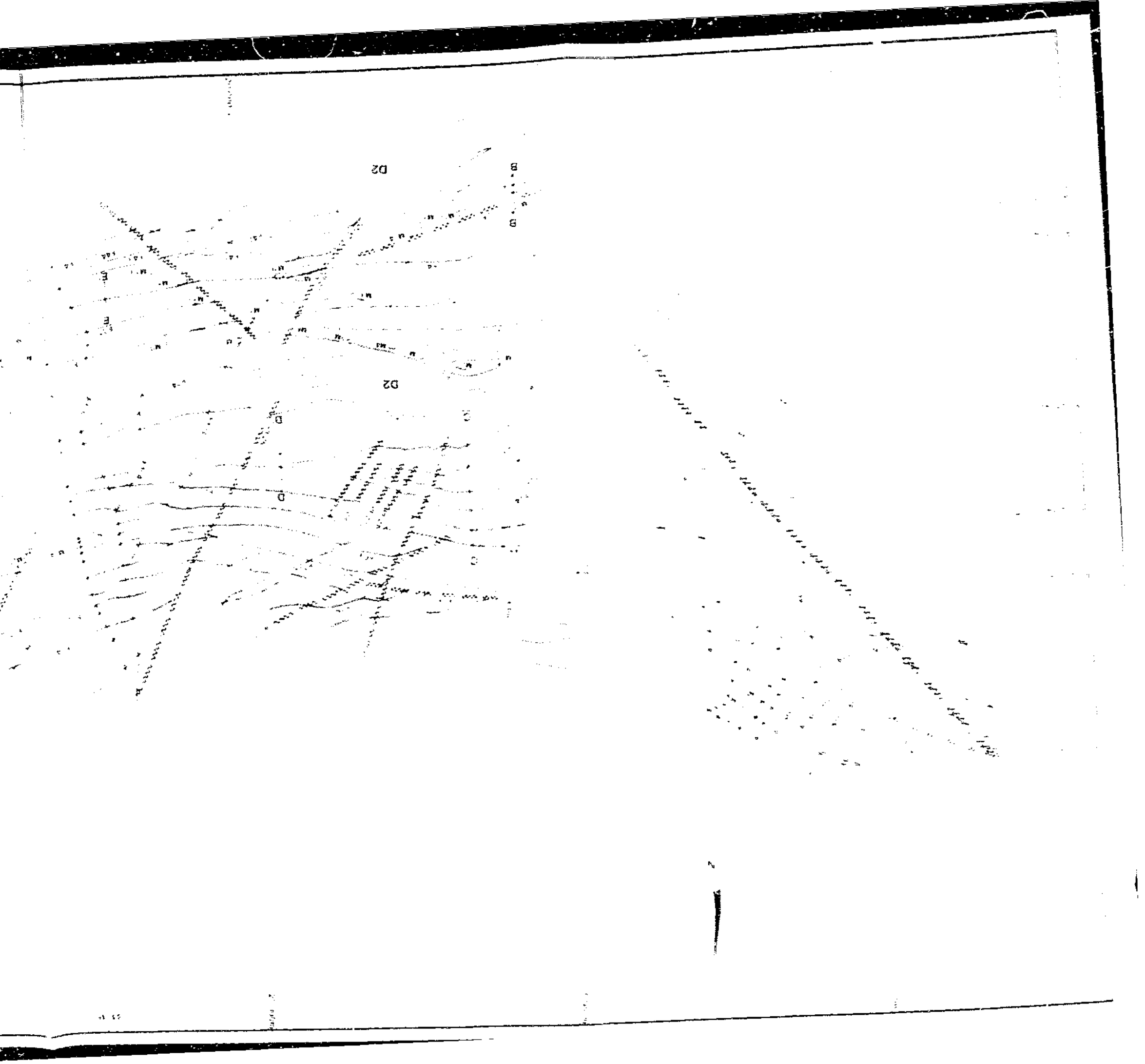
4

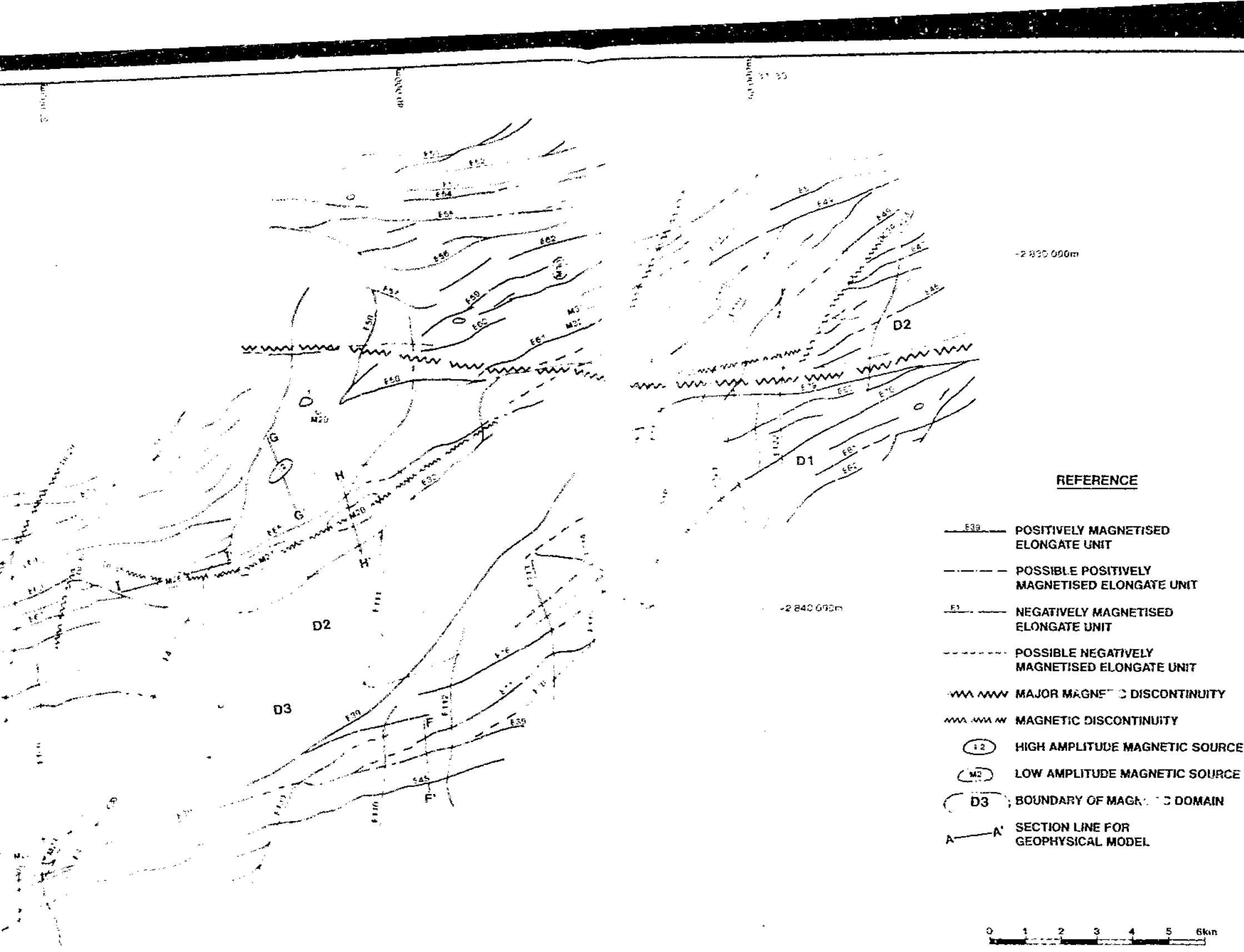
M.Sc Thesis



BABERTON
EULER DECONVOLUTION

5


D2
B
D2



REFERENCE

- E39 — POSITIVELY MAGNETISED ELONGATE UNIT
- POSSIBLE POSITIVELY MAGNETISED ELONGATE UNIT
- E1 — NEGATIVELY MAGNETISED ELONGATE UNIT
- POSSIBLE NEGATIVELY MAGNETISED ELONGATE UNIT
- MAJOR MAGNETIC DISCONTINUITY
- MAGNETIC DISCONTINUITY
- I2 — HIGH AMPLITUDE MAGNETIC SOURCE
- M2 — LOW AMPLITUDE MAGNETIC SOURCE
- D3 — BOUNDARY OF MAGNETIC DOMAIN
- A — A' SECTION LINE FOR GEOPHYSICAL MODEL

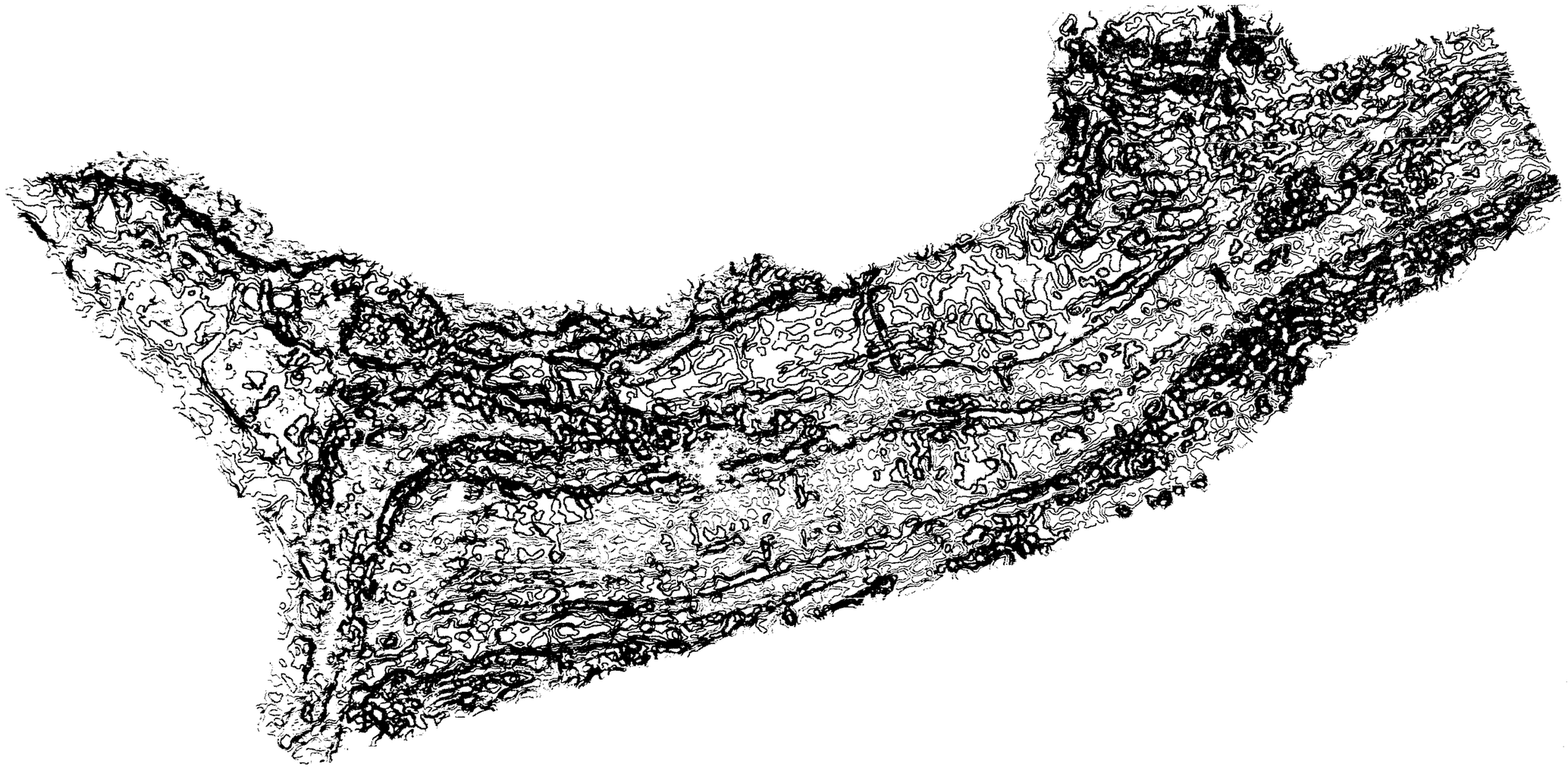
0 1 2 3 4 5 6km

BARBERTON

MAGNETIC INTERPRETATION

PLAN No. 6

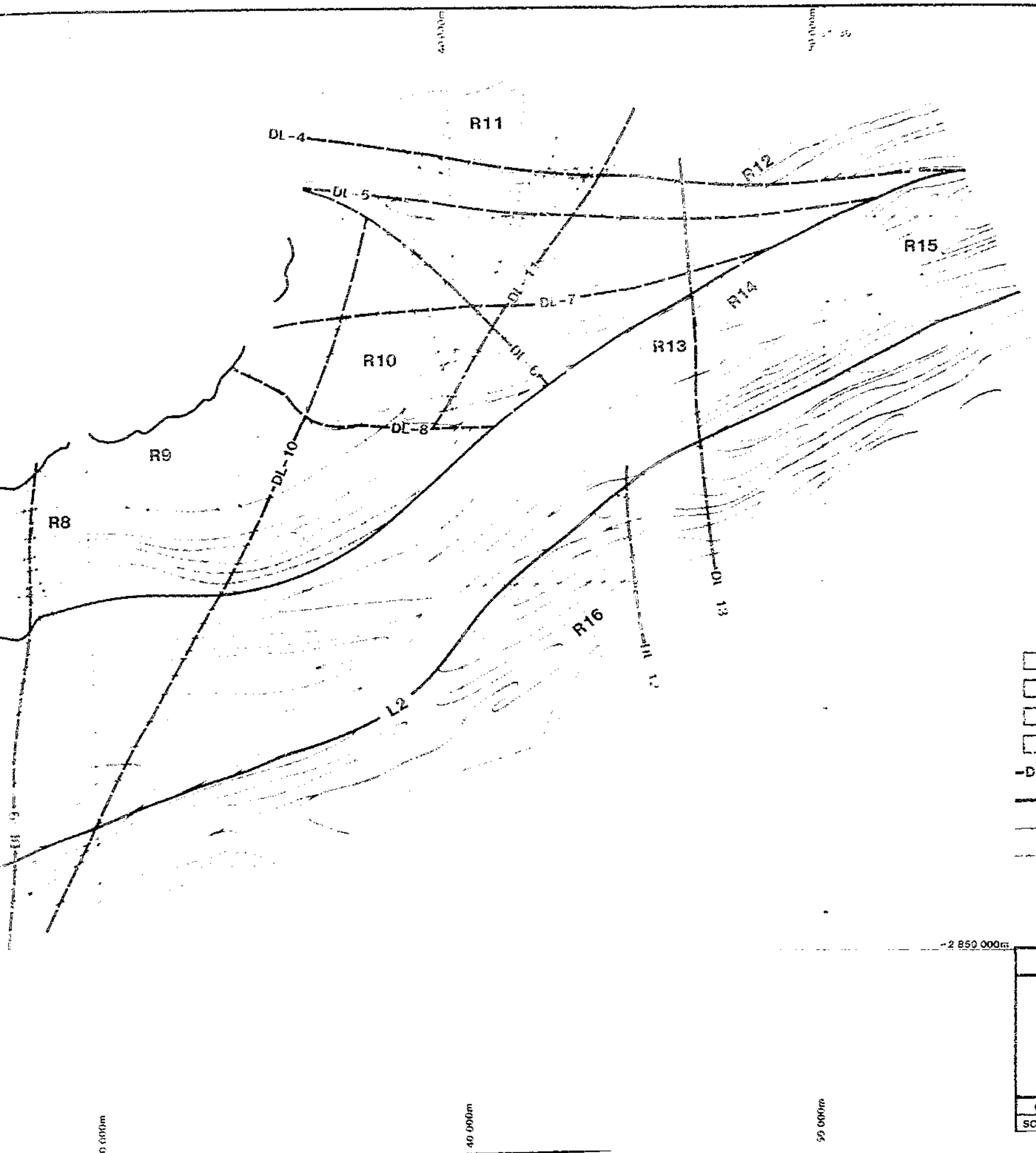
C.E.MOORE	S.D HAHN	M.Sc THESIS
SCALE 1 : 100 000		DWG No. Au/NW/ BAR/2
DATE DECEMBER 1993		



BARBERTON

RADIOMETRIC TOTAL-COUNT
CONTOUR MAP


R7
R6
R5
R4
R3
R2
R1



REFERENCE

- HIGH RADIOMETRIC COUNT RATE
- MODERATE RADIOMETRIC COUNT RATE
- LOW RADIOMETRIC COUNT RATE
- VERY LOW RADIOMETRIC COUNT RATE
- -DL-1- RADIOMETRIC DISLOCATION
- MAJOR LITHOLOGIC CONTACT
- LITHOLOGIC CONTACT
- POSSIBLE LITHOLOGIC CONTACT

0 1 2 3 4 5 6km

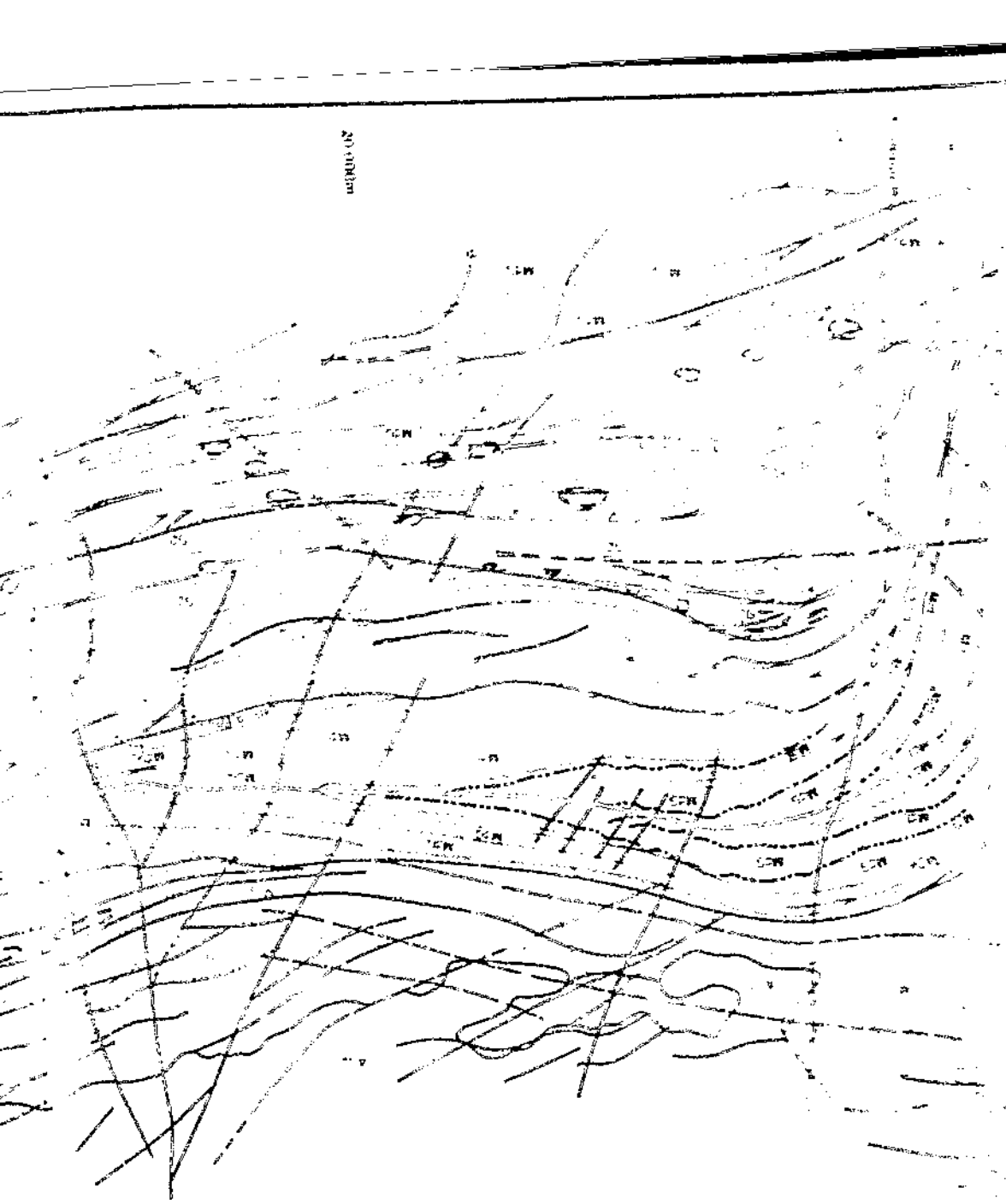
BARBERTON

RADIOMETRIC SURVEY INTERPRETATION

PLAN No. 8

C.B. MOORE	S.D.HAHN	M.Sc THESIS

SCALE 1 100 000





REFERENCE

MOODIES SEDIMENTS
- CONGLOMERATE SHALE
- SHALE
- FELSPATHIC QUARTZITE

- MAGNETIC SHALE AND LAVA
- FIG TREE SEDIMENTS
- ONVERWACHT LAVAS
- ONVERWACHT ACID VOLCANICS
- JAMESTOWN IGNEOUS COMPLEX
- NELSPRUIT GRANITE
- KAAP VALLEY GRANITE
- FAULT / SHEAR ZONE
- POSSIBLE FAULT / SHEAR ZONE
- LITHOLOGIC CONTACT
- POSSIBLE LITHOLOGIC CONTACT
- FOLD AXIS
- FELSIC INTRUSIVE
- POSITIVELY MAGNETISED ULTRAMAFIC INTRUSIVE
- NEGATIVELY MAGNETISED ULTRAMAFIC INTRUSIVE
- DIORITE DYKE
- DOLERITE DYKE

0 1 2 3 4 5 6 km

BARBERTON

INTERGRATED GEOPHYSICAL INTERPRETATION

PLAN No. 9

C B MOORE | D DOMINGUEZ | M G [illegible]

Author:Moore, Chris.
Name of thesis:Applications of high resolution airborne magnetic and radiometric data in the Barberton Greenstone belt of South Africa.

PUBLISHER:
University of the Witwatersrand, Johannesburg
©2015

LEGALNOTICES:

Copyright Notice: All materials on the University of the Witwatersrand, Johannesburg Library website are protected by South African copyright law and may not be distributed, transmitted, displayed or otherwise published in any format, without the prior written permission of the copyright owner.

Disclaimer and Terms of Use: Provided that you maintain all copyright and other notices contained therein, you may download material (one machine readable copy and one print copy per page)for your personal and/or educational non-commercial use only.

The University of the Witwatersrand, Johannesburg, is not responsible for any errors or omissions and excludes any and all liability for any errors in or omissions from the information on the Library website.